공학박사 학위논문

Study on Control of Dynamic Properties of Cellulose-Ionic Liquid Solution for Fabrication of Nanostructures

나노구조체 제조를 위한 셀룰로오스-이온성 액체 용액의 동역학적 특성 제어에 관한 연구

2019년 8월

서울대학교 대학원

재료공학부

안 용 준

Study on Control of Dynamic Properties of Cellulose-Ionic Liquid Solution for Fabrication of Nanostructures

나노구조체 제조를 위한 셀룰로오스-이온성 액체 용액의
동역학적 특성 제어에 관한 연구

지도교수 곽승엽

이 논문을 공학박사 학위논문으로 제출함
2019년 4월

서울대학교 대학원
재료공학부
안 용 준

안용준의 공학박사 학위논문을 인준함
2019년 7월

위 원 장 왕 희 영
부위원장 곽 승 엽
위 원 안 철 희
위 원 손 병 혁
위 원

Abstract

Study on Control of Dynamic Properties of Cellulose-Ionic Liquid Solution for Fabrication of Nanostructures

Yongjun Ahn
Department of Materials Science and Engineering
The Graduate School
Seoul National University

Cellulose, one of the most abundant polymers on the planet, has excellent properties such as high strength, biodegradability and biocompatibility. However, cellulose does not melt, and because of the limited solubility of the solvent, it is fairly unreasonable for use in relative industries. Recently, since the development of ionic liquids, which can easily dissolve cellulose at room temperature, related research has been increasing enormously. Ionic liquids is one of the type of salts consisting of large cation molecules and relatively small anions. The principle of cellulose dissolution is that the anion capable of hydrogen bonding disrupts the cellulosic hydrogen bonding network and

the cation penetrates into the relaxed network, thereby dissociating the structure of the cellulose. Despite a number of studies, there is a problem that the molar mass of the cellulose is decreased in the ionic liquid and the crystallinity after regeneration is not recovered, resulting in a decrease in strength. Therefore, this study aims to develop a cellulosic material having uniform nanostructure with fundamental understanding for depolymerization and recrystallization of cellulose in ionic liquid.

First, the depolymerization and its rate were investigated after dissolving the cellulose using an ionic liquid having different anions. The depolymerization of cellulose in ionic liquid was found to be acidic the hydrolysis. The acid generated from the ionic liquid was found to be produced more as the basicity of the anion was larger. The constant of viscosity average molar mass was obtained by using cellulose having molar mass distribution by hydrolysis in ionic liquid. In addition, it was observed for the lyotropic liquid crystalline of cellulose which was not previously reported.

Second, the mobility of hydrolyzed cellulose molecules in ionic liquids was determined and correlated with the recrystallization behavior. Cellulose has increased mobility when the molar mass was decreased, especially below the entanglement molar mass. The kinetic constants were calculated by analyzing

the correlation between the molecular diffusion coefficient and recrystallization for investigation of improving crystallinity.

Third, based on the hydrolysis behavior and mobility data, an ionic liquid was applied to the lignocellulosic biomass pretreatment process. Lignocellulose pretreatment aims to relax the structure and reduce the molar mass. As the solubility of the ionic liquid for cellulose increased, the crystallinity and removal efficiency of the non-cellulosic component increased significantly. This study has provided a reference for the selection of ionic liquids optimized for the structure of each lignocellulose.

Fourth, cellulose nanoparticles with uniform size and high dispersity were prepared using cellulose molecules to be controlled molecular motility in ionic liquid. During the hydrolysis, the reaction of the cation of the ionic liquid to the reducing end of the cellulose was induced to form cellulose nanoparticles similar to micelle structure. Cellulose nanoparticles showed high dispersity due to surface cation.

Fifth, process for separating rancid ingredients, such as free fatty acid and chlorophyll, of extra virgin olive oil is proposed using cellulose nanofiltration membrane functionalized by amine groups onto the surface. Similar to the principle of nanoparticle preparation, the cellulose moleculars with improved motility showed high porosity. The amine group was induced by substituting

the tosyl group and ethylenediamine in turn. The free fatty acids and chlorophyll, known as the rancid ingredients of extra virgin olive oil, were separated by the amine groups and pore size of the membrane, respectively. Moreover, it was confirmed that only the acid component can be selectively removed without changing the composition of the extra virgin olive oil.

In this study, celluloses were dissolved in ionic liquids under various conditions and their molecular properties were investigated. Based on the database, the technology for the preparation of nano-cellulose materials was established. Particularly, it is possible to open a new horizon for the cellulose process by developing a method to overcome the reduced molar mass and low crystallinity considered as be the limitation of conventional cellulose regenerated from ionic liquid.

Keywords

Cellulose; Ionic liquid; Rheological properties; Crystallization; Lignocellulose pretreatment; Nanoparticle; Nanofiltration

Student number: 2014-30197

Contents

Chapter 4

Effect of ionic liquid pretreatment on microstructure of lignocellulosic biomass

List of tables

List of figures

their neutralization point. To clearly show changing conductivity, these curves are shifted vertically by a factor B with the corresponding B value of 0, 0.5, 1 and 1.5, respectively.

Figure 2-5. FT-IR spectra of cellulose precipitated from (a) $[C_4C_1Im][Cl]$ and (b) $[C_4C_1Im][OAc]$, and (c) their number of reducing ends as function of reciprocal number average molar mass.

Figure 2-6. Dependence of dynamic storage modulus, G' (open symbols), and loss modulus, G" (filled symbols), on reduced angular frequency, ωa_T, for cellulose/$[C_4C_1Im][Cl]$ solutions dissolved for different times. These curves are shifted vertically by a factor B except for the solution dissolved for 144 h. The solid lines represent the curves reproduced by calculations using a generalized Maxwell model.

Figure 2-7. Relationship between (a) log a_T and $1/T$ and (b) activation energy, ΔE_a, and dissolution time, where a_T and T represent the horizontal shift factor and absolute temperature, respectively. The solid lines show the results of curve fitting using the WLF equation.

Figure 2-8. Dependence of intrinsic viscosity on the molar mass for cellulose/$[C_4C_1Im][Cl]$ solutions at 30 °C

Figure 2-9. Dependence of the radius of gyration, R_g, on the molar mass for cellulose/$[C_4C_1Im][Cl]$ solutions at 30 °C

Figure 5-4. (a) SEM and TEM images of pristine cellulose and the cellulose nanoparticles with different molar masses controlled by the dissolution time. The inserted photographs represent the stability in aqueous media. All samples were adjusted to the same concentration of 0.1 wt%, and each image was captured for the suspension after a month of sample preparation. (b) Dependence of the molar mass on the average size and zeta potential; the circle and triangle symbols represent the average size and zeta potential, respectively.

Figure 5-5. (a) XRD curves of pristine cellulose and the cellulose nanoparticles with different molar masses controlled by the dissolution time. (b) TGA curves and differential thermal analysis (insert) of pristine cellulose and the c ellulose nanoparticles with different molar masses.

Figure 6-1. Schematic representation of preparation procedure for cellulose **NF MEMBRANE** via freeze-thaw process

Figure 6-2. SEM (upper) and TEM (bottom) images of cellulose NF membrane with different molar mass

Figure 6-3. ^{13}C NMR spectra of tosyl cellulose NF membranes with degree of substitution DS_{tos} = 0.48, CNM-tosyl252, DS_{tos} = 0.95, CNM-tosyl165, and DStos = 1.71, CNM-tosyl92 recorded in DMSO-d_6 at 25 °C.

CHAPTER 1

Introduction

1.1. General description of cellulose processing

Depletion of fossil fuels and global warming caused by carbon dioxide emissions is a serious threat to the survival of humankind. Therefore, eco-friendly processes and materials are becoming a major issue in industry and academia. Lignocellulose is one of the most abundant resource on the earth and is emerging as an alternative material to resolve environmental problems. The efficiency and wide availability of lignocellulose is expected to play a key role in sustainable industrial development and is expected to enable de-fossilization in the chemical and energy industries.

Cellulose is the most abundant polymer in lignocellulose.[1] Cellulose is a linear polymer of glucose linked by β- (1→4) glucosidic bonds and has been used in our daily life through materials such as cotton, hemp, and pulp. The excellent properties such as biocompatibility and biodegradability of cellulose are expected to be used in various fields. Among the various properties, the high strength of cellulose is attracting attention in the functional materials and fiber-reinforced composite materials industry today.[2] In particular, cellulose with reduced diameter in nanometers exhibits properties such as high surface

energy, high thermal stability and structural stability.[3] Cellulose can be formed into various types of nanostructures and is expected to be able to exhibit new properties different from typical physical and chemical properties. Nano-structured cellulose is expected to exhibit excellent performance in membranes, biosensors, electrical and optical devices.[4-7]

However, cellulose is not melted and there is no solvent to dissolve the cellulose due to the rigidity of the molecular chains, the high crystallinity and the strong hydrogen bonds between the chains, which is difficult to apply as thermoplastic materials. Viscose rayon, developed by Courtaulds in the UK at the end of the nineteenth century, is the first molded material produced by wet spinning of cellulose. However, the xanthation process under severe conditions to dissolve cellulose caused the degradation of molecular chains, resulting in deterioration of physical properties. Complex processes and environmental pollution promoted various studies on cellulose dissolution. Typically, solvents such as N-Methylmorpholine N-oxide (NMMO)/H_2O, N,N-dimethylacetamide (DMAc)/lithium chloride (LiCl), and sodium hydroxide (NaOH)/urea system have been reported to be direct solvents that do not substitute cellulose. In particular, Lyocell, a cellulose fiber regenerated from NMMO/H_2O system, is being supplied exclusively from Lenzing (Austria) due to the process advantages and its excellent properties. However, the NMMO system has also been pointed out to be associated with high energy

consumption and deforestation by using high-purity pulp-based cellulose. Therefore, it has been continuously required for development of environmentally friendly solvents such as improvement of stability of solvent itself and development of low-carbon process.

In 2002, Rogers and colleagues[8] first reported the solubility of cellulosic materials in ionic liquids, and ionic liquids are attracting much attention as next-generation cellulose solvents. Ionic liquids have been used in cellulosic research as clean solvents because of their excellent properties such as low melting point, thermal and chemical stability, and high recovery efficiency compared to other solvents. Moreover, the ionic liquid acts as a solvent directly without the substitution process of cellulose and thus shows high energy efficiency. Therefore, ionic liquids suggested a new paradigm in the cellulose dissolution process.

However, the dissolution process of cellulose using an ionic liquid involves several problems. First is the decrease of the molar mass during the dissolution and second is the difficulty of low recrystallization and moldability. The decrease in cellulose molecular weight is caused by the weak acidity of the ionic liquid. Hydrogen atoms present in the cations of the ionic liquid can be transiently transited to halogen anions by external energy (heat). The form in which a hydrogen atom and an anion are combined is present as a generally known acidic substance (hydrogen chloride, acetic acid, etc.). Acidification of

the ionic liquid involves deconstruction (depolymerization) of the glucosidic bonds in cellulose and involves a decrease in molar mass. In addition, the reduction of uncontrolled molar mass has a negative impact on the physical properties.

The crystalline structure of cellulose is composed of regular assembly of hydrogen bonds. Depending on the type of crystalline structure, the crystalline form can be divided into Cellulose I, II, III, and IV. In the case of natural cellulose, it shows a cellulose I structure, and when it is recrystallized after dissolution, it is generally converted into a cellulose II structure. As mentioned above, cellulose has multiple hydrogen bonds and can be easily linked between each molecular chain. These properties interfere with regular recrystallization when solidifying after dissolution, resulting in low mechanical properties. Further, it is difficult to produce a material having a nano size due to non-uniform chain bonding, and it has not a uniform size. Therefore, in this study, we investigated cause of decrease of molecular weight of cellulose in ionic liquid in terms of kinetics, and proposed a method to prevent cellulose hydrolysis. The molar mass and the chain mobility of the cellulose were controlled by the dissolution condition, and high crystalline cellulose was prepared. Finally, a method for producing cellulose nanoparticles and NF membrane with uniform size was proposed.

1.2. Cellulose solvent

1.2.1. DMAc/LiCl system

McCormick and Turbac[9] first reported the feasibility of cellulose dissolution using N, N-dimethylacetamide and lithium chloride. This solvent system was used in the dissolution of polyamides and chitin in 1972. Cellulose/DMAc/LiCl systems were generally used for cellulose derivatives (cellulose acetate and nitrocellulose) and for analytical purposes (Gel Chromatography).[10]

In this solvent system, the cellulose is dissolveds by hydrogen bonding between the hydroxyl groups of cellulose and DMAc / LiCl. The dissolution occurs by the principle that hinders the hydrogen bonding of cellulose to the cellulose crystal structure swelled by DMAc,and then LiCl ion binds to the hydroxyl group. Cellulose should be pre-activated with distilled water, ethanol, and acetone in order before dissolution, and it was reported that the cellulose having a degree of polymerization of 130 and 1700 was dissolved to 15 wt% and 4 wt%, respectively. However, in the case of cellulose having a high degree of polymerization, it was observed that it was present in a swollen state without dissolving above a critical concentration.

One of the advantages of the DMAc / LiCl solvent system is its chemical stability. Unlike other solvent systems, it was observed that the decrease of

molar mass in cellulose solution was small at room temperature. McCormick et al. reported a viscosity reduction of only about 2% when stored at room temperature for 30 days in a 9 wt% solution, which was reported to be due to changes in intramolecular or intermolecular hydrogen bonding.[9]

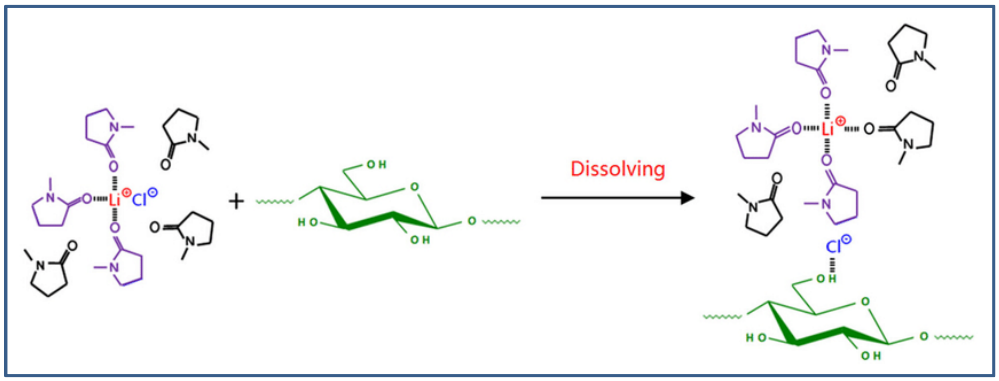

Figure 1-1. Dissolution mechanism of DMAc/LiCl system for cellulose[11]

1.2.2. Ammonia (NH_3)/ammonium thiocyanate (NH_4SCN) system

NH_3/NH_4SCN system was developed by Cuculo et al. in 1981. This system has high stability to cellulose and relatively low toxicity. When the cellulose (3.5 wt%) having a degree of polymerization of 210 is dissolved in NH_3/NH_4SCN (24.5/75.5 w/w), a cholesteric phase is formed. When 8 to 16 wt% is dissolved, a nematic phase is formed at 25 °C. In the case of NH_4SCN of 75.5% in cellulose/NH_3/NH_4SCN system, the minimum cellulose concentration capable of forming anisotropic phase is the maximum value. However, when this solvent is used, there is a disadvantage in the process of minimizing the evaporation of the solvent to prevent recrystallization of NH_4SCN.

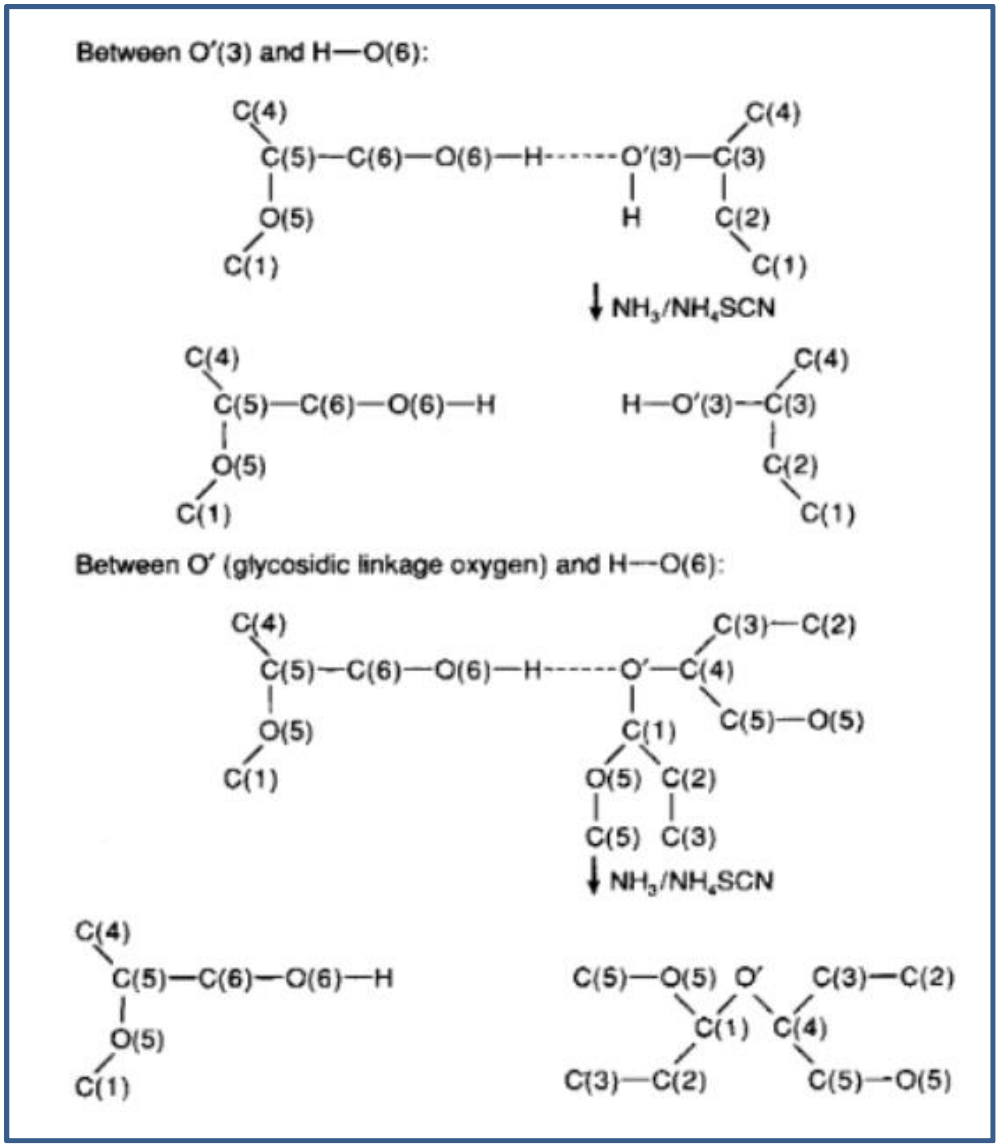

Figure 1-2. Dissolution mechanism of NH_3/NH_4SCN system for cellulose[12]

1.2.3. $Ca(SCN)_2 \cdot 3H_2O$ system

It was already known in 1905 that a mixture of $Ca(SCN)_2$ and water could dissolve cellulose. The composition of the solvent is 34.4 to 68.3 wt% of $Ca(SCN)_2$, 17.5 to 54.6 wt% of water, and the cellulose concentration is usually dissolved in concentration of 10 wt.% To 30 wt%. However, complete dissolution is difficult and requires about 120 ~ 140 ^oC heating at dissolution, resulting in a 40% reduction in degree of polymerization of cellulose. This solution forms a transparent gel that reversibly melts at 80 °C.

1.2.4. NMMO/H_2O system

NMMO was invented in 1939, but it began to be studied as a solvent for cellulose since 1970s. The anhydrous NMMO is a good cellulose solvent, but it has a melting temperature of 172 ºC or more, which leads to severe pyrolysis of cellulose molecules. Therefore, it is currently industrialized to form cellulose after dissolution using hydrated NMMO having a low melting temperature. In the case of hydrated NMMO, there are two crystal structures, NMMO and water bonded in the same ratio, and two molecules of NMMO combined with five molecules of water. The melting temperatures are 72 ºC and 39 ºC, respectively.

The N-O group of NMMO is capable of two hydrogen bonds to dissolve the cellulose. However, when more than 1.5 molecules are hydrated in NMMO, the dissolving power to cellulose decreases sharply. When two or more molecules are hydrated, NMMO binds preferentially with water and can not dissolve cellulose. It is known that an anisotropic cellulose solution can be easily formed when less than one molecule of water is hydrated in one molecule of NMMO. Although the fundamental understanding for the formation of the liquid crystalline phase of the cellulosic material is still unclear, it might ascribe to the reduction of the number of molecular chains

arranged by NMMO and the decrease of the interchain frictional force due to the high energy state of the flexible chain form by the steric hindrance.

NMMO is currently the only industrially used in the regenerated cellulose industry because of its ease of dissolution process. The recovery rate of NMMO is 99.9%, which is considered to be an eco-friendly method compared to other solvents. Kulpinski et al. tried to electrospin with cellulose/NMMO/H_2O solution and produced cellulose fibers of several micrometer unit.[13] It has been reported that high-efficiency cellulose fibers can be produced by this method. However, despite the fact that NMMO is an effective solvent for cellulose, a high-efficiency solvent system is still required because of the decrease of polymerization degree and the oxidation of cellulose during the dissolution process.

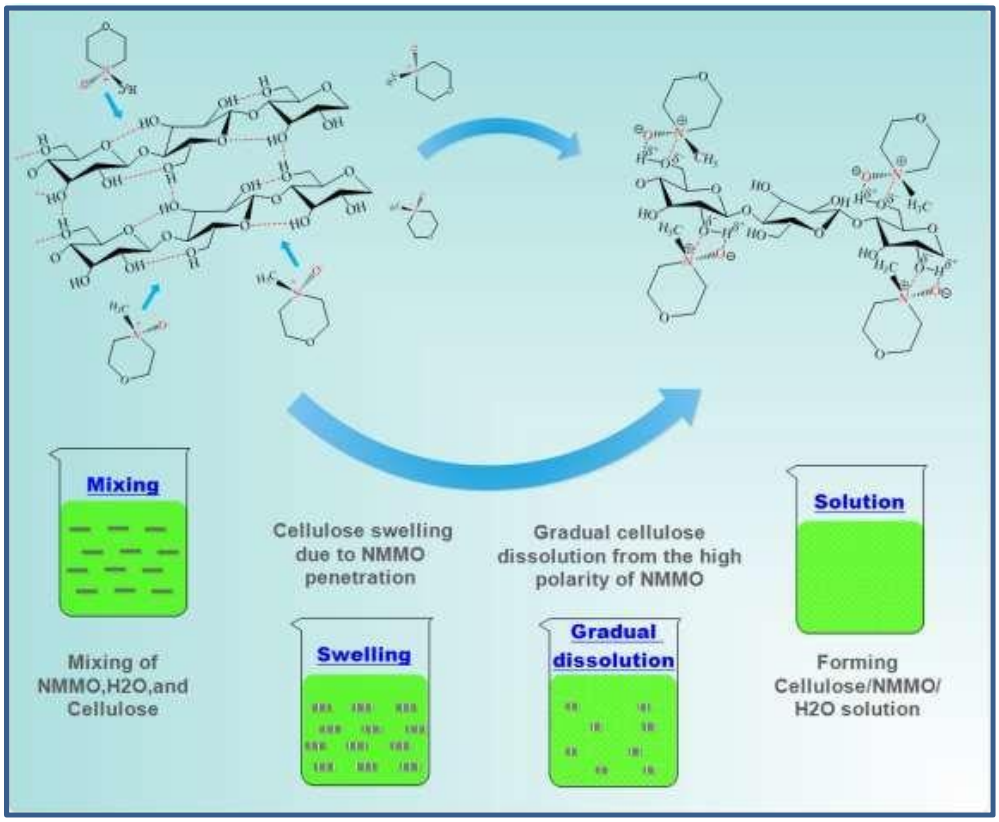

Figure 1-3. Dissolution mechanism of NMMO/H_2O system for cellulose[14]

1.2.5. Ionic liquid system

Ionic liquids are one of the liquid salt classes and exist as liquids at relatively low temperatures (<100 ºC). The polarity and non-polarity solubility of ionic liquids play a major role in many chemical processes, and the low vapor pressure, high thermal stability, good electrochemical properties, low melting point, and high regeneration yield of the ionic liquid itself. As a result, it has emerged as a next-generation clean solvent. Furthermore, one of the characteristics of ionic liquids is that it can change the chemical structure of anions and cations in ionic liquids. In particular, these ionic liquids have received much attention for use in carbohydrate and enzyme processes.

Cellulosic dissolution using ionic liquids was first attempted in 1934. Graenacher and his colleagues found that partial dissolution of cellulose was possible when N-ethylpyridinium chloride and cellulose were stirred in nitrogen gas.[15] In 2002, Rogers and colleagues succeeded in dissolving cellulose by using 1-allyl-3-methylimidazolium chloride and 1-methyl-3-methylimidazolium chloride.[8] The solubility of the ionic liquid has been reported to depend on the strength of the basicity of the anion and the hydrogen bonding strength with the cellulose hydroxyl group. Solubility in cellulose varies depending on the structure of the ionic liquid and is summarized in Table 1-1.

Cellulose dissolved in an ionic liquid is generally solidified in a polar solvent such as water or ethanol. The regenerated cellulose has a different rate of depolymerization depending on the basicity of the anion and is being studied as a technology for hydrolyzing cellulose and producing biofuel.

Table 1-1. Soubility of 3% cellulose in ionic liquids[15]

Ionic liquids	Solubility
1-buthyl-3-methylimidazolium chloride	+
1-allyl-3-methylimidazolium chloride	+
1-allyl-3-bethylimidazolium chloride	+
1,3-diallylimidazolium chloride	+
1-buthyl-2,3-dimethylimidazolium chloride	Slow
1-allyl-3-proparhylimidazolium chloride	Reacts
1-buthyl-2,3-dimethylimidazolium thiocyanate	-
1-buthyl-3-methylimidazolium saccharinate	-
1-buthyl-3-methylimidazolium tosylate	-
1-buthyl-3-methylimidazolium bisulfate	-
1-allyl-3-methylimidazolium dicyanamide	-
1-allyl-3-buthylimidazolium dicyanamide	-
1-allyloxy-3-methylimidazolium chloride	-

1.3. Dissolution mechanism of ionic liquid

In the early study for the dissolution of cellulose using ionic liquids, a simple prediction was made that chloride (Cl) anion binds to cellulose hydroxyl proton and imidazolium cation binds cellulosic hydroxyl oxygen. In other words, the complex hydrogen bond between hydroxyl groups of cellulose was expected to be disturbed by the ionic liquid, but the grounds for it were poor. In order to elucidate the dissolution phenomena of cellulose in ionic liquid, molecular modeling, using ^{13}C NMR, ^{1}H NMR, and ^{35}C NMR, was investigated, resulting that it was confirmed decreasing relaxation rate of C-1 and C-4 carbons of imidazolium ring and Cl anion during dissolution (Figure 1-4).[16] It was concluded that the hydroxyl proton of the carbohydrate and the chloride anion of the ionic liquid had a hydrogen bond at a molar ratio of 1: 1. These results have helped to develop the optimal ionic liquid for cellulosic dissolution by supporting the initial prediction.

Meanwhile, several researchers tried to investigate the process of dissolving cellulose in ionic liquid through molecular modeling. Youngs and his colleague,[17] a research associate at Queen's University in England, attempted to calculate the optimal molar ratio of solvents using DL POLY software. It was found that the molar ratio of glucose to ionic liquid was 1: 4, that is, when the molar ratio between the OH group of glucose and the Cl anion of ionic liquid were at 5: 4, cellulose could be completely dissolved (Figure 1-4). These

molecular modeling results are different from previous experimental results. However, the results are reported to show the highest solubility in other molar ratios than 1: 1. Studies relating to the solubility of cellulose with the molar ratio are still ongoing.

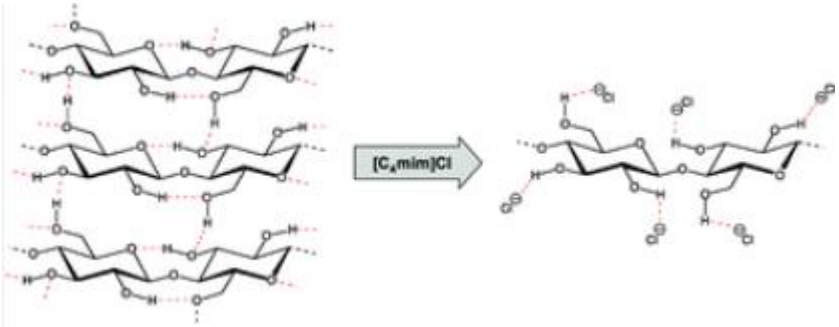

Figure 1-4. Schematic representation of cellulose dissolution in ionic liquid[16]

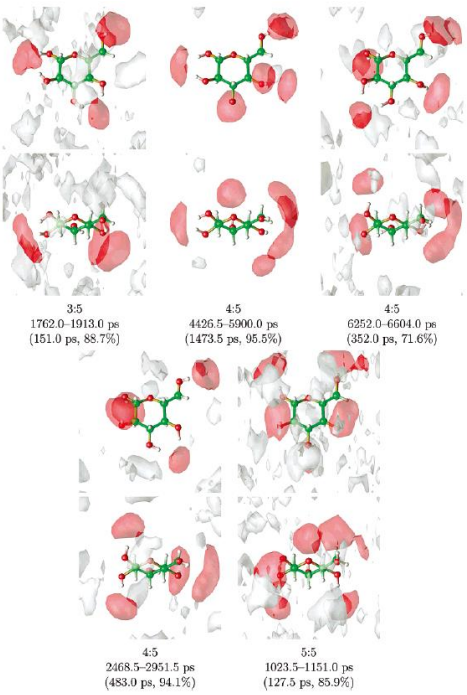

Figure 1-5. Spatial probability distributions of anions about the isolated glucose molecule, representing occurrences of the various possible chloride:OH ratios[17]

1.3.1. Effect of Anion for cellulose dissolution

Recent studies have shown that the higher hydrogen bonding basicity and dipolarity, the stronger the ability of anion to dissolve cellulose. Xu and colleagues found that the capacity of anions to accept hydrogen bonds is closely related to cellulose dissolution.[18] In the study, an ionic liquid composed of 1-butyl-3-methylimidazolium cations was used and they concluded that the hydrogen bonding capacity of anion and cellulose solubility were linearly related to each other; OAc^- > $HSCH_2COO^-$ > HCOO- > (C_6H_5) COO^- > $H_2NCH_2COO^-$ > $HOCH_2COO^-$ > $CH_3CHOHCOO^-$ > DCA^-.

Among the various ionic liquid series, 1-butyl-3-methylimidazolium dicyanamide is not soluble in cellulose, while 1-butyl-3-methylimidazolium acetate is the most efficient solvent for cellulose dissolution. This tendency does not seem to be related to the established pK_a value; HOAc: 4.75 > (C_6H_5) COOH: 4.18 > $CH_3CHOHCOOH$: 3.87 > $HOCH_2COOH$: 3.83> HCOOH: 3.72 > $HSCH_2COOH$: 3.684 > H_2NCH_2COOH: 2.35.[19-20] However, it is important that three of these anions have a hydrogen bond donor capable of interfering with the ability to accept hydrogen bonds to cellulose: $H_2NCH_2COO^-$, $HOCH_2COO^-$ and $CH_3CHOHCOO^-$.

1.3.2. Effect of cation for cellulose dissolution

The role of anions for cellulose dissolution is clear, and it is also confirmed that cations in ionic liquids also play a particular role in cellulose dissolution. It has been observed that ionic liquids containing imidazolium, pyridinium, ammonium and phosphonium cations can dissolve cellulose when paired with strong bases (hydrogen bond acceptors). The aromatic imidazolium and pyridinium cations are known to be the most efficient.

The high ability of pyridinium and imidazolium based ionic liquids to dissolve cellulose may be related to the aromatic properties of these cations and their ability to protect dissolved anionic/cellulose complexes. On the other hand, aromatic rings can be polarized,[21] whereas aromatic ILs have a lower relative intensities of interaction between cations and anions due to the decrease in the static charge. In the latter case, it is easier to form a hydrogen bond with cellulose. Studies including Graenche's patent show that cellulose can dissolve in the solution of these salts when basic solvents such as pyridine are present.[22]

As the alkyl chain length increases at the cation, the solubility power of the ionic liquid to the cellulose appears to decrease gradually. The low solubility of the cellulose in ionic liquid with long chain length cations is due to reduced effective anion concentration or hydrophobic interactions between the cations that screen for anion/cellulose bonds.[6]

1.4. Cellulose processing using ionic liquid

1.4.1. Non-toxic process

Green process products should be almost or completely free of toxicity to humans and the environment. Considering the ability of ionic liquids to process cellulose into many useful materials, there is little concern about the toxicity of any one of the cellulose itself or derivatives such as cellulose acetate or carboxymethylated cellulose. They are already useful and widely used in membranes, composites, separation media and medical applications.[23] They are considered non-toxic and non-harmful to our health or the environment. Therefore, it is important to necessary to understand the process characteristics to develop materials such as medical, food, and biosensors through cellulosic molding using ionic liquids.

1.4.2. Cellulose degradation for producing biofuel

The depletion of world petroleum supplies and environmental concerns related to the use of crude oil increases the demand for the development of environmentally friendly and non-petroleum-dependent energy sources.[24] The future alternative and sustainable energy source, lignocellulosic biomass, is capable of being converted into fermentable sugars, an intermediate that is ultimately converted to biofuels. However, current processes for converting lignocellulosic biomass to useful materials are inefficient. For example, the process of producing paper from wood, the most efficient conversion process, results in a utilization rate of biomass of 35% and the remainder of the lignocellulosic biomass is burned as waste.[25]

Cellulose of lignocellulosic biomass is shielded by lignin and hemicellulose matrix.[26] The process of overcoming and relaxing this structure is a key step in converting lignocellulosic biomass to biofuels and valuable chemicals. Dissolution and pretreatment of lignocellulose using ionic liquids as solvents have been extensively studied, offering a number of attractive features. In 2006, Fort et al. showed that 1-butyl-3-methylimidazolium chloride could be used to dissolve wood pulp.[27] 1-ehtyl-3-methylimidazolium acetate has been shown to be a better solvent for dissolving wood than 1-butyl-3-methylimidazolium chloride under the same working conditions and can also

be used to dissolve bagasse. Other sources of lignocellulosic biomass, such as bamboo, can also be dissolved in ionic liquids.

The pretreatment of lignocellulosic biomass has the advantage that the structure of cellulose is relaxed and the molecular weight can be lowered to increase the rate of the enzymatic hydrolysis at the same time. Many researchers have reported that cellulose recovered from ionic liquids shows amorphous structure and is favorable to convert to biofuels. However, there are some limitations to the treatment of lignocellulose with ionic liquids. The lignocellulose pretreatment process has only reported efficiency according to the ionic liquid, and systematic investigation in terms of kinetics is deficient. Moreover, uncontrolled hydrolysis of cellulose in chemical processes using cellulose has resulted in a reduction in physical performance, which limits the use of cellulose itself. Therefore, it is essential to understand the fundamental mechanism of hydrolyzed cellulose in ionic liquids and to control hydrolysis and crystalline structure.

1.5. Cellulose depolymerization

Recent experimental and theoretical studies have reported that ionic liquids would be decomposed via formation of a carbene intermediate and a proton. Heinze et al. investigated the interaction s of cations using simple cellulose model systems (cellooligomers, DP: 6 ~ 10).[28] On the basis of NMR studies, they suggested that 1-ethyl-3-methylimidazolium acetate forms a covalent bond between the C-1-carbone of the glucose unit and the C-2 of the imidazolium core (Figure 1-6). This suggestion was based on the fact that the C-1 carbon signal of the glucose unit disappeared after dissolution in ionic liquid. It has been shown that the carbenes derived from ionic liquid may also contribute to the degradation of the cellulose product, by the repeated elimination of formaldehyde units. Similar reactions have been experimentally observed by Ebner et al. using ^{13}C-labeling and fluorescence labeling experimental (Figure 1-7).[29] They verified formation of a covalent bonding between the C-2 carbon of 1-alkyl-3-methylimidazolium ILs and the reducing end of cellulose. Cramer et al. indicate that a small and more strongly interacting anion such as Cl^- can facilitate proton abstraction from the acidic C-2 position of the imidazolium, thus forming an intermediate carbene and an acid.[30] Rodriguez et al. demonstrate that elemental sulfur, which is abundant in raw biomass,[31] can also react with 1-ethyl-3-methylimidazolium acetate to

form a stable carbene and acetic acid.[32] Recently, Zhang et al. have shown that metal impurities may catalyze cellulose hydrolysis and subsequent sugar dehydration, even when present in IL at ppm levels.[33,34]

Clearly, the degradation of the product has to be avoided and to this end it seems straightforward to choose ILs, where the carbene formation is hindered. However, it is possible that the presence of the carbene is not only a side effect of the basicity of the strongly hydrogen bonding anions, and not only an undesirable source of degradation, but it is necessary for dissolving the the cellulose itself. The change of the cation results in the inaccessibility of the carbene, and considering the carbene formation as a necessity, it would, therefore, at least contribute to the drop in the solubility of the carbohydrate. Moreover, it has been shown that the formation of the carbene is diminished by the presence of water,[35,36] hence the precipitation effect by the addition of water can also be put into a different perspective.

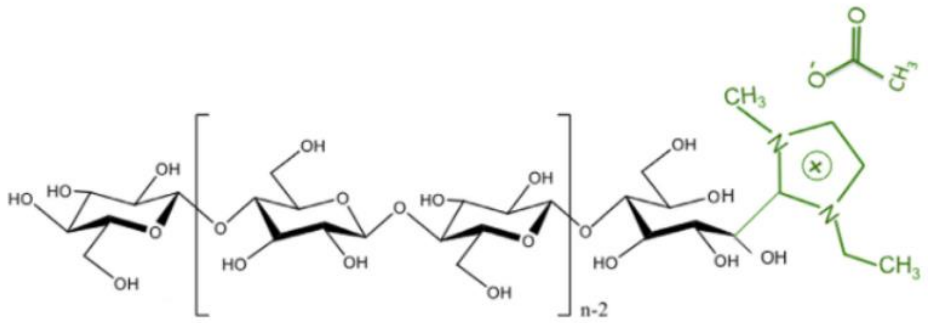

Figure 1-6. Schematic representation of cellulose and ionic liquid covalent binding[28]

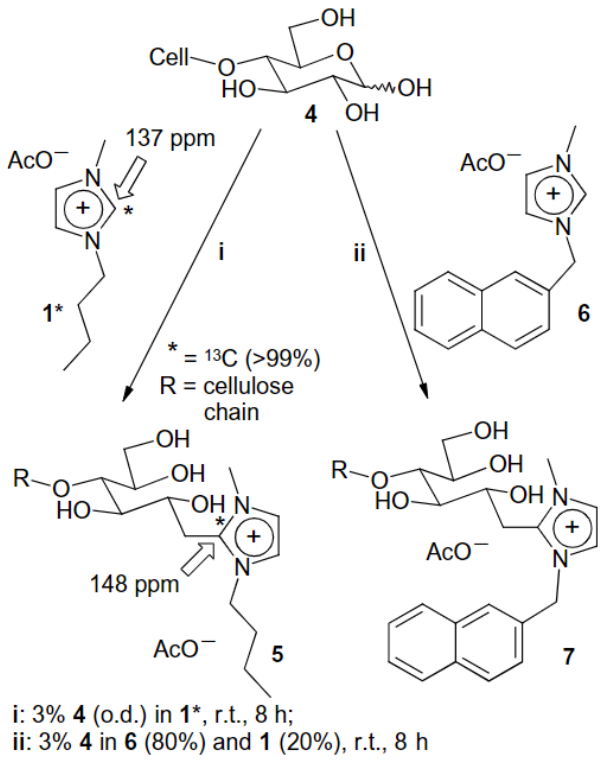

Figure 1-7. Reaction of ^{13}C- and fluorescent-labeled IL with cellulose[29]

1.6. Research objectives

The main objectives of this research is to develop a cellulosic material with uniform nanostructure by controlling the microstructure based on a fundamental understanding on the depolymerization of cellulose in ionic liquids. The depolymerization phenomenon of cellulose that has been overlooked in general cellulose process was analyzed in terms of rheological behavior, and the mobility of cellulose chains was investigated. Based on the database of molecular properties in ionic liquid, the control of cellulose microstructure was attempted to overcome the limitation for low crystallinity which is considered as one of problems to apply industrial field. In addition, a method to control morphology of cellulose reduced to nano-size level was investigated, and it was applied to food engineering process with evaluating performance.

In chapter 2, the effects of anions on cellulose depolymerization were investigated, and changes of the chain network and physical state of cellulose were observed. The changes in physical state were analyzed in terms of rheological properties with discussion on processibility of the cellulose/ionic liquid solution. Particularly, the constants for the viscosity average molecular weight under the ionic liquid were calculated.from the relationship between

the molar mass and the viscosity. In addition, fundamental database for producing the lyotropic solution of liquid crystalline cellulose have been established.

In chapter 3, a method for improving the crystallinity of cellulose recovered from an ionic liquid has been described. The mobility of the cellulose chains is described on the basis of the rheological properties with consideration for correlation with crystallinity. The cellulose controlled with molar mass showed high crystallinity similar to natural cellulose.

In chapter 4, the lignocellulose was pretreated with different kinds of ionic liquid, and the change of cellulose microstructure and the removal rate of non-cellulosic components such as lignin and hemicellulose were observed. Based on the database in chapters II and III, the changes of the network structure and composition of the cellulose were controlled according to the solubility and hydrolysis rate of the ionic liquid. In this chapter, the reference on selecting the optimal ionic liquid for lignocellulose pretreatment was provided according to types of lignocellulosic material.

In chapter 5, Studies on the nanoparticle formation of hydrolyzed cellulose in ionic liquid was carried out. The nanoparticles of cellulose were induced on the basis of the conformation of the cellulose and the intermolecular interaction between the molecules. In addition, nanoparticles with excellent

dispersibility were prepared using surface positive charge oriented from reduction of chain ends during cellulose hydrolysis.

In chapter 6, a cellulose NF membrane with amine groups on its surface was prepared and applied to the olive oil refining process. The control of the molar mass led to a change in the network structure of the cellulosic chains and consequently the pore size. Free fatty acid and chlorophyll, rancid ingredients of olive oil, were separated by surface amine groups and pore size, respectively. This study has resulted in reduction of process procedure and production cost of edible oil refining process.

References

1. Klemm, D.; Heublein, B.; Fink, H. P.; Bohn, A., Cellulose: fascinating biopolymer and sustainable raw material. *Angewandte Chemie International Edition* **2005,** *44* (22), 3358-3393.
2. Baillie, C., *Green composites: polymer composites and the environment*. CRC Press: 2005.
3. Vasita, R.; Katti, D. S., Nanofibers and their applications in tissue engineering. *International Journal of nanomedicine* **2006,** *1* (1), 15.
4. Liang, D.; Hsiao, B. S.; Chu, B., Functional electrospun nanofibrous scaffolds for biomedical applications. *Advanced drug delivery reviews* **2007,** *59* (14), 1392-1412.
5. Lu, P.; Ding, B., Applications of electrospun fibers. *Recent patents on nanotechnology* **2008,** *2* (3), 169-182.
6. Schiffman, J. D.; Schauer, C. L., A review: electrospinning of biopolymer nanofibers and their applications. *Polymer reviews* **2008,** *48* (2), 317-352.
7. Yoon, K.; Hsiao, B. S.; Chu, B., Functional nanofibers for environmental applications. *Journal of Materials Chemistry* **2008,** *18* (44), 5326-5334.
8. Swatloski, R. P.; Spear, S. K.; Holbrey, J. D.; Rogers, R. D., Dissolution of cellose with ionic liquids. *Journal of the American Chemical Society* **2002,** *124* (18), 4974-4975.

9. Dupont, A. L., Cellulose in lithium chloride/N,N-dimethylacetamide, optimisation of a dissolution method using paper substrates and stability of the solutions. *Polymer* **2003,** *44* (15), 4117-4126.
10. Dawsey, T. R.; McCormick, C. L., Lithium chloride/dimethylacetamide solvent for cellulose. A literature review. *Journal of Macromolecular Science - Reviews in Macromolecular Chemistry and Physics* **1990,** *C30* (3-4), 405-440.
11. Zhang, C.; Liu, R. G.; Xiang, J. F.; Kang, H. L.; Liu, Z. J.; Huang, Y., Dissolution Mechanism of Cellulose in N,N-Dimethylacetamide/Lithium Chloride: Revisiting through Molecular Interactions. *Journal of Physical Chemistry B* **2014,** *118* (31), 9507-9514.
12. Cuculo, J. A.; Smith, C. B.; Sangwatanaroj, U.; Stejskal, E. O.; Sankar, S. S., A study on the mechanism of dissolution of the cellulose/NH_3/NH_4SCN system. II. *Journal of Polymer Science Part A: Polymer Chemistry* **1994,** *32* (2), 241-247.
13. Kulpinski, P., Cellulose nanofibers prepared by the N-methylmorpholine-N-oxide method. *Journal of Applied Polymer Science* **2005,** *98* (4), 1855-1859.
14. Zhang, S.; Chen, C.; Duan, C.; Hu, H.; Li, H.; Li, J.; Liu, Y.; Ma, X.; Stavik, J.; Ni, Y., Regenerated cellulose by the lyocell process, a brief review of the process and properties. *BioResources* **2018,** *13* (2), 1-16.

15. Wang, H.; Gurau, G.; Rogers, R. D., Ionic liquid processing of cellulose. *Chemical Society Reviews* **2012,** *41* (4), 1519-1537.
16. Remsing, R. C.; Swatloski, R. P.; Rogers, R. D.; Moyna, G., Mechanism of cellulose dissolution in the ionic liquid 1-n-butyl-3-methylimidazolium chloride: A 13C and 35/37Cl NMR relaxation study on model systems. *Chemical Communications* **2006,** (12), 1271-1273.
17. Youngs, T. G. A.; Hardacre, C.; Holbrey, J. D., Glucose solvation by the ionic liquid 1,3-dimethylimidazolium chloride: A simulation study. *Journal of Physical Chemistry B* **2007,** *111* (49), 13765-13774.
18. Xu, A.; Wang, J.; Wang, H., Effects of anionic structure and lithium salts addition on the dissolution of cellulose in 1-butyl-3-methylimidazolium-based ionic liquid solvent systems. *Green Chemistry* **2010,** *12* (2), 268-275.
19. Kim, Y.; Kim, T.; Lee, W., Detection of corticosteroids in the presence of organic acids in a liquid chromatography eluent using the negative-ion mode of thermospray mass spectrometry. *Rapid Communications in Mass Spectrometry* **1997,** *11* (8), 863-868.
20. Namazian, M.; Halvani, S., Calculations of pK<inf>a</inf> values of carboxylic acids in aqueous solution using density functional theory. *Journal of Chemical Thermodynamics* **2006,** *38* (12), 1495-1502.
21. Ferreira, A. R.; Freire, M. G.; Ribeiro, J. C.; Lopes, F. M.; Crespo, J. G.;

Coutinho, J. A. P., An overview of the liquid-liquid equilibria of (ionic liquid + hydrocarbon) binary systems and their modeling by the conductor-like screening model for real solvents. *Industrial and Engineering Chemistry Research* **2011,** *50* (9), 5279-5294.

22. Heinze, T.; Dorn, S.; Schöbitz, M.; Liebert, T.; Köhler, S.; Meister, F., Interactions of ionic liquids with polysaccharides - 2: Cellulose. *Macromolecular Symposia* **2008,** *262* (1), 8-22.
23. Pinkert, A.; Marsh, K. N.; Pang, S.; Staiger, M. P., Ionic liquids and their interaction with cellulose. *Chemical Reviews* **2009,** *109* (12), 6712-6728.
24. van Spronsen, J.; Cardoso, M. A. T.; Witkamp, G. J.; de Jong, W.; Kroon, M. C., Separation and recovery of the constituents from lignocellulosic biomass by using ionic liquids and acetic acid as co-solvents for mild hydrolysis. *Chemical Engineering and Processing: Process Intensification* **2011,** *50* (2), 196-199.
25. Iskalieva, A.; Yimmou, B. M.; Gogate, P. R.; Horvath, M.; Horvath, P. G.; Csoka, L., Cavitation assisted delignification of wheat straw: A review. *Ultrasonics Sonochemistry* **2012,** *19* (5), 984-993.
26. Brodeur, G.; Yau, E.; Badal, K.; Collier, J.; Ramachandran, K. B.; Ramakrishnan, S., Chemical and physicochemical pretreatment of lignocellulosic biomass: A review. *Enzyme Research* **2011,** *2011* (1).
27. Fort, D. A.; Remsing, R. C.; Swatloski, R. P.; Moyna, P.; Moyna, G.;

Rogers, R. D., Can ionic liquids dissolve wood? Processing and analysis of lignocellulosic materials with 1-n-butyl-3-methylimidazolium chloride. *Green Chemistry* **2007,** *9* (1), 63-69.

28. Heinze, T.; Dorn, S.; Schoebitz, M.; Liebert, T.; Koehler, S.; Meister, F. Interactions of ionic liquids with polysaccharides–2: Cellulose*Macromol. Symp*. **2008**, *262*, 8-22.
29. Ebner, G.; Schiehser, S.; Potthast, A.; Rosenau, T. Side reaction of cellulose with common 1-alkyl-3-methylimidazolium-based ionic liquids*Tetrahedron Letters* **2008**, *49*, 7322-7324.
30. Cremer, T.; Kolbeck, C.; Lovelock, K. R. J.; Paape, N.; Wolfel, R.; Schulz, P. S.; Wasserscheid, P.; Weber, H.; Thar, J.; Kirchner, B.; Maier, F.; Steinrück, H.-P. Towards a Molecular Understanding of Cation–Anion Interactions—Probing the Electronic Structure of Imidazolium Ionic Liquids by NMR Spectroscopy, X-ray Photoelectron Spectroscopy and Theoretical Calculations*Chem. Eur. J.* **2010**, *16*, 9018-9033.
31. Monti, A.; Di Virgilio, N.; Venturi, G., Mineral composition and ash content of six major energy crops. *Biomass and Bioenergy* **2008**, *32* (3), 216-223.
32. Rodríguez, H.; Gurau, G.; Holbrey, J. D.; Rogers, R. D., Reaction of elemental chalcogens with imidazolium acetates to yield imidazole-2-chalcogenones: direct evidence for ionic liquids as proto-carbenes.

Chemical Communications **2011**, *47* (11), 3222-3224.

33. Zhao, H.; Holladay, J. E.; Brown, H.; Zhang, Z. C., Metal chlorides in ionic liquid solvents convert sugars to 5-hydroxymethylfurfural. *Science* **2007**, *316* (5831), 1597-1600.
34. Zhao, H.; Brown, H. M.; Holladay, J. E.; Zhang, Z. C., Prominent roles of impurities in ionic liquid for catalytic conversion of carbohydrates. *Topics in Catalysis* **2012**, *55* (1-2), 33-37.
35. Gurau, G.; Rodríguez, H.; Kelley, S. P.; Janiczek, P.; Kalb, R. S.; Rogers, R. D., Demonstration of chemisorption of carbon dioxide in 1, 3-dialkylimidazolium acetate ionic liquids. *Angewandte Chemie International Edition* **2011**, *50* (50), 12024-12026.
36. Brehm, M.; Weber, H.; Pensado, A. S.; Stark, A.; Kirchner, B., Proton transfer and polarity changes in ionic liquid–water mixtures: a perspective on hydrogen bonds from ab initio molecular dynamics at the example of 1-ethyl-3-methylimidazolium acetate–water mixtures—Part 1. *Physical Chemistry Chemical Physics* **2012**, *14* (15), 5030-5044.

CHAPTER 2

Hydrolysis of cellulose in ionic liquid: dependence of dissolution time on rheological properties and phase transition

2.1. Introduction

Dissolution of cellulose is fundamental importance for its processing and chemical derivatization. To design or improve a dissolution process, it is critical to understand the impact of ionic liquids (ILs) on the properties of cellulose and its solutions. Of particular importance is our understanding of the rheological behavior of cellulose in ILs. Rheological behaviors of polymer solutions play a significant role in processes for fibers, films, and nonwoven materials. Most studies on the rheological properties of cellulose/ IL solutions have focused on the influences of sources, concentrations and temperature on the rheological behavior of cellulose solutions.[1-2] Although the linear viscoelastic properties were comprehensively investigated for the cellulose/ ILs, there is few study on the influence of dissolution conditions on the changes of molecular properties and structure, such as molar mass and distribution. Recently, it has been reported that cellulose dissolved in some ionic liquids was fairly depolymerized along dissolution time.[3] It is expected

that there is some degree of molar mass reduction during dissolution process, which strongly influences on rheological properties. In addition, a more complete understanding of the interactions and the possibility of reactions occurring between cellulose and ILs requires further investigation. For example, the possibility of depolymerization of cellulose by some ILs was reported either theoretically or experimentally.

In a recent study on cellulose depolymerziation in ILs, Rodríguez, Gurau, Holbrey, and Rogers[4] showed experimentally that cellulose was significantly depolymerized by alkylmethylimidazolium-based IL during dissolution. However, thestudy did not reveal the cause or the mechanism for experimental results. Du and Qian[5] took attention on the formations of carbene and proton by ionic interaction between anion andcation. In the study, the free energy of carbene formation from different types of ILs was calculated using quantum mechanical calculation. They claimed that the resulted proton and the car-bene intermediate can hydrolyze the cellulose during dissolution. Similar reaction has been experimentally observed by Ebner et al.[6] using alkylimidazolium-based ILs. The theoretical approach was re-examined experimentally by Gazit and Katz.[3] Using various types of ILs and cellulose sources, they demonstrated the presence of free proton in cellulose/IL solution

In this chapter, cellulose-carbene reaction during IL-catalyzed depolymerization was investigate in typical condition for cellulose dissolution

and processing. The conformational change of the cel-lulose by the reaction was studied using reheological approach. Base titration and FT-IR were applied to reveal the presence of carbene and the difference in depolymerization behaviors of two ILs;1-butyl-3-methylimidazolium chloride ([C_4C_1Im][Cl]) and 1-butyl-3-methylimidazolium acetate ([C_4C_1Im][OAc]). The study found that the types of anion in ILs gave significant effect on the acidityand the depolymerization kinetics of the cellulose. Interpretation the relaxation behavior and the mobility was provided in terms of the molar mass and the chemical structure of the cellulose.

Based on depolymerization results, the molar mass dependence on viscoelasticity was investigated using the time-temperature superposition. The relaxation behaviors of the solutions for different molar mass were interpreted using the generalized Maxwell model. Mark-Houwink-Sakurada exponents and observation of phase transition behavior were employed to assess the relationship between the molar mass and the rheological properties, and the conformation of the dissolved cellulose. An understanding of the relationship between depolymerization and rheological properties would provide important information to help industries optimally the use cellulose-ionic liquid processing.

2.2. Experimental

2.2.1. Materials

Cellulose from poplar was kindly provided by Hyosung Co. (Korea). Its molar mass and composition were determined by GPC and composition analysis. Cellulose was dried overnight at 60 °C in a vacuum oven before use. 1-butyl-3-methylimidazolium chloride ([C_4C_1Im][Cl]), 1-butyl-3-methylimidazolium acetate ([C_4C_1Im][OAc]) and N,N-dimethylacetamide (DMAc, >99%) were purchased from BASF. Cellulose/IL was mixed in a sealed reaction vessel and stirred at 85 °C for 24–240 h. The cellulose concentration used in this study was fixed at 7 wt%.

2.2.2. Viscoelasticity measurements

Rheological measurements were performed on a stress-controlled rheometer (RS-1, ThermoFisher Scientific, Germany) equipped with 35 mm parallel plate geometry. Steady state viscosity measurements were carried out at 30 °C within a shear rate range of 10^{-3} – 10^{2} s^{-1}. Dynamic viscoelasticity was measured in a temperature range of 30 – 110 °C. The range of the oscillatory frequency was 10^{-2}–10^{2} Hz at each temperature. The data were reduced to the reference temperature (70 °C) data using time-temperature superposition principle. 19 The open edge of the specimen sandwiched between the plates

were covered with a thin layer of silicone oil (Shin-Etsu Chemical Co.) to prevent water uptake by the sample.

The intrinsic viscosity was determined from the viscosities of dilute cellulose/[C_4C_1Im][Cl] solutions calculated using Eqs. (1) and (2) proposed by Huggins and Kraemer.[7]

$$\frac{\eta_{sp}}{c} = [\eta] + K_h[\eta]^2 c \qquad (1)$$

$$\frac{ln\eta_r}{c} = [\eta] - K_k[\eta]^2 c \qquad (2)$$

where K_h is the Huggins coefficient, K_k is the Kraemer coefficient, $\eta_r = \eta_0/\eta_s$ (η_0 = zero shear rate viscosity; η_s = solvent viscosity) is the relative viscosity. The plots of η_{sp}/c and ln η_r/c versus c gave two straight lines with an identical intercept with y-axis (c = 0). The intercept corresponds to the intrinsic viscosity, [η]. The graphically determined intrinsic viscosities are summarized in Table 2-2.

2.2.3. Molar mass measurement

The prepared solution was poured into deionized water at room temperature, for cellulose precipitation. The precipitate was washed several times with deionized water until all residual ionic liquid was removed. The precipitated cellulose samples were dried in a vacuum oven for 1 day. For size-exclusion chromatography, the precipitated cellulose was dissolved in 9% LiCl/DMAc using the method reported by McCormick et al.[8] This dissolution method involved the following solvent exchange process. First, each cellulose sample was suspended in deionized water for 24 h. After filtration, the sample was immersed in anhydrous methanol for 30 min and filtered again. This process was repeated for three times. After solvent exchange with methanol, the same process was repeated for five times with DMAc. These solvent exchanges were carried out at room temperature. The cellulose samples were dissolved in 9 wt% LiCl/DMAc after being completely dried in a vacuum below 60 °C. GPC was performed on a YL9100 (Young Lin Instruments, Republic of Korea), equipped with a refractive index concentration detector (RI), and two angle light scattering detectors at 90° and 45°. A mobile phase consisting of 0.5 wt% LiCl in DMAc was used at a flow rate of 1 mL min^{-1}. The temperature was set at 40 °C. Light scattering (LS) constants were calibrated using standard polysaccharides with molar masses of 34.4, 19.4, 10.7, 4.7, 3.3 and 1.1 × 10^4 g mol^{-1}. The injection volume was 100 μL, and the run time was

30 min. The refractive index increment constant, dn/dc, representing cellulose in 9 wt% LiCl/DMAc was 0.055 $cm^3 \cdot g^{-1}$, based on a value reported in the literature. 23

2.2.4. Reducing ends measurement

In order to determine the degree of cellulose depolymerization, the number of cellulose reducing ends was measured via a colorimetric assay using 2,2'-bicinchoninate (BCA). The assay solutions were prepared by mixing two solutions. For assay solution A, Na_2CO_3 (5.4230 g), $NaHCO_3$ (2.4198 g), and bicinchoninic acid disodium salt hydrate (Sigma-Aldrich, >98%, 0.1944 g) were dissolved in milli-Q-purified water, and the volume of solution was adjusted to 100 mL. In assay solution B, $CuSO_4 \cdot 5H_2O$ (Sigma-Aldrich, >98%, 0.1242 g), and L-serine (Sigma-Aldrich, 0.1260 g) were dissolved in milli-Q-purified water, and the volume was adjusted to 100 mL. BCA reagent solution was prepared by combining solutions A and B in a 1:1 v/v ratio just prior to use. The BCA reagent solution was added to an aqueous slurry of cellulose solution at 80 °C for 1 h. Assay tubes were quenched in an ice bath and the absorbance at 560 nm was recorded using an Optizen 3220UV UV/Vis spectrophotometer (Mecasys).

The samples were subjected to FT-IR spectroscopy (Nicolet iS 5, ThermoFisher Scientific, Germany) with diamond attenuated total reflectance attachment. Scanning was conducted from 4000 to 650 cm^{-1} with 64 repetitious scans averaged for each spectrum. Resolution was 4 cm^{-1} and interval scanning was 2 cm^{-1}.

2.2.5. Optical microscope observation

The phase transition of cellulose/IL solutions with different molar masses and concentrations was observed using optical micrographs taken by BX41 Olympus polarized optical microscope. 1-methylimidazole (5 wt%) was added to prevent further hydrolysis during dissolution. 18 A 530 nm sensitive tint plate (U-TP530, Olympus) was used as a test plate compensator, which resulted in a magenta background for the micrographs.

2.2.6. Solution conductivity

The conductivity and the pH conductivity values were measured at 298 K using Microprocessor pH meter (pH-290L, iSTEK instruments, Republic of Korea) equipped with a conductivity electrode. The calibration of the pH meter was carried out with two buffers (pH values of 4.00 and 7.00). Approximately 1 g of cellulose/IL solution was diluted in 10 mL of deionized water for pH determination and acetonitrile for conductivity measurement. Dilution of IL in acetonitrile is not expected to influence conductivity results due to its virtually negligible conductivity comparing with IL.

2.3. Results and Discussion

2.3.1. Change of molar mass of cellulose dissolved in ionic liquids for different dissolution time

Figure 2-1 shows the calculated molar mass distribution of cellulose with various dissolution times. The molar mass distribution was fit to a Zimm-Schultz (Z-S) distribution[9] using Eq. (3). The solid lines represent the fits to the Z-S distribution. The parameters "*a*" and "*b*" in the Z-S distribution are related to the weight- and number-average molar masses according to Eq. (4) and (5).

$$\mathrm{w}(P_i) = \frac{a^{b+1}}{b!} M_i^b \exp(-aM_i) \quad (3)$$

$$a = \frac{1}{M_w - M_n} \quad (4)$$

$$b = \frac{M_w}{M_w - M_n} \quad (5)$$

The number-average (M_n) and weight-average (M_W) molar masses were calculated using Eq. (4) and (5), respectively, and summarized in Table 2-1. The polydispersity index, *Q,* is given by Eq. (6).

$$Q = \frac{M_W}{M_n} \quad (6)$$

The GPC curves of cellulose dissolved in [C_4C_1Im][Cl] shifted to lower molar masses with an increase in dissolution time. The shift to lower molar mass without curve splitting indicates that cellulose was homogeneously depolymerized during dissolution. The depolymerization in [C_4C_1Im][Cl] is consequently accompanied by an approximate decrease in average molar mass of one order magnitude. This trend is also observed for cellulose dissolution using [C_4C_1Im][OAc]. The cellulose depolymerization in ILs can be attributed to acid hydrolysis in IL. According to the previous study,[10] anions are able to form ionic bonding with proton in imidazolium cation. This reversible reaction accelerates dissociation of imidazolium and proton, which results in formation of H_3O^+ in water. Due to its strong hydrophilicity, there remain the limiting amount of water needed for cellulose hydrolysis in IL, which is calculated below 40 ppm in case of both ILs. On the other hand, the depolymerization of cellulose less occurred in [C_4C_1Im][OAc] than [C_4C_1Im][Cl]. This trend in greater rate of decreasing molar mass upon anion type of the IL used for cellulose dissolution is consistent with Rodríguez et al., [4] who remarkable differences of depolymerization was measured between [C_4C_1Im][Cl] and 1-ethyl-3-methylimidaozolium acetate.

In order to quantitatively compare the depolymerization kinetics, the plot of molar mass as a junction of time can be fitted by the zeroth order rate law, as

shown in Figure 2-2, and the depolymerization rate was calculated. From these data, [C_4C_1Im][Cl] exhibits a higher depolymerization rate. The depolymerization rate measured in [C_4C_1Im][Cl] was approximately 2 -fold faster than in [C_4C_1Im][OAc] corresponding to the molar mass ratio between samples dissolved in [C_4C_1Im][Cl] and [C_4C_1Im][OAc] for 240 h is 1:2. This data demonstrates that the anion type of ILs has a significant role in controlling the depolymerization rate. The capability for acid formation between two ILs might be different as proposed from Du and Qian.[5] To test this difference, we added 5 wt% N-methylimidazole, which is alkaline reagent for synthesis of dialkylimidazolium ILs,[11-12] to the cellulose/IL solutions sustained for different time. Figure 2-1 shows almost no change to molar mass of cellulose in [C_4C_1Im][Cl] added with N-methylimidazole. The prevention for the reduced molar mass may be ascribed to N-methylimidazole acting as a proton acceptor in acid-catalyzed hydrolysis reaction. However, the cellulose dissolved in [C_4C_1Im][OAc] was still depolymerized despite the addition of N-methylimidazole. It means that more proton is produced in [C_4C_1Im][OAc], indicating a lack of N-methylimidazole to prevent the cellulose depolymerization.

As shown in Figure 2-1, the molar mass distribution shifted toward lower molar mass as well as became broader as the dissolution time increased. The changes of the distributions were confirmed using van Gurp and Palmen plot

(i.e. vGP plot),[13] as illustrated in Figure 2-3. The loss tangent was plotted against the dynamic modulus. As the dissolution time increased, the minimum value of the phase angle increased and the curves became wider. As reported previously,[13] the shift of the vertical position and the broadness of the minimum phase angle were correlated to the changes of the molar mass and the polydispersity, respectively.

Table 2-1. Molar mass of cellulose in ILs for varying dissolution times

t (h)	Cellulose in $[C_4C_1Im][Cl]$		Cellulose in $[C_4C_1Im][OAc]$	
	M_n (10^3 g/mol)	M_w (10^3 g/mol)	M_n (10^3 g/mol)	M_w (10^3 g/mol)
Raw	250	283	250	283
24	195	252	249	279
48	161	210	233	271
72	123	165	214	255
96	106	145	193	238
120	89	128	167	209
144	73	108	164	192
168	61	92	149	180
192	42	71	140	171
216	35	63	131	165
240	29	55	119	146

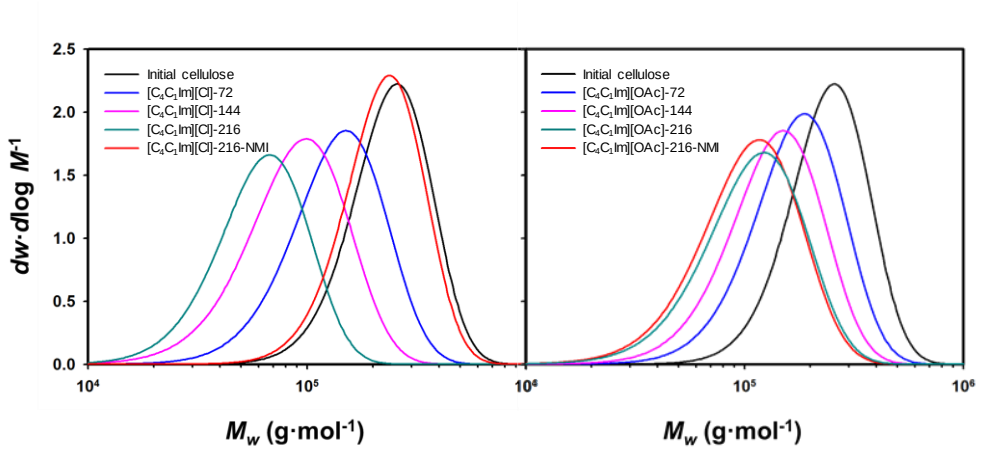

Figure 2-1. GPC curves of cellulose dissolved in [C_4C_1Im][Cl], [C_4C_1Im][OAc] and ILs added with 5% N-methylimidazole varing different dissolution time.

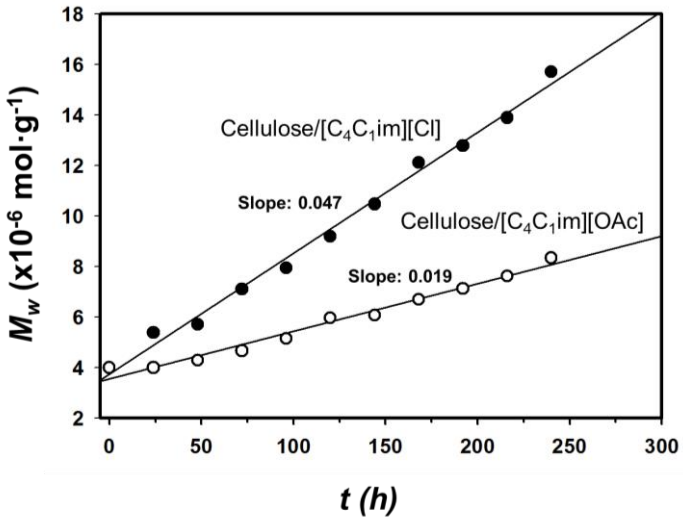

Figure 2-2. Change in reciprocal molar mass of cellulose dissolved in [C_4C_1Im][Cl] and [C_4C_1Im][OAc]

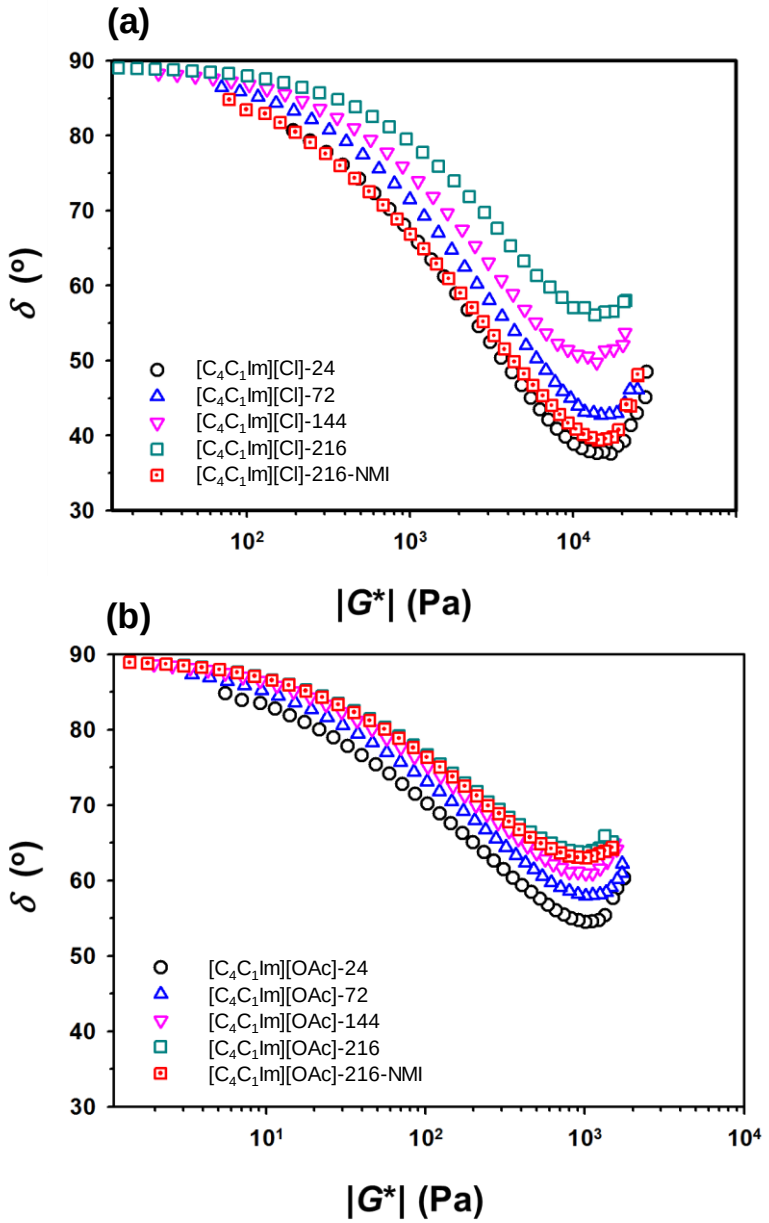

Figure 2-3. van Gurp-Palmen plots of cellulose in (a) $[C_4C_1Im][Cl]$ and (b) $[C_4C_1Im][OAc]$ solutions with different dissolution times

2.3.2. Formation of acidic condition during cellulose dissolution

It was found that ILs have different kinetics of depolymerization according to the types of anion. The data implicates the capability of acid formation and its concentration are changed according to the anion types of ILs. As studied previously,[3] the depolymerization was influenced mainly by the generated protons in the solution. In order to study the proton generation during dissolution, every solution was titrated using N-methylimidazole. During the titration, the conductivity and the pH value of the solutions were monitored (Figure 2-4). For the untitrated solutions, the conductivity became higher with increasing time because the long dissolution time allowed more chance for IL to generate protons. The higher formation rate of proton in $[C_4C_1Im][Cl]$ may act major role in extensively acidic depolymerization of cellulose. The trend in increasing conductivity upon the time is corresponded with pH values, which the acidity of each solution was reached up to approximately 3 and 5 of pH value for cellulose/$[C_4C_1Im][Cl]$ and $[C_4C_1Im][OAc]$ solutions, respectively.

The conductivity of the solutions consisting of $[C_4C_1Im][Cl]$ showed rapid drops upon introducing N-methylimidazole. The drop in conductivity continued until excess base was added to neutralize the acid, at which the conductivity was slightly increased. The neutralization point moved to higher base concentration as the dissolution time was increased. It demonstrates the

proton is continuously generated during the dissolution. It was also confirmed by the pH changes with titration (see the bottom Figure in Figure 2-4 (a)). In similar way, the conductivity of the $[C_4C_1Im][OAc]$ case was decreased with lower rate, and then increased. Interestingly, the neutralization points were significantly shifted to higher base concentration with increase of the dissolution time relative to $[C_4C_1Im][Cl]$. Although the conductivity of the $[C_4C_1Im][OAc]$ case was lower than the $[C_4C_1Im][Cl]$, more N-methylimidazole was consumed to be neutralized. Comparing to the $[C_4C_1Im][Cl]$ case, the pH change of the $[C_4C_1Im][OAc]$ case was negligible during titration after neutralization because more acidic products were formed in $[C_4C_1Im][OAc]$. This result was quantified in terms of the volume of N-methylimidazole for neutralization point versus the dissolution time as shown in Figure 2-4 (c). As shown in the Figure, large difference between the two solutions was observed. The neutralization for cellulose/$[C_4C_1Im][OAc]$ solution after 240 h required N-methylimidazole of 48,000 ppm while only 9,000 ppm was used for the cellulose/$[C_4C_1Im][Cl]$ solution. Strong conjugate base such as acetate anion can easily accept a proton from imidazolium cation and results in favorable formation of acid. On the contrast, weak conjugate base including chloride anion has less interaction between the anion and the proton in cation. In addition to the basicity, the size match of the cation and anions plays important role in the formation of stable ion pair. Collin et al.[14-

[16] reported that there was a greater chance to form an ion pair when the cation and anion have similar sizes. In that point of view, acetate anion has more chance to form acid comparing to chloride.

On the basis of the results, the formation of carbene intermediate produced by cation-anion pair was studied using FT-IR of the precipitated cellulose as shown in Figure 2-5 (a) and (b). The unexpected peak at 1562 cm^{-1} (C-N stretching vibration attributed from imidazole-type cation) appeared even after extensive wash for removal of the IL from the precipitated cellulose, which is the similar with previous work.[6, 17] The peak is considered as a result of carbene associated with the reducing end of cellulose. Theoretically, the dissociation of cation and anion in IL would result in carbene, highly reactive chemical intermediate. The carbene can further chemically combine to the reducing end of cellulose. For the precipitated cellulose from the $[C_4C_1Im][Cl]$ solution, the peak was getting larger as the dissolution time increased (Figure 2-5 (a)). However, the peak size was not remarkably increased for the $[C_4C_1Im][OAc]$ case. Based on the explanation above, chloride-based IL cleaves more effectively the glucosidic bonds of cellulose chain, resulting in more reducing ends. The more reducing ends gave more chance for carbene to combine with cellulose. The combination of carbene with reducing ends was also confirmed based on the relation between the number of the remained reducing end and the degree of splitting ($1/M_n$). In acid catalyzed hydrolysis

of cellulose, the reducing end is linearly increased with the degree of splitting if the reducing ends are not chemically changed.[18] Figure 2-5 (c), however, shows that the number of reducing ends was leveled off. The result indicates strongly that the reducing ends were combined with carbene at similar rate of its generation by depolymerization. It is an extra proof that the reducing ends generated by depolymerization was combined with carbene.

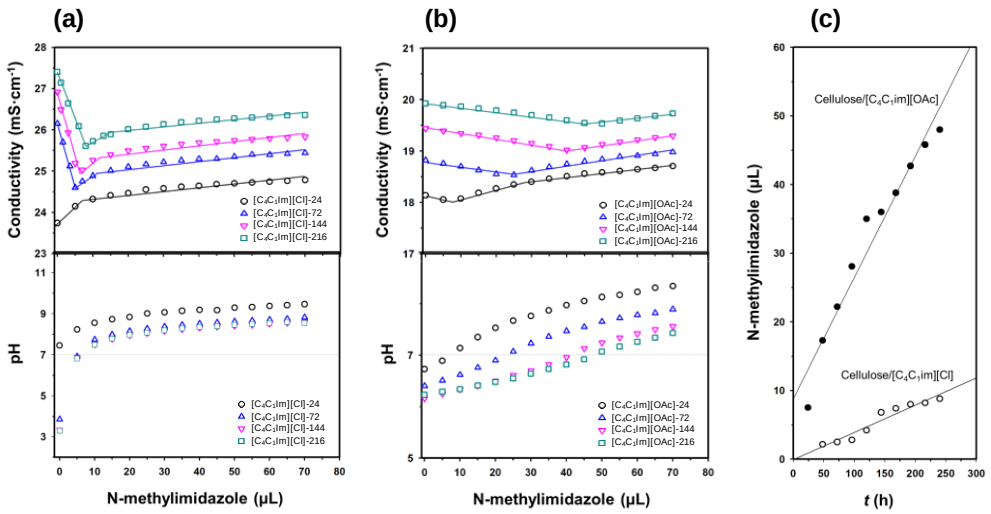

Figure 2-4. Conductivity and pH value of cellulose/IL solutions dissolved for different dissolution time as a function of volume of N-methylimidazole. (a) cellulose/[C_4C_1Im][Cl] solution, (b) cellulose/[C_4C_1Im][OAc] solution and (c) their neutralization point. To clearly show changing conductivity, these curves are shifted vertically by a factor B with the corresponding B value of 0, 0.5, 1 and 1.5, respectively.

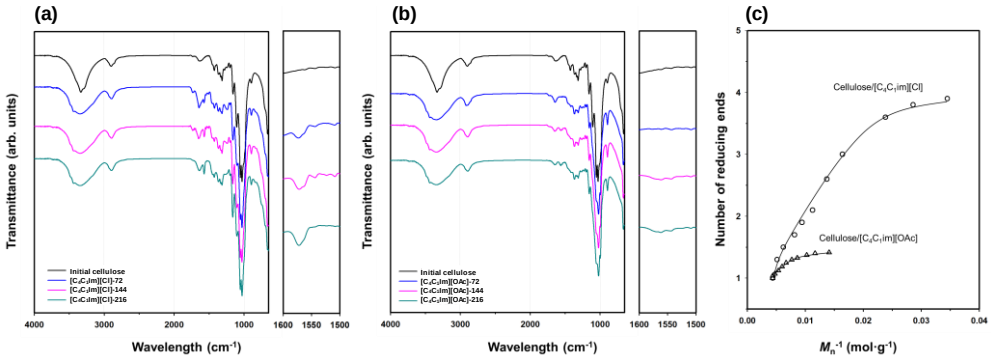

Figure 2-5. FT-IR spectra of cellulose precipitated from (a) $[C_4C_1Im][Cl]$ and (b) $[C_4C_1Im][OAc]$, and (c) their number of reducing ends as function of reciprocal number average molar mass.

2.3.3. Dynamic properties of cellulose in ionic liquid

As discussed previously in Section 2.3.2, cellulose in $[C_4C_1Im][Cl]$ exhibited higher depolymerization rates than one in $[C_4C_1Im][OAc]$. The rheological behaviors of cellulose in $[C_4C_1Im][Cl]$ dissolved at different times were observed to confirm the rapid change of cellulosic network structure and viscoelasticity by the dramatic decrease of the molar mass.

Figure 2-6 shows the master curves of 7 wt% cellulose/$[C_4C_1Im][Cl]$ solutions with various dissolution times, obtained by time-temperature superposition principle. All of the curves shifted upward by a factor B except for the curves at 144 h. Over the range of dissolution times (24–168 h), a plateau region between G' and G'' was observed when the relations of $G' \propto \omega^2$ and $G'' \propto \omega^1$ were held. Two cross-over points can be clearly seen, which is a typical behavior of entangled polymer solutions. The first cross-over corresponds to the macromolecular reptation, and the second crossover corresponds to entanglement relaxation. With increasing dissolution time, the first cross-over point shifts to a higher frequency, indicating the faster relaxation of the cellulose chains by low interaction (entanglement or hydrogen bonding) with its neighboring chains. For dissolution times above 192 h, the curve of G'' was larger than that of G' over the entire ω-region where the measurements were carried out. This behavior is usually observed for dilute solutions, for which

dynamic viscoelastic behavior is similar to that of the terminal region in the Rouse model. [19-21] Accordingly, the development of the network structure by entanglement was immature when the cellulose was dissolved for longer times.

The dependence of the viscoelastic behavior on temperature provides useful information on the qualitative aspects of the relaxation process in polymer chains. The dynamic moduli of cellulose/[C_4C_1Im][Cl] solutions were measured at a series of temperatures, taken at every 20 °C intervals from 30 to 110 °C. The time-temperature superposition principle was used to shift all the rheological data to a reference temperature of 70 °C. As shown in Figure 2-7 (a), the time–temperature superposition principle applied well to the viscoelastic curves of the cellulose/[C_4C_1Im][Cl] solutions. This result suggests that the relaxation mechanism does not change over the temperature range of 30–110 °C. The apparent activation energy for viscoelastic relaxation, ΔE_a, can be evaluated from the temperature dependence of the shift factor, a_T. The shift factor is defined as $\eta(T)T_{r\rho r}/(T_r)T_\rho$, where ρ is the density and the subscript r refers to properties of a reference state.[22] Since the change of density versus temperature is negligible, the definition of a_T can be simplified to $\eta(T)/(T_r)$. Near the glass transition temperature, T_g, the polymer flow is restricted to the free volume required to allow the necessary rotation of chain segments. Thus, the viscosity is described by the Williams-Landel-Ferry (WLF) equation shown in Eq. (7).

$$\log a_T = \frac{-C_1(T-T_r)}{C_2+(T-T_r)} \quad (7)$$

where C_1 and C_2 denote experimental constants and T_r is the reference temperature.

Then, activation energy at the reference temperature can be estimated from Eq. (8).

$$\Delta E_a(T = T_r) = R\frac{dlna_T}{d(1/T)}|_{T=T_r} = 2.303R(C_1/C_2)T_r^2 \quad (8)$$

The apparent activation energy of flow ΔE_a is plotted against the dissolution time as shown in Figure 2-7 (b). As the dissolution time increases, the activation energy was decreased and then leveled off when the time was longer than 196 h. As similar reason to the viscosity change, the decrease can be explained in terms of the reduction of the molecular size and its effect on flow. However, the molecular size did not contribute to the change of the activation energy further more when the size reached to a certain size, i.e. when the dissolution time exceeded 196 h.

The measured dynamic modulus data provided specific information about cellulose/[C_4C_1Im][Cl] solutions. The actual relaxation of a polymer chain has

a large spectrum of relaxation times, which can be described using the generalized Maxwell model represented in Eqs. (9) and (10).

$$G'(\omega) = \sum_{i=1}^{N} \frac{G_i(\omega\tau_i)^2}{[1+(\omega\tau_i)^2]} \quad (9)$$

$$G''(\omega) = \sum_{i=1}^{N} \frac{G_i(\omega\tau_i)}{[1+(\omega\tau_i)^2]} \quad (10)$$

where G_i and τ_i are the initial modulus and relaxation time corresponding to the *i*th Maxwell element in the Maxwell model.

The calculated G_i and τ_i allow the evaluation of overall viscoelastic characteristics of cellulose/[C_4C_1Im][Cl] solutions. These parameters are calculated using Eqs. (11), (12), and (13).

$$G_N^0 = \sum G_i \quad (11)$$

$$M_e = \frac{\rho RT}{G_N^0} \quad (12)$$

$$\bar{\tau} = \frac{\sum \tau_i^2 G_i}{\sum \tau_i G_i} \quad (13)$$

where G_N^0, M_e, ρ, R, T, and $\bar{\tau}$ are plateau modulus, entanglement molar mass, density, ideal gas constant, absolute temperature and mean relaxation time, respectively. The calculated values of $\bar{\tau}$, G_N^0, M_e and intrinsic viscosity,

zero-shear viscosity for cellulose/[C_4C_1Im][Cl] solutions with various dissolution times are listed in Table 2-2.

The solid lines in Figure 2-6 represent the curves calculated using generalized Maxwell model with an appropriate combination of G_i and τ_i values for the solutions. These curves, represented by Eqs. (9) and (10), are in good agreement with the experimental data. The well-fitted curves indicates the similarity and the universality in the shape of their viscoelastic curves.[20, 23] The storage modulus G_i shows a frequency-independent plateau over a certain frequency range, which is the plateau modulus G_N^0 of the solution. The estimated G_N^0 was insensitive to the molar mass, indicating that entangled molar mass was almost constant as calculated by Eq. (12) and shown in Table 2-2.

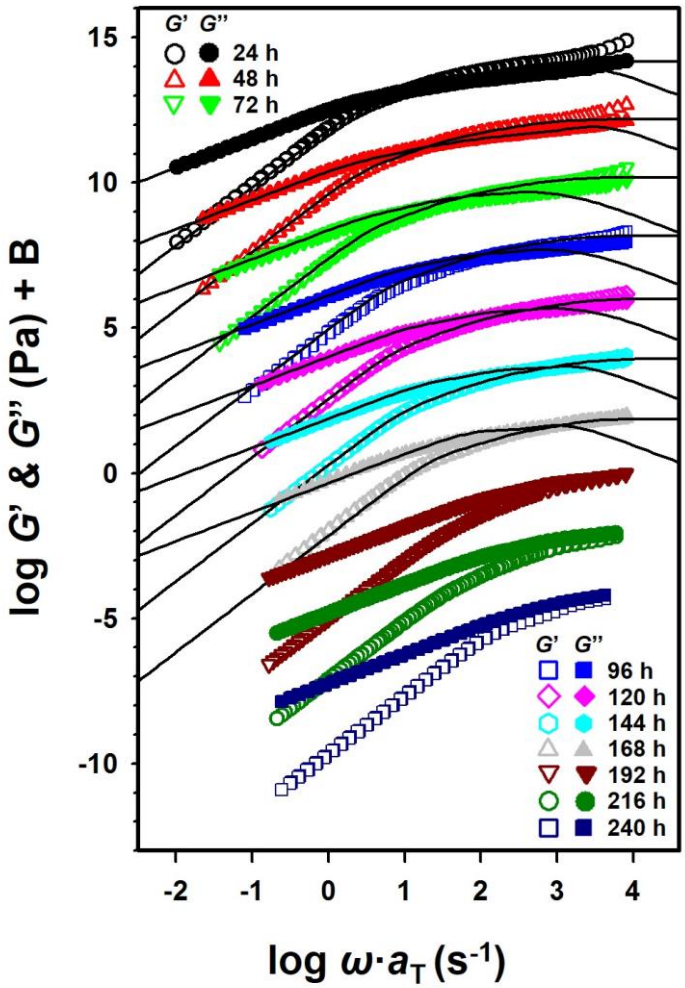

Figure 2-6. Dependence of dynamic storage modulus, G' (open symbols), and loss modulus, G" (filled symbols), on reduced angular frequency, ωa_T, for cellulose/[C_4C_1Im][Cl] solutions dissolved for different times. These curves are shifted vertically by a factor B except for the solution dissolved for 144 h. The solid lines represent the curves reproduced by calculations using a generalized Maxwell model.

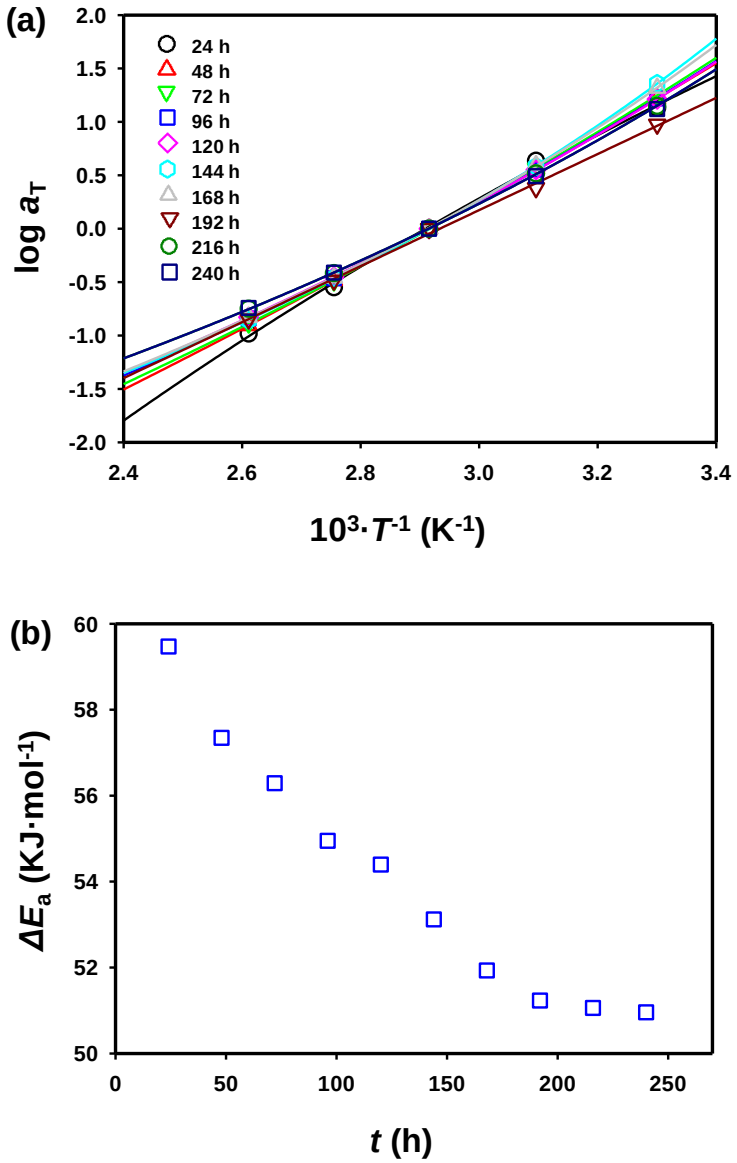

Figure 2-7. Relationship between (a) log a_T and $1/T$ and (b) activation energy, ΔE_a, and dissolution time, where a_T and T represent the horizontal shift factor and absolute temperature, respectively. The solid lines show the results of curve fitting using the WLF equation.

Table 2-2. Viscoelastic characteristics of cellulose in [C_4C_1Im][Cl]

t (h)	$\bar{\tau}$ (10^{-2} s)	G_N^0 (10^3 Pa)	M_e (10^3 g/mol)	$[\eta]$ (cm^3/g)	$\eta 0$ (10^2 Pa s)
24	27.75	21.04	8.98	228	22.72
48	16.74	21.01	9.00	225	11.01
72	10.65	20.98	9.02	219	5.20
96	6.46	21.23	8.91	179	2.93
120	4.93	20.93	9.04	171	1.92
144	3.82	20.88	9.06	157	0.87
168	2.48	20.14	9.39	152	0.56
192a	-	-	-	151	0.24
216a	-	-	-	121	0.21
240a	-	-	-	110	0.19

[a]the generalized Maxwell model cannot be adopted for these data

2.3.4. Correlation between molar mass and rheological behavior

Mark-Houwink-Sakurada (MHS) equation is efficient to describe molecular properties of a polymer, which is correlating the intrinsic viscosity and the molar mass. Figure 2-8 shows a double logarithmic plot of the calculated intrinsic viscosity against the molar mass for cellulose in $[C_4C_1Im][Cl]$ at 30 °C. The Figure contains the data published from other researchers.[1, 8, 24] From the experimental data, the parameters of the MHS equation (Eq. (14)) were obtained using Eq. (15)

$$[\eta] = KM_W^{\alpha} \qquad (14)$$

$$[\eta] = (0.64 \pm 0.3)M^{(0.47\pm0.06)}/cm^3\ g^{-1} \qquad (15)$$

Using Eq. (15), the parameters K and α for the cellulose samples were obtained. The exponent α and coefficient K was determined to be 0.47 and 0.64, respectively, suggesting that $[C_4C_1Im][Cl]$ may be a theta solvent for cellulose.[1] Compared to other results (cellulose/DMAc/LiCl solution), α in the study was much lower.[8] It indicates that the intermolecular interactions were significantly lower by an ionic liquid in the study. The inter-/intra-molecular hydrogen bonds should be broken because the chloride anions released from

the ionic liquid were associated with the backbone.

From the obtained intrinsic viscosity and molar mass, the radius of gyration R_g was estimated using the Flory approach for flexible polymer chains as shown in Eq. (16).[25]

$$R_g{}^2 = \frac{1}{6}\left[\frac{[\eta]}{\Phi}M\right]^{2/3} \qquad (16)$$

where, Φ is Flory constant $2.8 \times 10^{23}\ mol^{-1}$. The radius of gyration ranged from 11.3 to 25.1 nm for the molecules with molar mass from 55 to 283 kg mol^{-1} respectively. Figure 2-9 shows the change of the radius of gyration along the molar mass. Figure 2-9 also includes the data reported previously from other researchers.[1, 26-27] All the data showed good linear relationships. This relationship can be expressed on the assumption that $R_g = bN^{\upsilon}/\sqrt{6}$. An exponent of υ was calculated as 0.54, which suggests the conformation of the cellulose molecules in [C_4C_1Im][Cl] can be considered as a Gaussian chain in a theta solvent.

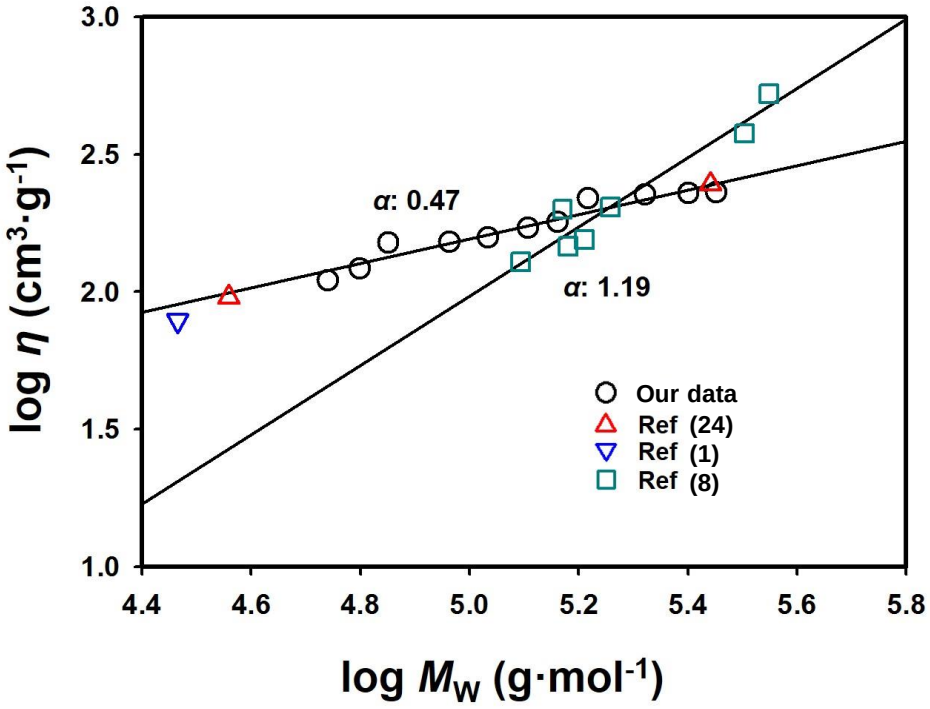

Figure 2-8. Dependence of intrinsic viscosity on the molar mass for cellulose/[C_4C_1Im][Cl] solutions at 30 °C

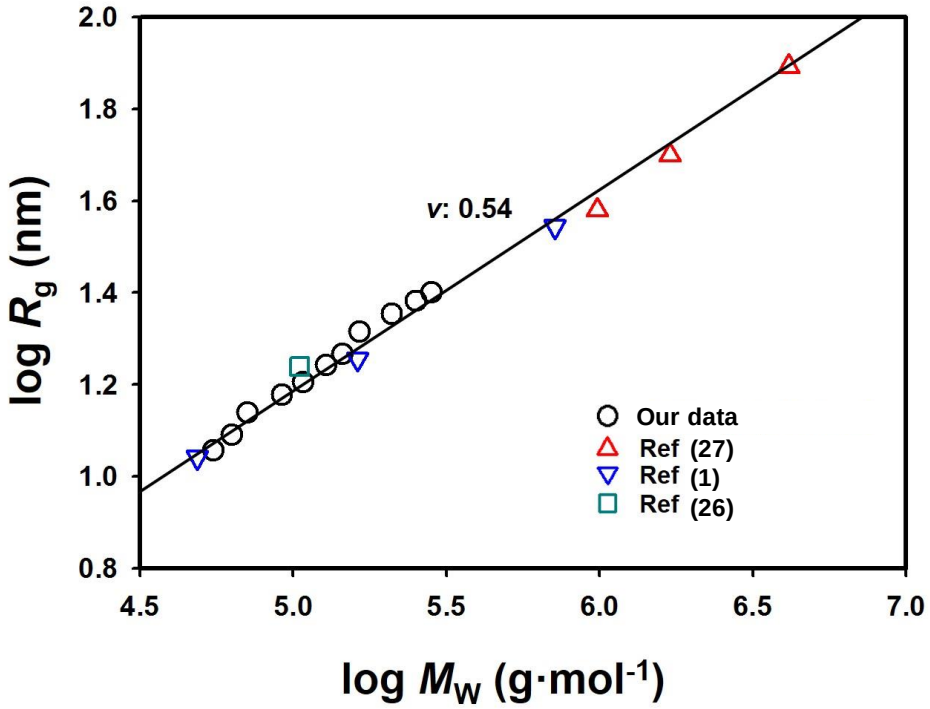

Figure 2-9. Dependence of the radius of gyration, R_g, on the molar mass for cellulose/$[C_4C_1Im][Cl]$ solutions at 30 °C

2.3.5. Phase transition behavior of cellulose/ionic liuquid solution

Cellulose solutions are, in principle, able to form cholesteric phase in suitable solvents in certain concentrations. It is also known that the formation of liquid crystalline phase strongly depends on molecular conformation and topological constraint. To further clarify the influence of different physical state, above and below critical molar mass, on the phase transition, the birefringence observation and the rheological behavior were compared. Figure 2-10 shows the polarized optical micrographs of the cellulose/[C_4C_1Im][Cl] solutions at 30 ºC. For 55 kg·mol^{-1} molar mass solution, the change of visible color and phase transition are clearly distinguished. Below 10 wt% concentration, the solution is completely isotropic, and then the anisotropic texture gradually became more obvious with further increasing concentration. At 13 wt% of concentration, fingerprint-like textures appeared of cholesteric phase. As the cellulose concentration further increased, apparent optical textures appeared. For 252 kg·mol^{-1} molar mass solution, overall tendency for change from isotropic to anisotropic phase is similar with high molar mass solution, but cholesteric phase could not be observed distinguishingly. The reason for the absence of fingerprint-like pattern and appearance of nonaligned cholesteric phase in the higher molar mass solutions may lie in their large domain size

which accelerate aggregation of liquid crystalline phase.

The distinguishable behavior for phase transition also can be observed in rheological behaviors as shown in Figure 2-11. For the solutions with low molar mass, the viscosities of low molar mass solutions was steeply increased up to maximum value at a concentration by 10 wt%, a slightly decreased by 14 wt%, and increased again. This trend means typical behavior for lyotropic liquid crystalline solutions.[28] Compared to the low molar mass solution, zero shear viscosity was exponentially increased with increasing concentration, suggesting sol-gel transition of cellulose/[C_4C_1Im][Cl] solution.[29] The different behavior of phase transition can be explained in terms of absence of inter-connected structure by reduction below critical molar mass. As shown in Figure 2-12, each anisotropic domain forms self-organization network chain by entanglement above the critical molar mass. The solution of united clusters makes gel state with drastic increase of viscosity. Below the critical molar mass, the cellulose chains can also have opportunities to form liquid crystalline domains but do not have inter-connection of each domain due to insufficient chain length for entanglement. As a result, the cellulose/[C_4C_1Im][Cl] solution passes through viscosity drop (cholesteric phase) between sol-gel transitions.

On the basis of this speculation, it would be possible to explain on the formation of cholesteric phase of cellulose above and below critical molar

mass. The quantitative analysis for characteristic time provides physical state of cellulose chain. This time constant τ is approximated as followed:

$$\tau = \frac{12\eta_0}{\pi^2 \upsilon k_B T} \tag{17}$$

Where υ, k_B and T are a number of molecules per unit volume, Boltzmann constant and the absolute temperature, respectively. Based on values of η_0 and τ obtained above, we estimate the υ values, above and below the critical molar mass, to be 4.85×10^{-6} mol $\cdot$ cm^{-3} and 5.39×10^{-6} mol $\cdot$ cm^{-3}, respectively. It implies that cellulose chains were more packed closely and the states change from entangled to unentangled region. The dense structure makes more chance to interact each chains, which may help to transit from isotropic state to cholesteric phase.

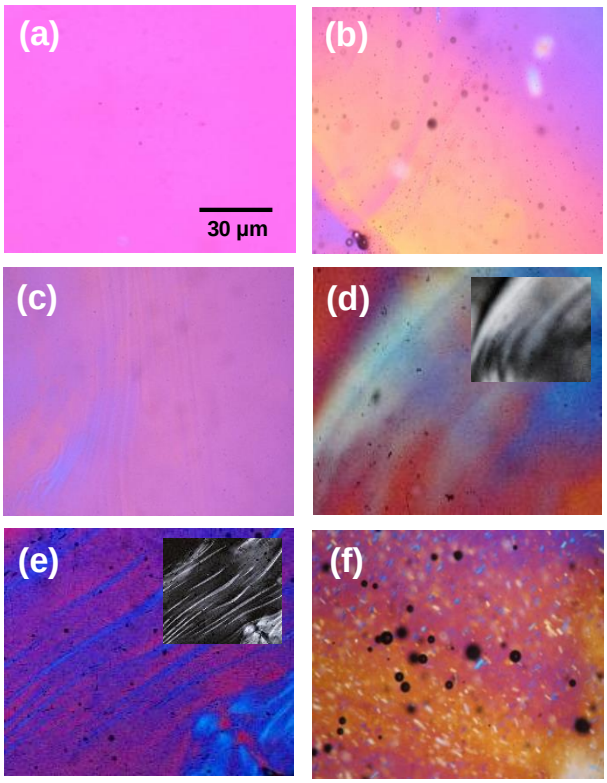

Figure 2-10. Polarized optical micrographs of cellulose/[C_4C_1Im][Cl] solutions as a function of concentration with different molar masses for cellulose/[C_4C_1Im][Cl] solutions at 30 ºC. The polarized optical micrographs in the left column are for (a) isotropic solution, (c) 13 wt% and (e) 15 wt% solutions having a molar mass of 55 kg/mol. The images on the right are for (b) 9 wt%, (d) 10 wt% and (f) 11 wt% solutions consisting of 252 kg/mol. The insets are the micrographs taken without the sensitive tint plate insertion. The polarized image of 11 wt% solution with a high molar mass indicates that solubility of [C_4C_1Im][Cl] for cellulose having 252 kg/mol is limited above 11 wt%.

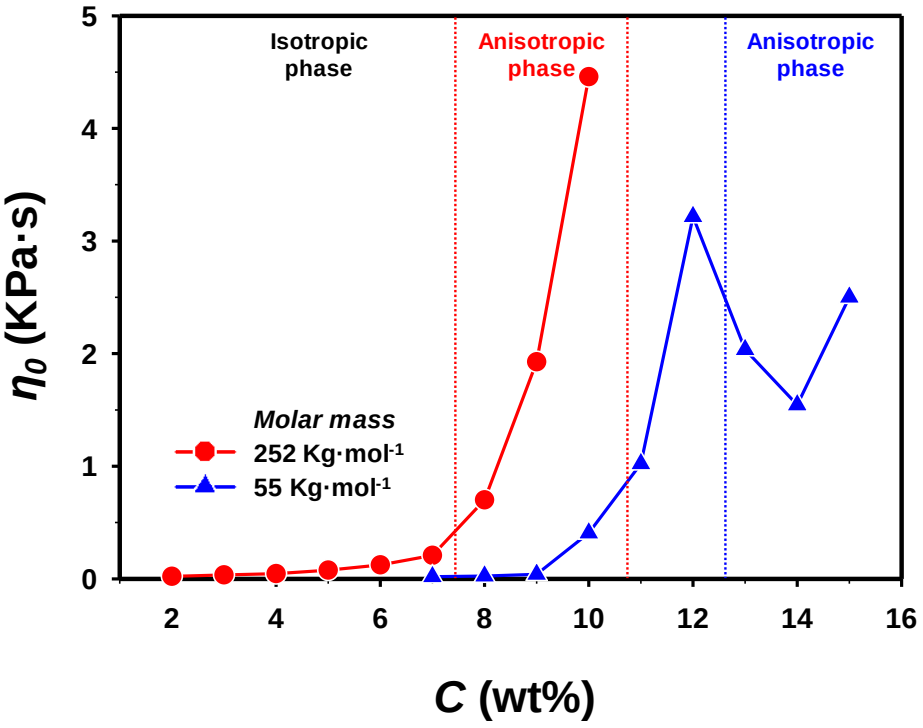

Figure 2-11. Dependence of the zero-shear viscosity on the molar mass and concentration for cellulose/[C_4C_1Im][Cl] solutions at 30 °C.

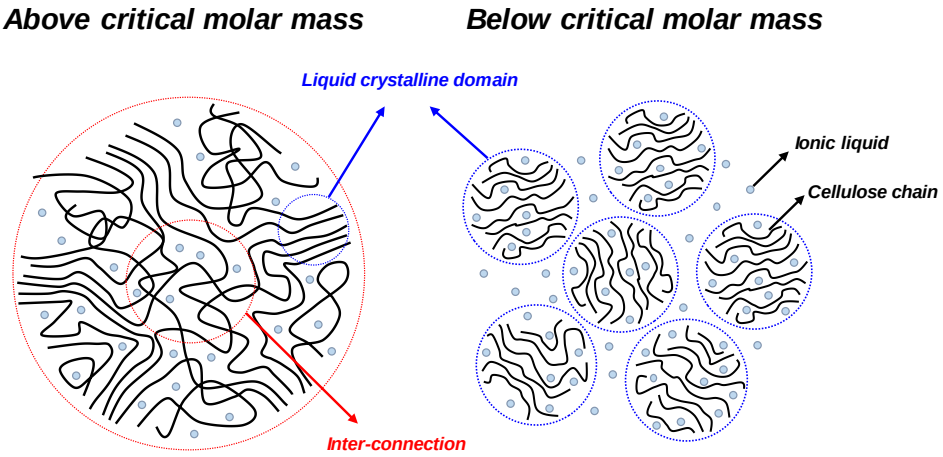

Figure 2-12. Schematic representation of different mechanisms for the formation of liquid crystalline phase above and below the critical molar mass. Depending on the molar mass, cellulose forms either networked anisotropic structures or separated liquid crystalline domains.

2.4. Conclusions

In this chapter, the effect of anion in ionic liquid was investigated for degree and the kinetics of depolymerization of cellulose in ionic liquid. Comparing to acetate, chloride anion depolymerized cellulose more effectively due to higher acidity which exhibits 2-fold higher depolymerization rate. In turns, the chain conformation was greatly changed by chloride anion during depolymerization, confirmed by the rheological observation. The study also showed the presence and the chemical reaction of carbene.

Depolymerization decreased the inter-molecular entanglement and friction, and, in turn, showed a decrease in the viscosity and terminal region in dynamic test, as well. The activation energy decreased as cellulose was depolymerized. However, chain isolation by severe depolymerization resulted in leveled-off activation energy. The dependence of molar mass on phase transition suggested a correlation between physical state and cholesteric phase, which showed the different behavior above and below critical molar mass. The exponents for Mark-Houwink-Sakurada and the result of the radius of gyration suggests that the cellulose in ionic liquid existed as a Gaussian chain in a theta solvent.

References

1. Gericke, M.; Schlufter, K.; Liebert, T.; Heinze, T.; Budtova, T., Rheological properties of cellulose/ionic liquid solutions: from dilute to concentrated states. *Biomacromolecules* **2009,** *10* (5), 1188-1194.
2. Lu, F.; Song, J.; Cheng, B.-W.; Ji, X.-J.; Wang, L.-J., Viscoelasticity and rheology in the regimes from dilute to concentrated in cellulose 1-ethyl-3-methylimidazolium acetate solutions. *Cellulose* **2013,** *20* (3), 1343-1352.
3. Gazit, O. M.; Katz, A., Dialkylimidazolium ionic liquids hydrolyze cellulose under mild conditions. *ChemSusChem* **2012,** *5* (8), 1542-1548.
4. Rodríguez, H.; Gurau, G.; Holbrey, J. D.; Rogers, R. D., Reaction of elemental chalcogens with imidazolium acetates to yield imidazole-2-chalcogenones: direct evidence for ionic liquids as proto-carbenes. *Chemical Communications* **2011,** *47* (11), 3222-3224.
5. Du, H. B.; Qian, X. H., The effects of acetate anion on cellulose dissolution and reaction in imidazolium ionic liquids. *Carbohydrate Research* **2011,** *346* (13), 1985-1990.
6. Ebner, G.; Schiehser, S.; Potthast, A.; Rosenau, T., Side reaction of cellulose with common 1-alkyl-3-methylimidazolium-based ionic liquids. *Tetrahedron Letters* **2008,** *49* (51), 7322-7324.

7. Huggins, M. L., The viscosity of dilute solutions of long-chain molecules. IV. Dependence on concentration. *Journal of the American Chemical Society* **1942,** *64* (11), 2716-2718.
8. McCormick, C. L.; Callais, P. A.; Hutchinson, B. H., SOLUTION STUDIES OF CELLULOSE IN LITHIUM-CHLORIDE AND N,N-DIMETHYLACETAMIDE. *Macromolecules* **1985,** *18* (12), 2394-2401.
9. Peebles, L. H., *Molecular weight distributions in polymers*. Interscience Publishers New York: 1971; Vol. 18.
10. Cremer, T.; Kolbeck, C.; Lovelock, K. R.; Paape, N.; Wölfel, R.; Schulz, P. S.; Wasserscheid, P.; Weber, H.; Thar, J.; Kirchner, B., Towards a Molecular Understanding of Cation–Anion Interactions—Probing the Electronic Structure of Imidazolium Ionic Liquids by NMR Spectroscopy, X-ray Photoelectron Spectroscopy and Theoretical Calculations. *Chemistry–A European Journal* **2010,** *16* (30), 9018-9033.
11. Padmanabhan, S.; Kim, M.; Blanch, H. W.; Prausnitz, J. M., Solubility and rate of dissolution for Miscanthus in hydrophilic ionic liquids. *Fluid Phase Equilibria* **2011,** *309* (1), 89-96.
12. Sun, N.; Rodríguez, H.; Rahman, M.; Rogers, R. D., Where are ionic liquid strategies most suited in the pursuit of chemicals and energy from lignocellulosic biomass? *Chemical Communications* **2011,** *47* (5), 1405-1421.

13. Trinkle, S.; Friedrich, C., Van Gurp-Palmen-plot: a way to characterize polydispersity of linear polymers. *Rheologica Acta* **2001,** *40* (4), 322-328.
14. Collins, K. D., Charge density-dependent strength of hydration and biological structure. *Biophysical journal* **1997,** *72* (1), 65.
15. Collins, K. D., Ions from the Hofmeister series and osmolytes: effects on proteins in solution and in the crystallization process. *Methods* **2004,** *34* (3), 300-311.
16. Collins, K. D., Ion hydration: Implications for cellular function, polyelectrolytes, and protein crystallization. *Biophysical chemistry* **2006,** *119* (3), 271-281.
17. Mahadeva, S. K.; Kim, J., Influence of residual ionic liquid on the thermal stability and electromechanical behavior of cellulose regenerated from 1-ethyl-3-methylimidazolium acetate. *Fibers and Polymers* **2012,** *13* (3), 289-294.
18. Zhang, Y.-H. P.; Lynd, L. R., Determination of the number-average degree of polymerization of cellodextrins and cellulose with application to enzymatic hydrolysis. *Biomacromolecules* **2005,** *6* (3), 1510-1515.
19. Osaki, K.; Inoue, T.; Uematsu, T.; Yamashita, Y., Evaluation methods of the longest Rouse relaxation time of an entangled polymer in a semidilute solution. *Journal of Polymer Science Part B: Polymer Physics* **2001,** *39* (14), 1704-1712.

20. Osaki, K.; Takatori, E.; Tsunashima, Y.; Kurata, M., The universality of viscoelastic properties of entangled polymeric systems. *Macromolecules* **1987,** *20* (3), 525-529.
21. Rouse Jr, P. E., A theory of the linear viscoelastic properties of dilute solutions of coiling polymers. *The Journal of Chemical Physics* **1953,** *21* (7), 1272-1280.
22. Ferry, J. D., *Viscoelastic properties of polymers*. John Wiley & Sons: 1980.
23. Carella, J. M.; Graessley, W. W.; Fetters, L. J., Effects of chain microstructure on the viscoelastic properties of linear polymer melts: polybutadienes and hydrogenated polybutadienes. *Macromolecules* **1984,** *17* (12), 2775-2786.
24. Takahashi, Y.; Takada, A.; Imaichi, K.; Nakamura, Y. In *Viscoelastic properties of cellulose in 1-buthyl-3-methylimidazolium chloride*, AIP Conference Proceedings, 2008; pp 318-320.
25. Huggins, M. L., Principles of Polymer Chemistry. *Journal of the American Chemical Society* **1954,** *76* (10), 2854.
26. Lv, Y.; Wu, J.; Zhang, J.; Niu, Y.; Liu, C.-Y.; He, J.; Zhang, J., Rheological properties of cellulose/ionic liquid/dimethylsulfoxide (DMSO) solutions. *Polymer* **2012,** *53* (12), 2524-2531.
27. Tamai, N.; Tatsumi, D.; Matsumoto, T., Rheological properties and molecular structure of tunicate cellulose in LiCl/1, 3-dimethyl-2-

imidazolidinone. *Biomacromolecules* **2004,** *5* (2), 422-432.

28. Song, H.; Zhang, J.; Niu, Y.; Wang, Z., Phase transition and rheological behaviors of concentrated cellulose/ionic liquid solutions. *Journal of Physical Chemistry B* **2010,** *114* (18), 6006-6013.
29. Song, H.; Niu, Y.; Wang, Z.; Zhang, J., Liquid crystalline phase and gel-sol transitions for concentrated microcrystalline cellulose (MCC)/1-ethyl-3-methylimidazolium acetate (EMIMAc) solutions. *Biomacromolecules* **2011,** *12* (4), 1087-1096.

CHAPTER 3

Recrystallization behavior of cellulose hydrolyzed in ionic liquid

3.1. Introduction

Both dissolution and regeneration of cellulose continue to be important for enhancing the performance of cellulose and for broadening its areas of application; research in this regard has been pursued for more than a century. Especially comprehensive understanding on recrystallization of cellulose in ionic liquid plays a significant role for regeneration process for fiber, film and nonwoven.[1-3] Despite of progress in recent years, one of the main challenges of developing cellulosic materials is the fundamental understanding and the predictability of crystallization, which influences on physical and chemical stability, of the cellulose regenerated from ionic liquid. Molecular mobility is generally considered to be a key factor determining the crystallization of cellulose, and has the subject of many.[4-7] In addition, crystallinity depended on molecular mobility is crucial for applications because mechanical strength needs to appropriate crystalline under external pressure or elongation.[8-10] However, most studies reported quite low crystallinity of cellulose regenerated from ionic liquids,[11-14] and there are few studies reported on the contribution

of molecular mobility to crystallization.

Factors of molecular properties, such as molar mass, have been represented to contribute to the physical properties of cellulose materials. As discussed in chapter 2, it was presented that cellulose materials having various molar mass were prepared from cellulose/1-butyl-3-methylimidazolium chloride ([C_4C_1Im][Cl]) solution, and studied on relationship between molecular structure and mobility. In the basis on the correlation, it was hypothesized that the molecular mobility, as estimated by rheometer, related to the probability of the molecules being in the appropriate conformation for crystallization.

In this chapter, a preparation method of highly ordered cellulose II crystalline material was presented using cellulose hydrolyzed in [C_4C_1Im][Cl], based on investigation on correlation between the chain mobility and crystallization. Different length of time was applied to control the molar mass of cellulose. Characterization of the cellulose/[C_4C_1Im][Cl] solution with the different molar mass was carried out by rheological properties and crystallinity, and finally attempted to draw a quantitative correlation between the molecular mobility and crystallization at a temperature for a certain time. This study can provide a fundamental understanding of the crystallization behavior of cellulose after hydrolysis and thus aid the development of better cellulose regeneration processes using ionic liquids.

3.2. Experimental

3.2.1. Materials and sample preparation

Cellulose was obtained as a powder from Hyosung Co. (Seoul, Republic of Korea). The cellulose powder was dried for overnight at 60 oC in a vacuum oven before use. 1-butyl-3-methylimidazolium chloride ([C_4C_1Im][Cl], purity ≥99%) were purchased from BASF (Germany). Nine percent (w/w) solution of lithium chloride (LiCl) and DMAc (purity≥99%, distilled over CaH_2) were purchased from Deasung Chemical & Metal Co. (Seoul, Republic of Korea) and used for GPC measurement. Reagent-grade methanol (Sigma Aldrich) was distilled over anhydrous calcium sulfate before used.

Cellulose was dissolved in [C_4C_1Im][Cl] at 85 °C using a mechanical stirrer, and the solution was kept in the reservoir at same temperature. To study the effect of duration time on the molar mass and crystallization of cellulose, testing solutions were sampled daily from the solution reservoir for 240 h. The sampled cellulose solution was immersed and regenerated in distilled water for a day. After several washing to remove the residual [C_4C_1Im][Cl], the sample was dried in an oven for one day.

3.2.2. Measurement of rheological properties

A stress controlled rheometer (HAKKE RS-1, ThermoScientific, Germany) was used to study the viscoelastic properties of the cellulose/[C_4C_1Im][Cl] solutions. The gap was about 1 mm parallel plate geometry. Before the oscillatory shear measurements, a stain sweep from 0.1 to 100% with a fixed frequency of 6.28 rad/s was performed for each solution to determine the linear viscoelastic regime. The chosen strains of 10% fell well within the linear viscoelastic regime for the frequency range of 0.01 – 100 rad/s at various temperatures ranging from 30 to 110 ºC. To prevent water uptake by the sample during the measurements, the edges of the specimen sandwiched between the plates were covered with a thin layer of silicone oil (Shin-Etsu Chemical Co.).

From the obtained viscoelastic properties and molar mass of cellulose/[C_4C_1Im][Cl] solution, the radius of gyration R_g was estimated using Flory approach for flexible polymer chains as following;[15]

$$R_g{}^2 = \frac{1}{6}\left[\frac{[\eta]}{\Phi}M\right]^{2/3} \qquad (1)$$

Where, $[\eta]$ ($cm^3 \cdot g^{-1}$) is the intrinsic viscosity, M ($g \cdot mol^{-1}$) is the molar mass and Φ is Flory constant of 2.8×10^{23} mol^{-1}, respectively. The calculated

values of radius of gyration were summarized in Table 3-2.

3.2.3. XRD measurement

X-ray diffraction profiles of the regenerated cellulose were performed using Powder X-ray diffraction (Ultima IV, Rigaku, Japan) with Cu K_α (λ = 0.154 nm) at 45 KV and 40 mA. A reflection–transmission spinner was used as a sample holder and the spinning rate was set at 10 rpm throughout the experiment. The patterns were collected in the 2θ range of 8 – 40° with a step size of 0.05° and an exposure time 180 s. To quantitatively estimate the conversion to crystalline, the following empirical equation was adopted in the recrystallized cellulose substitutes;[16]

$$CrI = \frac{I_{total} - I_{am}}{I_{total}} \times 100 \qquad (2)$$

Where *CrI* is the crystallinity index for cellulose II structure, I_{total} is the diffraction intensity at peak position for 21.5° and Iam is the intensity at suitable locations for the amorphous background (16°).

3.3. Results and Discussion

3.3.1. Molecular mobility of cellulose solutions

Figure 3-1 shows the complex viscosity of cellulose solutions kept at different times. Regardless of the duration time, the cellulose solutions showed a typical shear-thinning behavior. The plateau viscosity dramatically decreased as the duration time increased. The decrease of viscosity resulted from the reduction in molar mass. The reduction in molar mass in turn, resulted in a reduction in molecular size, which then resulted in less chain entanglement of chains and a lower viscosity. When the incubating time was longer than 8 days, the solution showed Newtonian behavior. The size of the hydrolyzed cellulose chain at long incubating times was too small for entanglement to occur. In these cases, only intermolecular interaction contributed to the viscosity hence no shear thinning behavior was observed. For a similar reason, shear thinning began as the incubating time increased due to higher angular velocity, which is often observed in conventional linear polymers in solution. This higher angular velocity was attributed to the fact that polymers with higher molar mass show greater chain-to-chain entanglement, and the chains can be disentangled by shear force at lower frequencies.

To assess the rheological behavior more quantitatively, non-Newtonian flow behavior observed for cellulose/$[C_4C_1Im][Cl]$ solution was studied

with the quantitative Cross model.[17] It is known to describe well the dependence of viscosity on shear rate. According to Cox-Merz rule,[18] which applies to many polymer solution, the steady shear viscosity, $\eta(\dot{\gamma})$, is identical to the absolute value of complex shear viscosity:

$$\eta(\dot{\gamma}) = |\eta^*(\omega)| \qquad \text{if} \quad \dot{\gamma} = \omega \qquad (3)$$

Both $\eta(\dot{\gamma})$ and $|\eta^*(\omega)|$ are known to approach the same constant value, the zero-shear viscosity η_0, at very low share rate or frequency:

$$\eta_0 = \lim_{\gamma \to 0} \eta(\dot{\gamma}) = \lim_{\omega \to 0} |\eta^*(\omega)| \qquad (4)$$

By substituting the steady shear terms with dynamic terms in the Cross model using Eq (3) and (4), we obtained a modified Cross model that has the form of:

$$|\eta^*(\omega)| = \frac{\eta_0}{1 + (\tau\omega)^n} \qquad (5)$$

The exponent n and τ are known as the power law exponent and characteristic relaxation time. Viscoelastic characteristic parameters η_0

and τ were obtained by fitting the dynamic shear viscosity curves using Eq (5). These viscoelastic characteristics are plotted against the molar mass in Figure 3-2 (a). It is seen that the zero shear viscosities of cellulose/[C_4C_1Im][Cl] solutions fall on a master curve, where it follows the classical power low relationship, $\eta_0 = KM_w^{\alpha}$. The power law exponent α for cellulose/[C_4C_1Im][Cl] solution was fitted to the two slopes of 1.1 and 3.7. It indicated that the change of viscosity was mainly determined by critical point (molar mass) and assigned to unentangled and entangled region. This behavior suggests that chain to chain entanglement state of cellulose is changed above and below critical molar mass.

In addition, these viscoelastic properties are dependent on the molecular structure related with relaxation mechanism. According to the Doi-Edwards theory of viscoelasticity, the ratio τ/η_0 is determined only by the polymer type and the concentration because the molar mass dependence of τ and η_0 follow the same power-law relationship.[19] As shown in Figure 3-2 (b), the value of τ/η_0 is similar among cellulose/[C_4C_1Im][Cl] solutions although each cellulose solutions have different molar mass. The similar values of τ/η_0 imply universality in the relaxation processes of cellulose /[C_4C_1Im][Cl] solutions with different molar mass.

For a polymer solution with high molar mass, the shear viscosity is controlled by the chain network structure, and the decrease in viscosity

with increasing shear rate is caused by the shear-induced change to the network.[20] Therefore, the zero-shear viscosity can be related to polymer chain characteristics as:

$$\eta_0 = K\zeta_0\Phi^{3.5}\bar{n}^{3.5} \qquad (6)$$

Here, K is a constant that depends on the polymer species, ζ_0 is the polymer segmental friction coefficient, Φ is the volume fraction of polymer, and $\bar{n}$ is the average number of segments in a polymer chain, which is almost similar to weight average degree of polymerization. Since Φ is constant in this work, and K is assumed to be the same among each cellulose solutions, Eq (6) is reduced to a simple relationship between ζ_0, η_0 and $\bar{n}$.

$$\zeta_0 \propto \eta_0\bar{n}^{-3.5} \qquad (7)$$

According to Eq (7), the relative value of the segmental friction coefficient can be estimated from the zero shear viscosity and weight average molar mass (these data is same as chapter 2), and listed in Table 3-1. The relative values for the friction was slightly decreased with duration time. The reduction of the friction is related with the molecular

size. In polymer dynamics, friction coefficient is proportional to molecular size. As the molecular size is decreased in same solvent, the frictional force between neighboring chains, therefore, would be reduced, which leads to the decrease of viscosity. This suggests that the cellulose more freely move into solvent and other chains.

The molar mass not only influences the zero shear viscosity but also the shear thinning behavior. The relaxation time predicts that the viscosity begins to decrease with increasing shear rate in the range where the product of this relaxation time. The quantitative analysis for shear thinning provides physical state for polymer chains, which represents the characteristic time. This time constant τ_b is approximated and is related to the zero shear viscosity as followed:

$$\tau_b = \frac{12\eta_0}{\pi^2 \upsilon k_B T} \qquad (8)$$

Where υ, k_B and T are the number of molecules per unit volume, Boltzmann constant and the absolute temperature, respectively. Based on the characteristic relaxation time τ obtained from Cross model, the number of molecules per unit volume may be calculated as shown in Table 3-1. The value of υ for cellulose/[C_4C_1Im][Cl] solution slightly

decreased with the reduction of the molar mass. It implies that cellulose chain was more packed closely to its neighbor chains with a decrease in molecular size. The dense structure makes more chance to interact each chains, which may influence on recrystallization process.

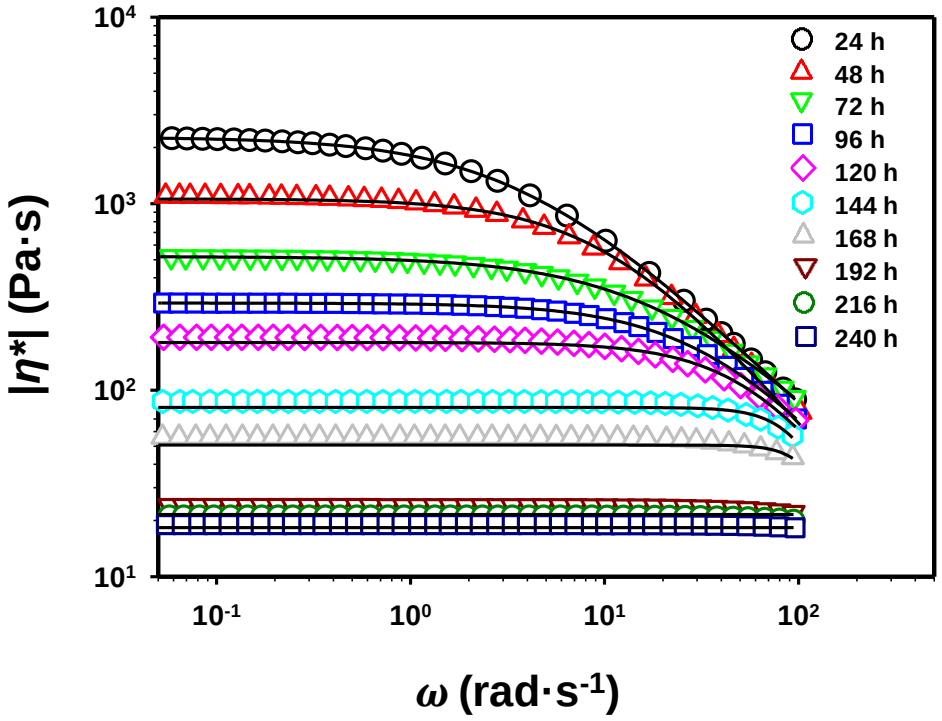

Figure 3-1. Complex viscosity curves of cellulose/[C_4C_1Im][Cl] solution at 30 ^oC as a function of oscillatory shear frequency and the Cross model datafit curves

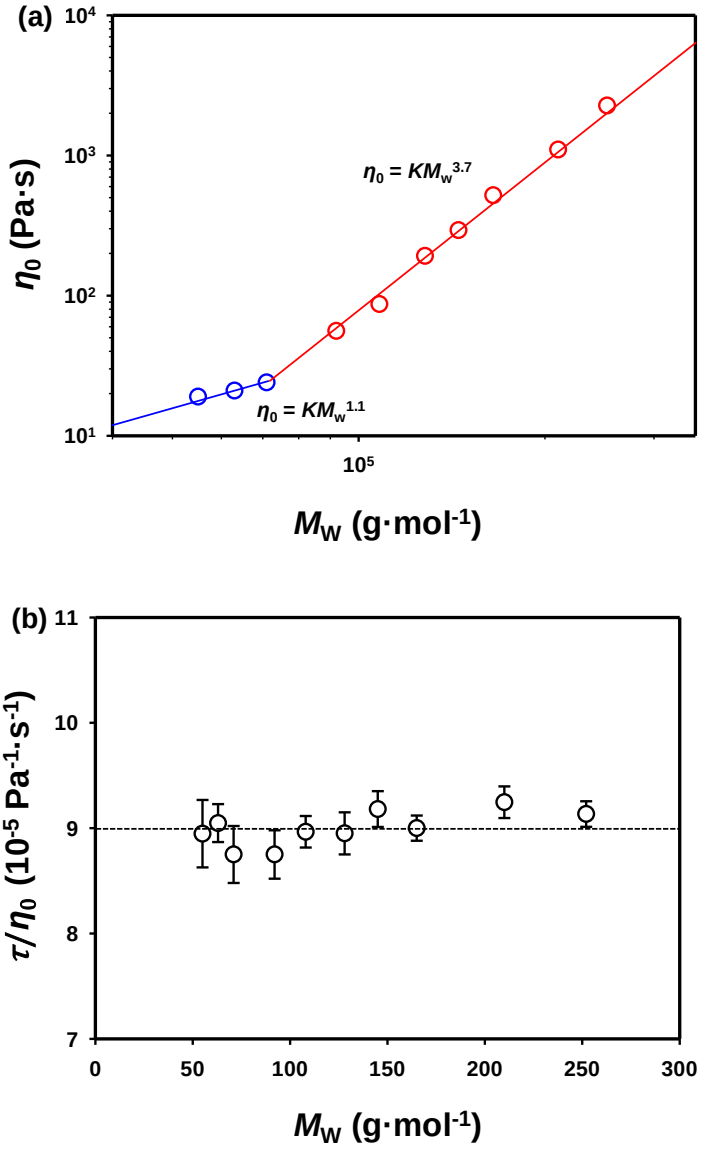

Figure 3-2. Viscoelastic characteristic properties of cellulose/[C_4C_1Im][Cl] solution obtained by Cross model data-fitting results and relationship to molar mass: (a) zero-shear viscosity versus weight average molar mass; (b) τ/η_0 versus the molar mass

Table 3-1. Viscoelastic characteristics of cellulose in $[C_4C_1Im][Cl]$

t (h)	$\eta_0\bar{n}^{-3.5}$ (10^{-8} Pa s)	υ (10^{-6} mol/cm^3)
24	1.53	4.85
48	1.50	5.10
72	1.44	5.12
96	1.36	5.15
120	1.35	5.21
144	1.19	5.26
168	1.18	5.29
192	1.06	5.31
216	1.03	5.33
240	0.97	5.39

3.3.2. Microstructure of recrystallized cellulose

Figure 3-3 (a) shows the XRD patterns of cellulose regenerated from solutions having different molar mass. Regardless of the molar mass, all regenerated cellulose had a cellulose II crystalline structure, as reported previously.[21] With a decrease in molar mass, the characteristic peaks at 12.0˚, 20.5˚, and 21.5˚ became larger and sharper. These data mean that cellulose having lower molar mass forms well-defined and large crystalline phase.

The crystallinities obtained from XRD profiles under same regeneration condition are shown in Figure 3-3 (b). If we assumed that all solutions had same recrystallization time, the rate of crystalline conversion for cellulose with high molar mass was relatively low. The cellulose molecule is rigid and polar, and the crystalline phase is closely packed with a density of ~1.5 g/cm^3. As a result, the rigidity of the cellulose molecule reduces the possible conformations leading to lower configurational arrangement and suggesting that high energy of attaining the specific conformation is required in crystalline lattice. In addition, the entanglement between chains restricts that the molecules attaches regularly to each other. These result in low conversion rate of amorphous state to crystalline phase. However, as the molar mass of the cellulose decreased, especially below the critical molar mass, M_{cr}, the conversion

rate to the crystalline was surprisingly increased with a decrease in the molar mass. It is very interesting that these high values of the cellulose regenerated from ionic liquid are close to a value of original cellulose I crystalline (about 85%),[22-23] which has not been reported in our best knowledge. Based on the physical state of the cellulose, the transition from entangled to unentangled regime by a reduction of the molar mass improve the mobility to rearrange regular conformation of the cellulose molecule. This suggests that the mobility of cellulose dissolved in $[C_4C_1Im][Cl]$ strongly influences on the crystalline conversion during regeneration. The discussion on this topic would be continued in the next section.

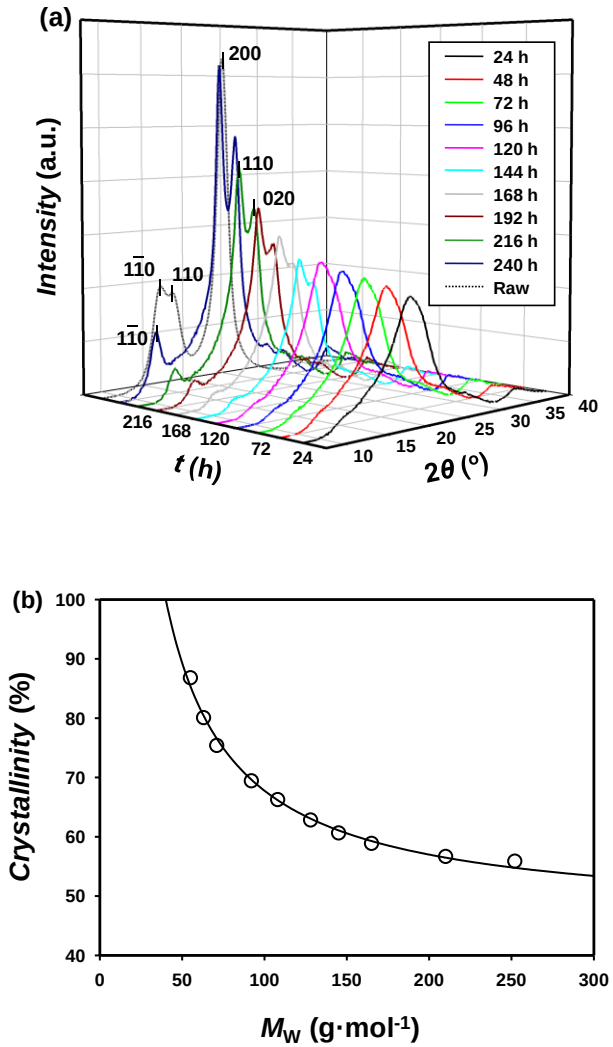

Figure 3-3. Structural change of cellulose after recrystallization from $[C_4C_1Im][Cl]$; (a) XRD curves of cellulose having different molar mass; (b) crystallinity obtained from XRD profiles

3.3.3. Correlation between crystallinity and molecular mobility

Molecular mobility has been suggested to be key determinant of the crystallization. The molecular motion such as translation and rotation are essential in physical or chemical processes. These motions of most molecules in single or multiple component systems, as reflected in the diffusion, are generally coupled to shear viscosity. The relationship between the diffusion coefficient (transition: D_{trans}, rotation: D_{rot}) and shear viscosity, η, is given by the Stokes-Einstein equation:

$$D_{trans} = \frac{k_B T}{6\pi\eta r} \qquad (9)$$

$$D_{rot} = \frac{k_B T}{8\pi\eta r^3} \qquad (10)$$

Where r is the molecular radius, k_B is the Boltzmann constant, and T is absolute temperature. Because the rate constant, k, for a molecular mobility-controlled reaction is proportional to the diffusion coefficient,[7] reaction rate constants at a constant temperature can be correlated to the ratio of their viscosity, as shown in Eq (11):

$$\frac{k_1}{k_2} = \left(\frac{D_1}{D_2}\right)^{\xi} = \left(\frac{\eta_2}{\eta_1}\right)^{\xi} \qquad (11)$$

Where ξ is termed the correlation index, where $0 \leq \xi \leq 1$, and expresses the extent of correlation between the diffusion and the rate of a reaction. For cellulose/[C_4C_1Im][Cl] solution, Figure 3-4 shows the correlations between the molecular mobility and the rate constant for crystallization of cellulose at room temperature above and below critical molar mass. The extent of correlation shown in Eq (11) as ξ was obtained from the slope of a plot of log k versus log η. An interesting aspect of the correlation is the weaker dependence on molecular mobility in the entangled regime that in the unentangled regime. Below critical molar mass, the extent of correlation is about 0.22 while above critical molar mass it is only about 0.06. As molar mass increased, molecular motion slows down, and the rate of crystallization is expected to depend increasingly on the diffusion process. It can be explained in terms of physical state of cellulose chain. In unentangled polymer solution, molecular translation and rotation are usually faster than the change of molecular structure itself so that the overall rate does not depend on diffusion of the reactant. However, in the entangled solution, molecular diffusion is relatively slow and, in most cases, the rate of reaction. It is likely that molecular motion becomes partially rate limiting in chain entanglement.

For this behavior, another possible explanation for this results is a change in the cellulose mobility at the critical molar mass. Using Arrhenius relationship, $\log \eta \propto \Delta E_a/RT$, apparent activation energy can be estimated for the molecular mobility in both regime. Figure 3-5 shows the activation energy of flow is plotted against the molar mass. As the molar mass decreased, the activation energy was exponentially decreased. It suggests that the cellulose chains having low molar mass are isolated from its neighbor chains as explained in rheological properties. During the crystallization of a linear polymer, the chain rearranges its position into a more ordered pattern and hence forms a crystalline structure. The polymer having a higher molar mass is more likely to entangle with other chains, which make rearrangement difficult. The polymer chain with a low molar mass (i.e. a more hydrolyzed cellulose) can form a more crystalline structure with a better crystal order.

In addition, the degree of chain extension also plays an important role in crystallization. Even though a cellulose chain is less entangled, it cannot easily form a crystalline structure if it is not extended. It is even more important for polymers such as cellulose to form a fringed micelle crystalline structure.[24] Table 3-2 lists the calculation results for the ratio of the radius gyration to the fully extended chain length for cellulose having different molar mass. As these data suggest, extendibility index,

L/*D*, for the cellulose chain increases with the reduction of molar mass. This conformation results in the parallel alignment to form the fringed micelle crystalline of cellulose. For the reasons mentioned above, hydrolyzed cellulose has a well-structured cellulose II crystalline.

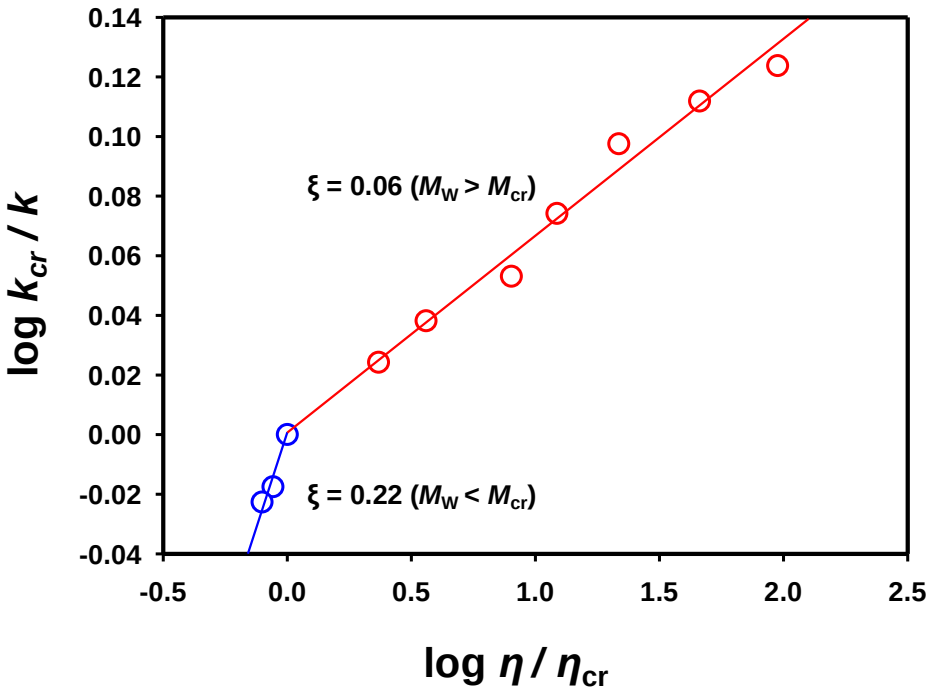

Figure 3-4. Correlation between viscosity and rate constants for crystallization of cellulose above and below its critical molar mass

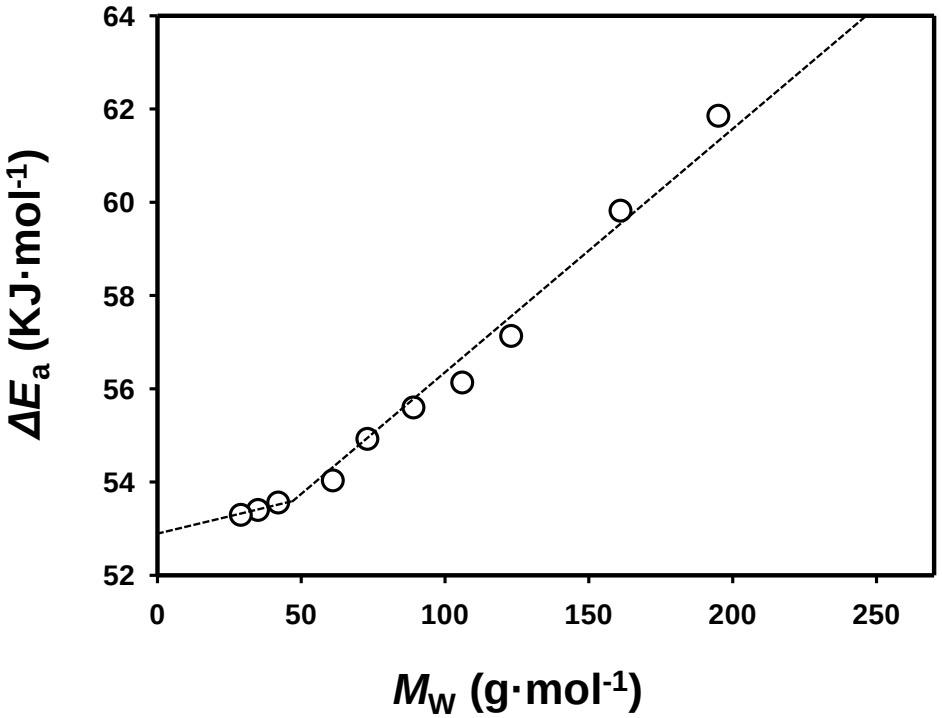

Figure 3-5. Relationship between activation energy and molar mass of cellulose

Table 3-2. Radius of gyration and chain extendibility of cellulose/[C_4C_1Im][Cl]

Degree of Polymerization[a]	Fully extended length (10^{-9} nm)[b]	Radius of gyration (10^{-9} m)	L/D[c]
1555	2333	21.75	107.24
1296	1944	21.25	91.49
1018	1527	20.25	75.41
895	1342	18.10	74.17
790	1185	17.17	68.99
666	1000	15.66	63.82
567	851	14.85	57.35
438	657	14.21	46.24
388	583	12.87	45.31
339	509	11.93	42.65

[a]Degree of polymerization was calculated using molar mass of cellulose repeatingunit (162 g/mol).

[b]Based on size of glucose molecule (1.5 nm), fully extended length was estimated.

[c]Ratio of fully extended chain length (L) and radius of gyration (D) was calculatedas extendibility index.

3.4. Conclusions

In this chapter, preparation of well-defined cellulose II crystalline was investigated using the cellulose regeneration from [C_4C_1im][Cl]. The crystallization of cellulose in [C_4C_1im][Cl] was strongly correlated with molecular mobility associated with molar mass. As the molar mass of cellulose decreased, the intermolecular friction and entanglement simultaneously decreased, especially below critical molar mass. The drastic increase of crystallinity with the improved mobility suggested a correlation between the mobility and conversion to crystalline, which showed the different behavior above and below the critical molar mass. The discrepancy led to drastic decrease of activation energy for the recrystallization and in turn resulted in higher crystallinity. This study opens up a route to the development of well-ordered cellulosic material and to a fundamental understanding of the effects of molecular mobility on recrystallization of cellulose in ionic liquid.

References

1. Ahn, Y.; Hu, D.-H.; Hong, J. H.; Lee, S. H.; Kim, H. J.; Kim, H., Effect of co-solvent on the spinnability and properties of electrospun cellulose nanofiber. *Carbohydrate polymers* **2012,** *89* (2), 340-345.
2. Kothari, S. H.; Kumar, V.; Banker, G. S., Comparative evaluations of powder and mechanical properties of low crystallinity celluloses, microcrystalline celluloses, and powdered celluloses. *International journal of pharmaceutics* **2002,** *232* (1), 69-80.
3. Kreze, T.; Malej, S., Structural characteristics of new and conventional regenerated cellulosic fibers. *Textile Research Journal* **2003,** *73* (8), 675-684.
4. Averous, L.; Boquillon, N., Biocomposites based on plasticized starch: thermal and mechanical behaviours. *Carbohydrate Polymers* **2004,** *56* (2), 111-122.
5. Bag, R.; Beaugrand, J.; Dole, P.; Kurek, B., Viscoelastic properties of woody hemp core. *Holzforschung* **2011,** *65* (2), 239-247.
6. Eriksson, M.; Notley, S. M.; Wågberg, L., Cellulose thin films: degree of cellulose ordering and its influence on adhesion. *Biomacromolecules* **2007,** *8* (3), 912-919.
7. Guo, Y.; Byrn, S. R.; Zografi, G., Physical characteristics and chemical

degradation of amorphous quinapril hydrochloride. *Journal of pharmaceutical sciences* **2000,** *89* (1), 128-143.

8. Isogai, A.; Saito, T.; Fukuzumi, H., TEMPO-oxidized cellulose nanofibers. *Nanoscale* **2011,** *3* (1), 71-85.
9. Mwaikambo, L. Y.; Ansell, M. P., Chemical modification of hemp, sisal, jute, and kapok fibers by alkalization. *Journal of Applied Polymer Science* **2002,** *84* (12), 2222-2234.
10. Wang, B.; Sain, M.; Oksman, K., Study of structural morphology of hemp fiber from the micro to the nanoscale. *Applied Composite Materials* **2007,** *14* (2), 89-103.
11. Freire, M. G.; Teles, A. R. R.; Ferreira, R. A.; Carlos, L. D.; Lopes-da-Silva, J. A.; Coutinho, J. A., Electrospun nanosized cellulose fibers using ionic liquids at room temperature. *Green Chemistry* **2011,** *13* (11), 3173-3180.
12. Ohkawa, K.; Hayashi, S.; Nishida, A.; Yamamoto, H.; Ducreux, J., Preparation of pure cellulose nanofiber via electrospinning. *Textile Research Journal* **2009,** *79* (15), 1396-1401.
13. Quan, S.-L.; Kang, S.-G.; Chin, I.-J., Characterization of cellulose fibers electrospun using ionic liquid. *Cellulose* **2010,** *17* (2), 223-230.
14. Xu, S.; Zhang, J.; He, A.; Li, J.; Zhang, H.; Han, C. C., Electrospinning of native cellulose from nonvolatile solvent system. *Polymer* **2008,** *49*

(12), 2911-2917.

15. Flory, P. J., Principles of polymer chemistry. **1953**.
16. Nelson, M. L.; O'Connor, R. T., Relation of certain infrared bands to cellulose crystallinity and crystal lattice type. Part II. A new infrared ratio for estimation of crystallinity in celluloses I and II. *Journal of Applied Polymer Science* **1964,** *8* (3), 1325-1341.
17. Cross, M. M., Polymer rheology: influence of molecular weight and polydispersity. *Journal of Applied Polymer Science* **1969,** *13* (4), 765-774.
18. Cox, W. P.; Merz, E. H., CORRELATION OF DYNAMIC AND STEADY FLOW VISCOSITIES. *Journal of Polymer Science* **1958,** *28* (118), 619-622.
19. Graessley, W. W., Some phenomenological consequences of the Doi-Edwards theory of viscoelasticity. *Journal of Polymer Science Part B: Polymer Physics* **1996,** *34* (16), 2667-2674.
20. Graessley, W. W., Viscosity of entangling polydisperse polymers. *The Journal of Chemical Physics* **1967,** *47* (6), 1942-1953.
21. Zhang, L.; Ruan, D.; Zhou, J., Structure and properties of regenerated cellulose films prepared from cotton linters in NaOH/urea aqueous solution. *Industrial & Engineering Chemistry Research* **2001,** *40* (25), 5923-5928.
22. Kljun, A.; Benians, T. A.; Goubet, F.; Meulewaeter, F.; Knox, J. P.;

Blackburn, R. S., Comparative analysis of crystallinity changes in cellulose I polymers using ATR-FTIR, X-ray diffraction, and carbohydrate-binding module probes. *Biomacromolecules* **2011,** *12* (11), 4121-4126.

23. Schenzel, K.; Almlöf, H.; Germgård, U., Quantitative analysis of the transformation process of cellulose I→ cellulose II using NIR FT Raman spectroscopy and chemometric methods. *Cellulose* **2009,** *16* (3), 407-415.
24. Scallan, A., A quantitative picture of the fringed micellar model of cellulose. *Textile Research Journal* **1971,** *41* (8), 647-653.

CHAPTER 4

Effect of ionic liquid pretreatment on microstructure of lignocellulosic biomass

4.1. Introduction

The need for alternative resources for fossil-based fuel has accelerated investigations on sustainable energy and bio-based materials. Lignocellulosic biomass, the most abundant material on the earth, is considered to be a promising candidate with great potential to serve as a substitute for fossil fuels. Lignocellulosic biomass (lignocellulose) is a complex composite of cellulose, lignin and hemicellulose as well as other materials. Among these components, cellulose is the major carbon-source for bio-fuel and sugar products. In particular, sugars obtained from cellulose are attractive starting materials for large-scale production in a bio-refinery,[1-6] although the potential of lignocellulosic biomass has not been fully exploited due to poor accessibility of enzymes. Native lignocellulosic biomass is inherently recalcitrant to biodegradation, owing to the presence of lignin, high crystallinity of cellulose, and complex bonding between them. Lignin in lignocellulose acts as a physical or chemical barrier, protecting cellulose and hemicellulose from enzymatic degradation, and decreasing the efficiency of enzymatic

hydrolysis.[7, 8] The high crystallinity of the native cellulose structure (cellulose I) also hinders the accessibility of enzymes into polysaccharides. Accordingly, the conversion of the crystalline structure of cellulose I to other crystal forms such as cellulose II, cellulose III_{II} and cellulose III_{I} or to an amorphous structure, can significantly improve the susceptibility to hydrolysis.[9] Pretreatment of the biomass involving physicochemical, structural, and compositional changes is critical to overcome its recalcitrance to hydrolysis.[10-12]

Ionic liquid-pretreatment for lignocellulosic biomass has emerged as a novel technology. Since Swatloski et al.[13] reported cellulose dissolution using ionic liquid, many ionic liquids have been synthesized and tested for lignocellulose dissolution. Representatively, superior solubility of those based on acetate and chloride anion combined with dialkylimidazolium cations was reported to dissolve high amounts of each components, such as cellulose, lignin and hemicellulose, in lignocellulose under mile condition.[9] Pretreatment of the lignocellulose by ionic liquids removes lignin as well as decreasing the level of crystallinity by weakening intra-/inter-molecular hydrogen bonds. In early studies, Dadi *et al.*[14] reported that the enzymatic hydrolysis yield of Avicel was dramatically improved after pretreatment with 1-buthyl-3-methylimidazolium chloride since the resulting decrease in crystallinity improved enzyme accessibility to the substrate. Other researchers[15, 16] studied the changes of

crystalline structure and crystallinity using 1-ethyl-3-methylimidazolium acetate to pretreat various biomasses under a range of conditions. Although previous researches demonstrated the potential of ionic liquids for pretreatment in a bio-refinery, a systematic study on the influence of anion type remains to be done. In point of structural change of lignocellulose, the anion type in ionic liquids should be also considered due to its significance for disturbing the microstructure. Therefore, it is still required for an understanding on the physical state of the lignocellulose molecule associated differently with anion types of the ionic liquid in order to control the crystalline conversion.

In this chapter, the effect of ionic liquid types on the lignocellulose pretreatment was investigated using typically used ionic liquids, 1-ethyl-3-methylimidazolium acetate and 1-ethyl-3-methylimidazolium chloride. The selected ionic liquids are expected to represent properties of other ionic liquids consisting of similar anion, such as formate, iodide and bromide anions, due to their similar properties. Two types of ionic liquid with different anions were compared for pretreatment efficiency of lignocellulose: the influence of the anion type on the composition and the crystalline structure was investigated. The molecular interactions and the mobility were observed by considering the rheological behavior, which was used to demonstrate differences in crystalline change. This study provides a fundamental understanding of the action of ionic

liquid and provides recommendations for which materials and conditions should be selected for pretreatment of the lignocellulosic biomass. In addition, the study is also expected to provide information concerning the mechanism of crystalline transition of lignocellulose by investigating the relationship between the dynamics of lignocellulose molecules and its composition.

4.2. Experimental

4.2.1. Materials

Three different lignocelluloses were investigated in this study: cotton (*Gossypium arboretum*) stalks, hemp (*Cannabis sativa*) stalks and acacia (*Acacia auriculiformis*) pruning. Cotton and hemp were kindly provided by Hempleekorea Co., and acacia was provided by Moorim P&P Co. Microcrystalline cellulose (MCC, from Sigma Aldrich) was used as a control. 1-ethyl-3-methylimidazolium acetate(EmimOAC, ~95%) and 1-ethyl-3-methylimidazolium chloride (EmimCl, ~95%) were purchased from Sigma Aldrich. Anhydrous Lithium Chloride (LiCl) and N,N-dimethylacetamide (DMAc) were purchased from Daejung Chemicals & Methals Co. To remove moisture, DMAc was distilled over CaH_2 before use.

4.2.2. Pretreatment and recrystallization method

The biomass samples were milled to 20 mesh (particle size: 200 – 800 μm) before pretreatment and were then incubated with EmimOAC or EmimCl at 4 % (w/w) for 2 h at 80 ºC or 120 ºC. The temperatures were chosen to avoid thermal decomposition of the ionic liquid which could affect the efficiency of the pretreatment.[17] After the ionic liquid-pretreatment, the samples were transferred to a beaker, and acetone/water (1:1 v/v) was added in order to

separate and remove the lignin from the cellulose.[18] The mixture was stirred for 1 h at room temperature and then the precipitated substrates were separated from the coagulant by filtration through a ceramic funnel with nylon filter paper, under vacuum. The material was washed with water at least four times to remove the ionic liquid and then dried in a vacuum oven for 2 days at 60 ºC. The pretreatment conditions used for the lignocelluloses are summarized in Table 4-1.

4.2.3. Fourier-transform infrared spectroscopy (FT-IR)

The samples were subjected to FT-IR spectroscopy using a PerkinElmer spectrum BX spotlight spectrophotometer with diamond attenuated total reflectance attachment. Scanning was conducted from 4000 to 700 cm^{-1} with 64 repetitious scans averaged for each spectrum. Resolution was 4 cm^{-1} and interval scanning was 2 cm^{-1}.

Table 4-1. Pretreatment conditions and ionic liquids used in this study

Sample code	Abbreviation	Name	Pretreatment Temp. (ºC)
EmimOAC 80 ºC	EmimOAC	1-ethyl-3-methylimidazolium acetate	80
EmimOAC 120 ºC			120
EmimCl 80 ºC	EmimCl	1-ethyl-3-methylimidazolium chloride	80
EmimCl 120 ºC			120

4.2.4. Lignocellulosic biomass composition

The composition of the samples before and after the pretreatment was determined according to the analytical procedure of the National Renewable Energy Laboratory (NREL) No. 002.[19, 20] Briefly, samples (150 mg each) were treated with 72% (v/v) sulfuric acid at 30 ºC for 3 h, followed by diluted acid (4%) at 121 ºC. Hydrolyzed products were analyzed by HPLC (Young-Lin Model YL9100, Korea) equipped with an RI detector and a Shodex sugar SP0810 column operated at 85 ºC. The mobile phase consisted of deionized water with a flow rate of 0.6 ml/min. The amounts of cellulose and hemicellulose were calculated from the glucose and xylose contents multiplied by a conversion factor of 0.9 and 0.88 respectively.[21] The amount of acid-insoluble lignin after acid hydrolysis was measured as the mass of insoluble residue remaining.[19] The amount of acid-soluble lignin was measured by a UV-Vis spectrophotometer at 205 nm with an extinction coefficient value of 110 $Lg^{-1}cm^{-1}$ (NREL, 1996)

4.2.5. Thermogravimetric analysis (TGA)

Thermogravimetric analysis of the biomass samples was performed using a PerkinElmer instrument, Pyris Diamond TG/DTA. The thermal stability of 0.5 mg of each sample was studied from room temperature to 600 ºC at a rate of 10 ºC/min. The rate of purge gas (Nitrogen) flow was controlled at 70 mL/min.

4.2.6. Measurement of rheological properties

In order to avoid cellulose degradation, a DMAc/LiCl solvent system was employed for measuring steady-state and dynamic viscoelastic behaviors. The lignocellulose was activated using the method reported by McCormick *et al*.[22] where the lignocellulose samples were dissolved in the solvent, 9 wt% DMAc/ LiCl, after being completely dried in vacuum below 60 ºC.

Rheological measurements were carried out on a strain-controlled rheometer (RS-1, Thermo Electron Co., Germany) with 40 mm plate-plate geometry. Frequency sweeps within the linear region controlled strain were performed at various temperatures ranging from 30 to 110 ºC. All data were reduced to a reference temperature of 30 ºC by time-temperature superposition (TTS). Steady shear experiments were carried out at 30 ºC with a shear rate of 0.01–500 s^{-1}. To prevent moisture uptake by the sample during experiments, the edges of the specimen were coated with silicon oil between the plates.

In order to estimate and quantify the chain mobility, the activation energy (ΔE_a) of the lignocellulose solutions was calculated using the Williams-Landel-Ferry equation and the results are summarized in Table 4-3.

$$\ln a_T = \frac{-c_1(T - T_r)}{c_2 + (T - T_s)}$$

Where c_1 and c_2 denote experimental constants and T_r is reference temperature (here T_r = 303 K). Then, ΔE_a at the reference temperature was estimated from the following equation:

$$\Delta E_a(T = T_r) = R\frac{dlna_T}{d(1/T)}|_{T=T_r} = 2.303R(C_{1/}C_2)T_r^2$$

4.2.7. X-ray diffraction (XRD) measurement

The microstructures of the native and the pretreated samples were analyzed by wide-angle X-ray diffraction (WAXD, Ultima IV, Rigaku, Japan). The scans were collected from 2θ = 8 to 40° with a step size of 0.01° at 1 s per step. The following empirical equation was adopted to estimate the cellulose crystallinity in the native and pretreated biomass samples:[23]

$$\mathrm{CrI} = (I_{total} - I_{am})/I_{total} \times 100$$

Where I_{total} is the diffraction intensity at peak position for 22.5° for cellulose I and I_{am} is the intensity at suitable locations for the amorphous background (18°). For cellulose II, the main peak appears as a doublet at 21.5°, and the amorphous peak appears at 16°.

4.3. Results and Discussion

4.3.1. Composition of ionic liquid-pretreated lignocellulose

Figure 4-1 shows the FT-IR spectra of the native and the pretreated MCC, cotton, hemp and acacia. The characteristic peaks of lignin and hemicellulose in the lignocelluloses appeared at 1732 cm^{-1} (C=O unconjugated stretching, hemicellulose), 1515-1505 cm^{-1} (C=C aromatic symmetrical stretching, lignin), 1425 cm^{-1} (C=C stretching in aromatic groups, lignin and hemicellulose) and 1240 cm^{-1} (C–O aryl group, lignin).[24] With the exception of acacia, the characteristic peaks were decreased with increasing temperature, regardless of the type of ionic liquid. However, with EmimOAC pretreatment, there was a more rapid decrease as the temperature increased, than after treatment with EmimCl. When the biomasses were pretreated with EmimOAC at 120 ºC, the peaks almost disappeared. For acacia, the significant difference of FT-IR spectra was not observed in any of the experimental conditions. When MCC, cotton and hemp were pretreated with EmimOAC, a new peak appeared at 3447 cm^{-1} (OH stretching intramolecular hydrogen bonds of cellulose II).[25] This result indicates that the crystalline structure is transformed from cellulose I to II only by EmimOAC.

The composition of each biomass was measured using HPLC (Table 4-2). The Table shows more efficient decomposition and removal of lignin and

hemicellulose pretreated in EmimOAC than EmimCl as confirmed by the FT-IR results. The removal of lignin and hemicellulose seems to be related to the solubility of the ionic liquids for cellulose, lignin and hemicellulose. Compared to other anions in ionic liquids, EmimOAC has better solubility for cellulose, lignin and hemicellulose,[9, 26, 27] suggesting that non-cellulosic component would have more freedom to separate from the biomass after dissolution when solvent has more solubility for each component.[20] As a result, the lignin and hemicellulose in the EmimOAC-pretreated biomass was substantially reduced. However, EmimCl is less effective dissolution at separating each components because of low solubility compared to EmimOAC.[9, 26, 27] The insufficient dissolution (heterogeneous state) of lignocellulose in EmimCl results in the low efficiency of lignin and hemicellulose reduction. On the basis of this explanation, the effect of increasing pretreatment temperature can be interpreted as the solubility enhancement for the lignocelluloses. At high temperature, the lignocellulose in ionic liquids became more homogeneous and loosening, leading to the efficient removal of non-cellulosic components.

The removal efficiency of the lignin and hemicellulose was also dependent on their initial content. In low lignin content, lignocellulose samples were more effectively delignified than for samples with a higher content. The lignin removal efficiency in cotton was approximately 70% when it was pretreated

with EmimOAC at 120 ºC, however, the efficiency for the pretreated acacia under the same conditions was only 20%. This trend was similar to hemicellulose. The difference in the efficiency is attributed to limited solubility of the ionic liquid and the known recalcitrance of lignin for dissolution. Lignin in lignocellulose surrounds and combines with cellulose, which acts as chemical barrier.[28] There is an increased likelihood of forming strong complex between cellulose and non-cellulose, which further impedes their separation when the non-cellulosic content is high. Consequentially, lignocelluloses having high lignin content is not easily dissolved in ionic liquid.

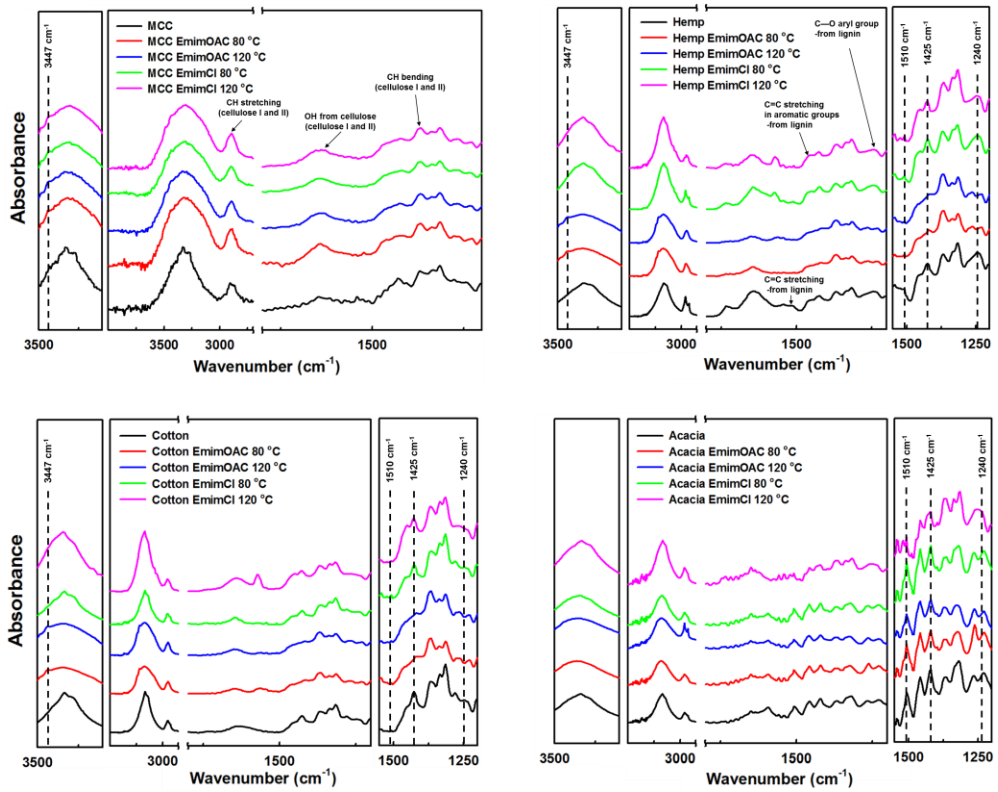

Figure 4-1. FT-IR spectra of MCC, cotton, hemp and acacia samples pretreated with EmimOAC or EmimCl at 80 ºC and 120 ºC

Table 4-2. Composition of cellulose, hemicellulose and lignin in native and pretreated cotton, hemp and acacia[a]

Substrate	Cellulose (%)	Hemicellulose (%)	Acid-Sol. lignin (%)	Acid-Insol. lignin + ash (%)
Cotton	67± 3	16 ± 2	2 ± 0.7	11 ± 2
Cotton EmimCl 80 ºC	70 ± 2	15 ± 1	1 ± 0.7	10 ± 3
Cotton EmimCl 120 ºC	72 ± 3	15 ± 1	1 ± 0.2	10 ± 1
Cotton EmimOAC 80 ºC	78 ± 4	12 ± 1	1 ± 0.2	5 ± 2
Cotton EmimOAC 120 ºC	83± 3	12 ± 3	1 ± 0.5	3 ± 1
Hemp	52 ± 7	25 ± 2	2 ± 1	15 ± 4
Hemp EmimCl 80 ºC	54 ± 1	23 ± 1	2 ± 0.5	14 ± 3
Hemp EmimCl 120 ºC	56 ± 1	23 ± 2	2 ± 0.7	13 ± 2
Hemp EmimOAC 80 ºC	62 ± 2	23 ± 3	1 ± 0.4	7 ± 5
Hemp EmimOAC 120 ºC	71 ± 3	19 ± 2	1 ± 0.7	6 ± 4
Acacia	49 ± 4	13 ± 3	3 ± 0.5	29 ± 6
Acacia EmimCl 80 ºC	50 ± 6	13 ± 1	3 ± 0.6	28 ± 7
Acacia EmimCl 120 ºC	51 ± 7	12 ± 2	2 ± 1	27 ± 4
Acacia EmimOAC 80 ºC	55 ± 2	10 ± 3	2 ± 1	27 ± 5
Acacia EmimOAC 120 ºC	59 ± 3	9 ± 1	1 ± 0.6	24 ± 4

[a]All measurements are an average of triplicate samples.

4.3.2. Thermal stability of ionic liquids and pretreated lignocellulose

The thermal decomposition of ionic liquids during pretreatment is a critical issue because the decomposed ionic liquids alter the efficiency of lignocellulose pretreatment.[17] To confirm the chemical integrity of ionic liquids, the observation for their decomposition behavior was conducted using TG analysis. Figure 4-2 (a) shows that both EmimOAC and EmimCl maintained their weight in the temperature range used in this study (80 and 120 ºC). In addition, Figure 4-2 (b) demonstrates that the weight loss of EmimOAC and EmimCl for 2 h under isothermal condition was only 0.6% and 0.4%, respectively. This behaviors indicate that both ionic liquids nearly maintained their chemical structure, suggesting the thermal decomposition of ionic liquids can be neglected in this study.

Molecular weight is well known to plays an important role in explaining crystallization behavior. However, the molecular weight of lignocellulose is not easy to be measured directly using gel permeation chromatography due to its complex composition. Therefore, the relationship between the thermal stability and the molecular weight as alternative method was investigated to observe the cellulose molecular weight. Figure 4-3 shows the derivative thermogravimetric (DTG) curves of the native and the pretreated samples. The

broad signal below 100 ºC indicates the removal of water in the samples. The DTG curves of the native samples show a sharp and narrow peak at 360 ºC, which is typical thermal decomposition temperature of cellulose. When the samples were pretreated, the thermal degradation started at a lower temperature. The pretreatment temperature differently affected the thermal behavior according to anion type. For the EmimOAC-pretreatment at 80 ºC, MCC, cotton and hemp show two major decompositions at 280 and 330 ºC. However, pretreatment at 120 ºC resulted in a single decomposition below 300 ºC. In particular, the acacia samples treated at 120 ºC initiated degradation below 200 ºC and shows a broad range of degradation temperature. This indicates that the cellulose was decomposed during the pretreatment at high temperature. The change of the decomposition temperature can be explained in terms of the decrease in molecular weight.[29, 30] It is generally known that the decomposition temperature is decreased with a lower thermal resistance of polymer chain relating with the molecular weight. Therefore, the cellulose in lignocelluloses is expected to have lower molecular weight with ionic liquid-pretreatment at high temperature. This speculation may be considered to be valid, regarding the result the similar behavior was observed for DTG curves of cellulose samples having different molecular weight.[31]

The degradation temperature of the samples treated with EmimCl was lower and split when the treatment was carried out at high temperature, which is

similar to the results with EmimOAC. However, each decomposition peak for the sample treated with EmimCl appeared at a higher temperature than for the samples treated with EmimOAC. As explained above, the thermal stability of cellulose could be depended on the molecular weight, suggesting that EmimOAC-pretreated lignocellulose hydrolyzed more extensively than the EmimCl-pretreated sample. In a previous study on cation-anion interactions in ionic liquid, it was reported that the acetate anion has a stronger ability to form ionic bonding with cations than with the chloride anion.[26] This ability means that an acetate anion and a proton from a cation can combine easily to form carbene and acid, which in turn results in the possibility of acid-catalyzed hydrolysis occurring during the pretreatment.[29] In addition, the generated carbene leads to ring-opening reaction at end group of glucose. Based on these points, the sample pretreated with EmimOAC showed reduced thermal stability compared to the one with EmimCl.

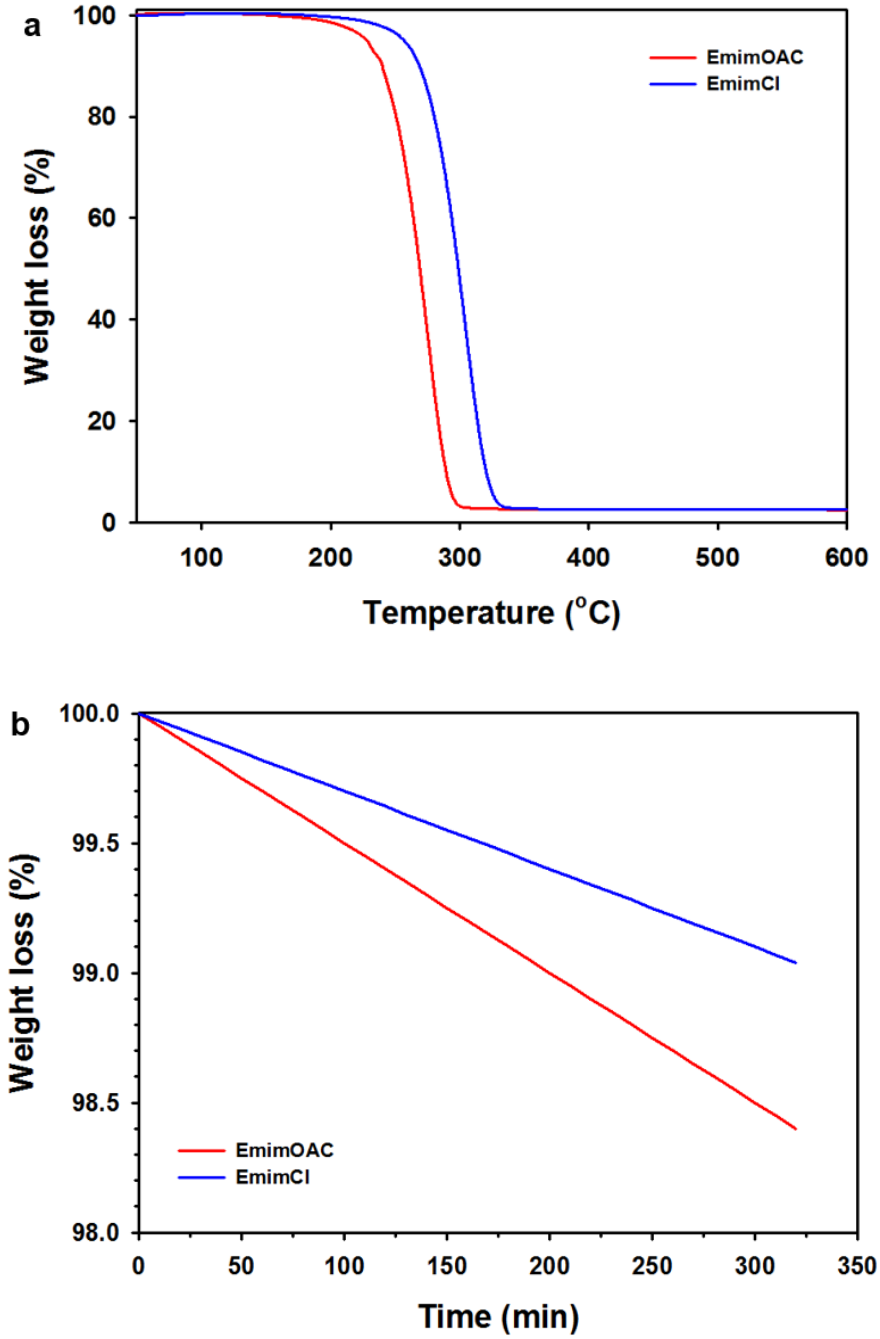

Figure 4-2. (a) TG curves and (b) isothermal TG analysis of EmimOAC and EmimCl at 120 ºC

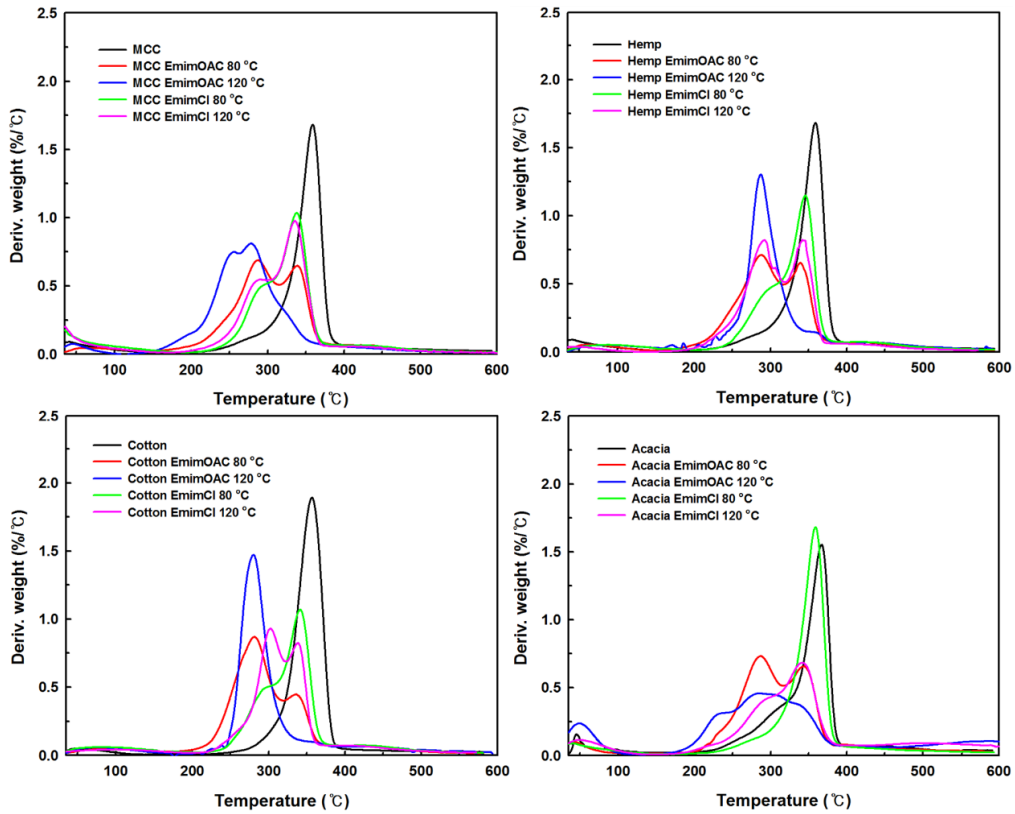

Figure 4-3. TG-DTG curves of MCC, cotton, hemp and acacia samples pretreated with EmimOAC or EmimCl at 80 ºC and 120 ºC

4.3.3. Rheological behavior of ionic liquid-pretreated lignocellulose

Figure 4-4 shows the viscosity changes of 4% solutions for the native and the pretreated samples. The viscosity represents the molecular mobility, such as chain rigidity, chain to chain interaction and molecular weight. The change of the quantitative value in the rheological behavior demonstrated the transition of physical interaction between lignocellulose molecules by ionic liquid-pretreatment. For the native lignocellulose solutions, a conventional polymeric fluid behavior with high viscosity was seen, exhibiting a Newtonian plateau at low shear rate and a shear thinning at high shear rate. This indicates that the lignocellulose solutions have chain entanglements or junction points between the lignocellulose molecules, meaning that the cellulose is constrained by the lignin and hemicellulose. For the pretreated lignocellulose solutions, the viscosity was rapidly decreased while the Newtonian plateau evidently became broad and shear-thinning shifted to a higher shear rate. The EmimOAC pretreated sample solution, in particular, exhibited a significant viscosity drop with Newtonian flow behavior. The shear-thinning shifting and the viscosity drop can be attributed primarily to molecular weight and a restricted chain effect. It resulted from the decreased molecular weight and the removal of lignin and hemicellulose as explained above.[32]

In order to fundamentally understand the flow behavior of the lignocellulose, the changes of storage (G') and loss (G'') moduli as a function of angular frequency for the lignocellulose solutions at 30 ºC were measured by time-temperature superposition principles and the results are shown in Figure 4-5. The data was shifted along the vertical axis by factor B to prevent data overlap, with the corresponding B value of -3, 0 and 3. For the native lignocellulose solutions, a plateau region and cross-over point between G' and G'' where the relations of $G' \propto \omega^2$ and $G'' \propto \omega^1$ hold, were observed. According to the rubber elasticity theory, this suggests the presence of an extensive quantity of entangled networks or crosslinking. The cross-over point at low frequency indicates a slow relaxation of the cellulose chain constricted by entanglement and crosslinking from neighboring chains and lignin. The Newtonian flow was observed in the EmimOAC pretreated lignocellulose solution. The curve of G'' was larger than that of G' in the whole ω-region where the measurements were carried out, indicating that the solutions were more like viscous liquids and suggesting that the intermolecular interaction was weakened by the pretreatment.

For all solutions, the ΔE_a value of the EmimOAC-pretreated lignocellulose solutions was lower than that of EmimCl-pretreated lignocellulose solutions as shown in Table 4-3. This indicates that EmimOAC pretreatment improved the chain mobility more efficiently than EmimOAC, which may also be

explained in terms of changes of molecular weight and chemical bonding. As described above, the cellulose decomposition and the removal of the lignin and hemicellulose occurred simultaneously during the ionic liquid pretreatment. The hydrolysis of the lignocellulose results in weakening of the entanglement and chemical bonding between cellulose and other components. The reduction of the intermolecular interaction by the pretreatment enhances the chain mobility, which may lead to improve the rearrangement and recrystallization of cellulose during precipitation.

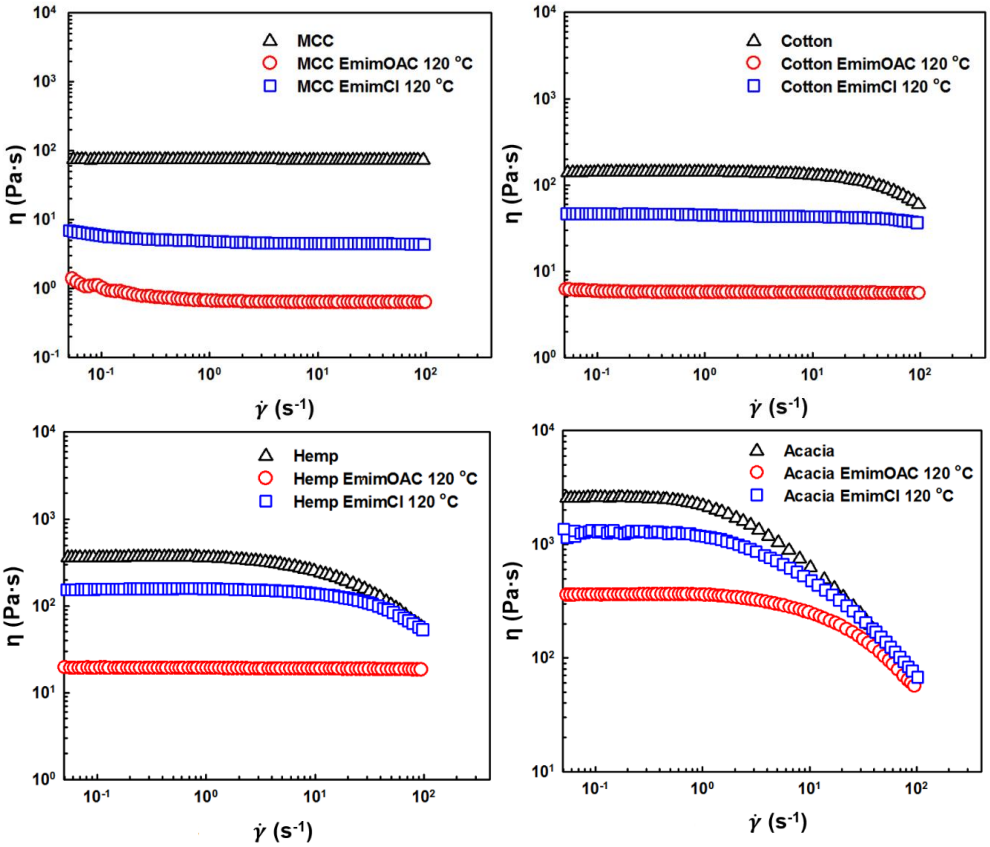

Figure 4-4. Steady shear viscosity change of MCC, cotton, hemp and acacia samples pretreated with EmimOAC or EmimCl at 120 ºC

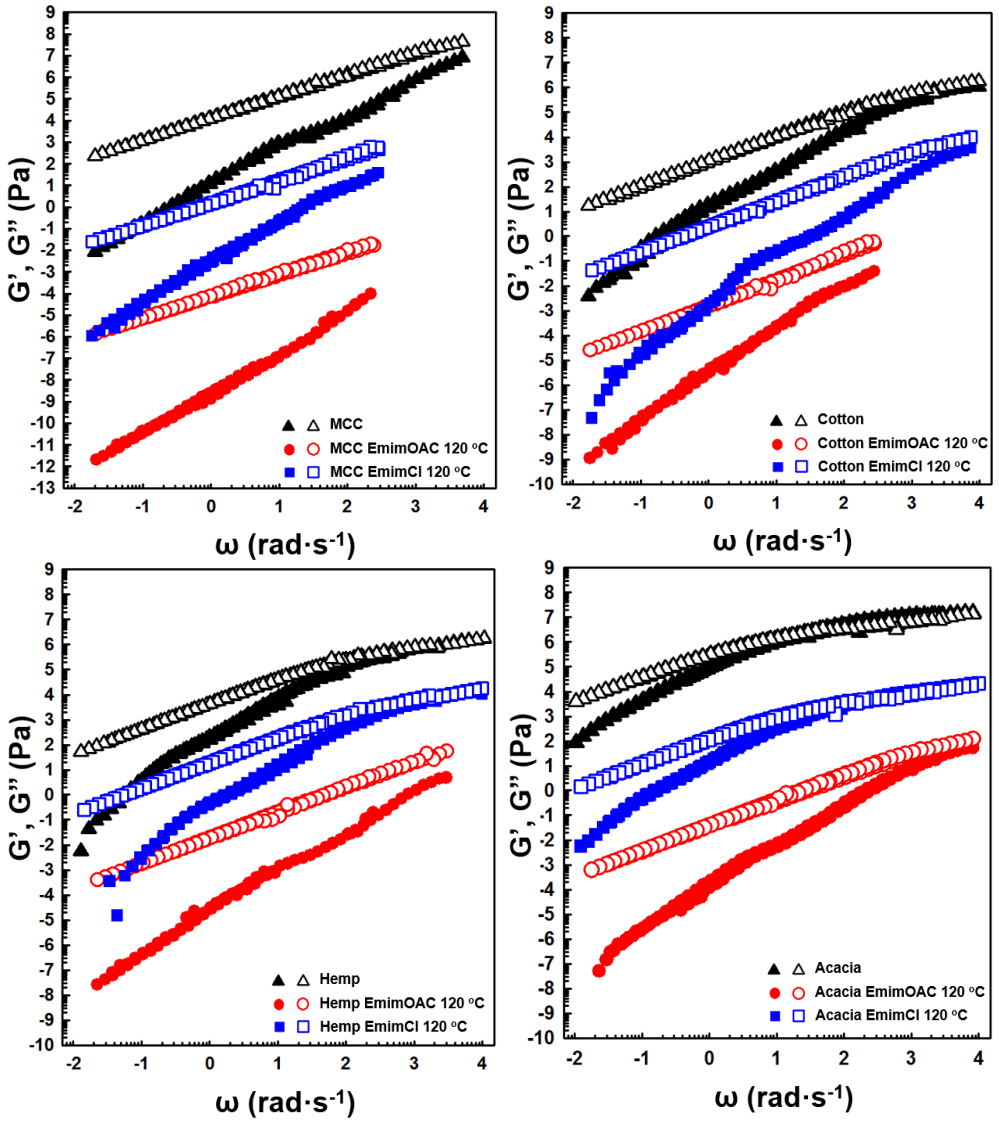

Figure 4-5. Dependence of dynamic storage modulus, *G*' (filled symbo ls), and loss modulus, *G*'' (open symbols), on reduced angular frequen cy for MCC, cotton, hemp and acacia samples pretreated with EmimO AC or EmimCl at 120 °C. These curves are shifted vertically to avoid overlap except for samples pretreated with EmimCl.

Table 4-3. Dependence of activation energy on pretreatment using different ionic liquids[a]

Sample	Activation energy (kJ/mol)		
	Raw	EmimOAc 120 °C	EmimCl 120 °C
MCC	49 ± 1	45 ± 1	47 ± 2
Cotton	54 ± 2	46 ± 1	50 ± 1
Hemp	57 ± 1	50 ± 1	54 ± 1
Acacia	59 ± 4	57 ± 1	57 ± 2

[a]Activation energy is the average of triplicates.

4.3.4. Microstructure of ionic liquid-pretreated lignocellulose

Figure 4-6 shows the X-ray diffraction patterns of the native and the pretreated biomasses. The main peak of four native samples was located around 22.5°, which indicates the distance between hydrogen bonds in cellulose I. There was a broad peak at ~ 16°, which is known to be a composite of two peaks, forms I_α (16.7° and 14.9°) and I_β (16.8° and 14.3°).[16] Results after pretreatment with the ionic liquid showed a significant influence on the crystalline structure and a strong dependence on the anion types present. With the exception of the acacia samples, the main peak at 22.5° disappeared and a new asymmetric doublet peak at 20.0° and 21.5° appeared while the broad peak at ~16° disappeared and a new peak was detected at 12° after the pretreatment with EmimOAC. This indicates that the samples were recrystallized as cellulose II, which is in accordance with the FT-IR results. For the EmimCl pretreatment, all biomasses substrates were recrystallized to the cellulose I or remained as an amorphous structure. The dependency of the transition on anion type can be explained by the lignin and hemicellulose content during the pretreatment. Pretreatment with EmimCl did not significantly affect the lignin and hemicellulose content due to the low solubility,[9] as dicussed in results of FT-IR and composition analysis. This indicates that the lignocellulose maintained a microfibril structure with a strong attachment between cellulose and other components (lignin and hemicellulose) described in previous studies,[33-35]

suggesting the microfibil formation of a network structure consisting of cellulose, lignin and hemicellulose, which reduced cellulose mobility and hindered recrystallization. The interruption of recrystallization by lignin can be also understood from a consideration of neat cellulose recrystallization under mechanical tension. Samayam *et al.*[16] reported that mechanical tension during recrystallization of cellulose hindered the transformation to cellulose II although cellulose I could readily be converted to cellulose II under low/no tension. In a similar way, the strong combination of cellulose, lignin and hemicellulose retains the crystalline structure of cellulose I despite the pretreatment, as shown in Figure 4-7. The conversion from cellulose I to II, therefore, requires sufficiently swollen or dissolved state to rearrange cellulose molecules. This speculation can be demonstrated additionally in terms of homogenously swollen structure derived from high temperature. The loosen structure by increasing temperature should allow that the cellulose molecules are easily diffused and moved in ionic liquid, indicating fast rearrangement for crystalline transition. The pretreatment at high temperature help the transition from cellulose I to cellulose II.

The XRD pattern responded to the increase of the pretreatment temperature by displaying different trends according to the ionic liquid. The cellulose II structure was still observed in the XRD curves of the cotton and the hemp treated with EmimOAC at higher temperature. However, the EmimCl-

pretreated samples showed smaller and broader peak intensity, indicating that the samples consisted almost of amorphous structure. This results from the differences in chain mobility as explained in the section dealing with rheological behavior. Compared to the chloride anion, the acetate anion effectively weakens intermolecular interaction during the pretreatment and improves the chain mobility, which in turns improves the chance for recrystallization. In addition to this, the sample pretreated with EmimCl still contained more lignin compared to the sample after treatment with EmimOAC (Table 4-2). Because the presence of bound lignin restricts range of motion of the cellulose chains, lignocellulose with more lignin has less likelihood of being recrystallized.

A difference of crystalline structure according to lignocellulose types was also observed. The crystalline structure of acacia (with a lignin content above 20 %) was different from the other substrates (with a lignin content below 10 %). Although the peak of acacia became broader, the peak location still remained at 16º and 22.5º, regardless of the ionic liquid type. This means that the pretreated acacia still had cellulose I structure rather than cellulose II. As mentioned in the composition results, lignin interrupts swelling and dissolution of cellulose and hinders the conversion of the crystalline structure from cellulose I to II.

The crystallinity index of each sample was calculated from the XRD curves

(Table 4-4).[36] Regardless of the ionic liquid type, the crystallinity index of the all pretreated samples rapidly decreased, corresponding to the results of the crystalline structure. As the pretreatment temperature increased, the crystallinity displayed a tendency that was dependent on the ionic liquid. The crystallinities of MCC, cotton and hemp treated by EmimOAC were slightly increased with the higher pretreatment temperature. In contrast to the results of the EmimOAC pretreatment, the crystalline structure of the cotton and the hemp pretreated with EmimCl almost disappeared completely at high temperature. As explained above, the swollen structure after treatment with EmimOAC was sufficient to result in an improvement of chain mobility which in turn, improved the crystallinity.

In the point of lignocellulose type, the different trends of the crystallinity change were observed according to the pretreatment temperature. The crystallinity of the lignocellulose containing high lignin content above 10% was decreased with increasing temperature, whereas the crystalline having small amount of lignin was well developed. In well swollen state of the cellulose, the crystalline conversion readily occurred after structural collapse by the pretreatment as described above. The transition can be facilitated with well development of the crystalline at high temperature. In the case of structure constrained strongly by lignin, the cellulose could be more collapsed at high temperature, but it is insufficient to convert crystalline form because external

network of lignin and cellulose is still sustained. This results suggest that the effect of temperature is differently applied to the lignocellulose consisting of thick cell wall such as acacia.

The difference in the crystallinity behavior could also be explained in terms of molecular weight. The cellulose pretreated with EmimOAC at high temperature underwent more extensive hydrolysis (Figure 4-3). The reduction in the molecular weight of cellulose decreased the inter chain entanglements (Figure 4-5). This improved the chain mobility during recrystallization; therefore, the cellulose had a higher probability of forming cellulose II with high crystallinity. As a result, the sample from the EmimOAC pretreatment contains cellulose II with high crystallinity. Previous studies showed that the crystalline structure of regenerated cellulose was dependent on hydrolysis conditions. Some researchers[37-40] have noted that while cellulose hydrolyzed under harsh condition had the possibility to achieve the cellulose II crystalline form, if mild conditions were used, recrystallization to cellulose II was more difficult. For the acacia sample pretreated with both EmimOAC and EmimCl, the crystallinity decreased as the temperature increased. Despite effective dissolution at high temperature, the cellulose chain was still strongly constrained by the remaining lignin and hemicellulose. The combination of cellulose and other components does not permit the cellulose to be rearranged to the crystalline form, which is in accordance with the results of the

rheological behavior and activation energy (Table 4-3 and Figure 4-5). This resulted in a decrease in crystallinity after pretreatment at high temperature.

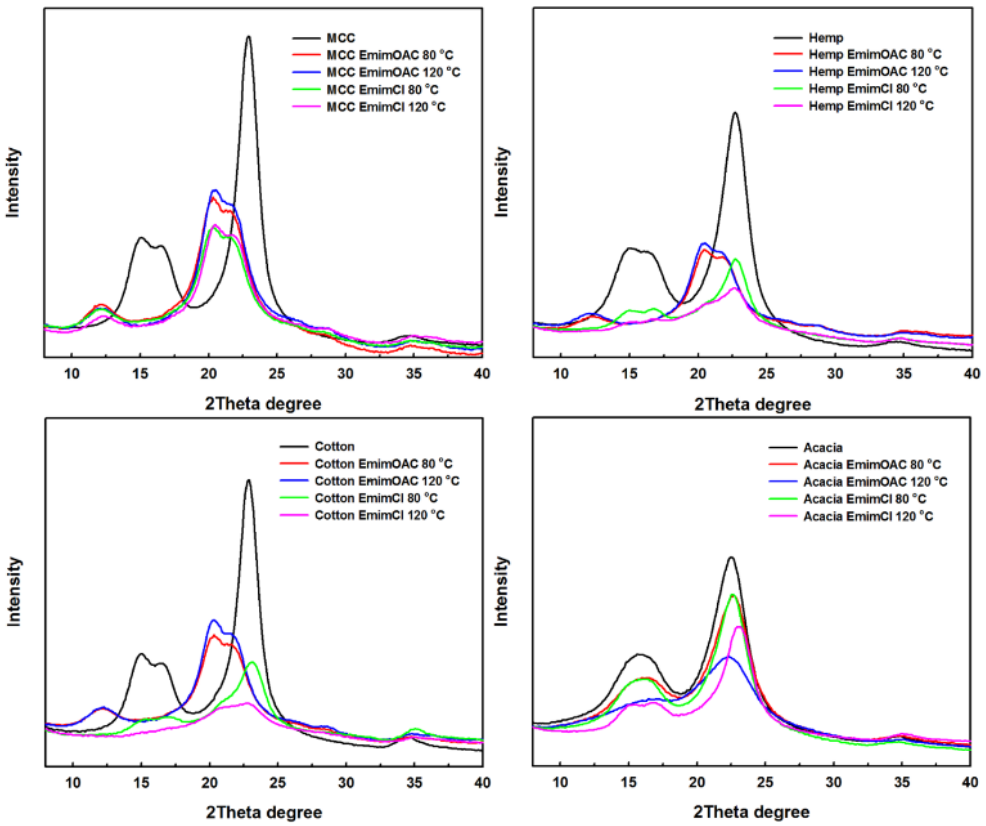

Figure 4-6. XRD patterns of MCC, cotton, hemp and acacia samples pretreated with EmimOAC or EmimCl at 80 ºC and 120 ºC

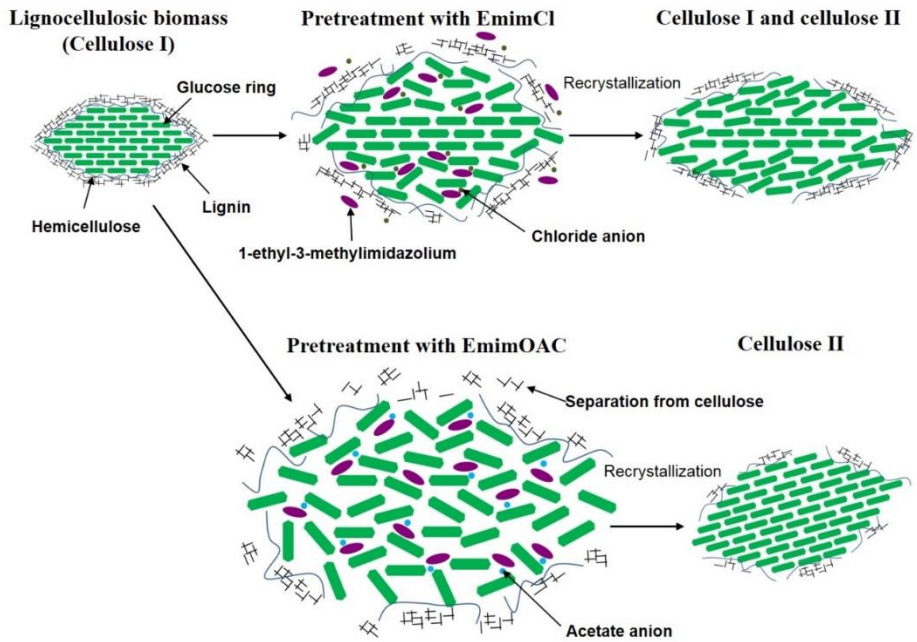

Figure 4-7. Schematic representation of pretreatment and recrystallizati on of lignocellulosic biomass showing the penetration of ionic liquid i nto the biomass and dissolution of cellulose. Depending on lignin cont ent and ionic liquid type, the cellulose recrystallizes to either uniform cellulose II or a mixed crystalline form including cellulose I and II.

Table 4-4. Crystallinity index (CrI) and crystalline structure of MCC, cotton, hemp and acacia samples pretreated with EmimOAC or EmimCl at 80 ºC and 120 ºC[a]

Sample	Raw		EmimOAC 80 ºC		EmimOAC 120 ºC		EmimCl 80 ºC		EmimCl 120 ºC	
	CrI	Structure	CrI	Structure	CrI	Structure	CrI	Structure	CrI	Structure
MCC	0.82 ± 0.01	Cell I[b]	0.72 ± 0.01	Cell II[c]	0.78± 0.02	Cell II	0.67 ± 0.02	Cell II	0.71 ± 0.03	Cell II
Cotton	0.79 ± 0.01	Cell I	0.59 ± 0.03	Cell II	0.64± 0.03	Cell II	0.55 ± 0.04	Cell I	-[d]	-
Hemp	0.75 ± 0.02	Cell I	0.62 ± 0.03	Cell II	0.64± 0.04	Cell II	0.54 ± 0.05	Cell I	-	-
Acacia	0.62 ± 0.03	Cell I	0.60 ± 0.05	Cell I	0.35± 0.07	Cell I	0.61 ± 0.05	Cell I	0.57 ± 0.05	Cell I

[a]All measurements are an average of triplicate samples.

[b]Cell I: cellulose I

[c]Cell II: cellulose II

[d]The calculation of the crystallinity index in cotton and hemp pretreated with EmimCl at 120 ºC was not available due to unclear diffraction patterns.

4.4. Conclusions

In this chapter, the compositional and structural transitions of three lignocelluloses pretreated with two different ionic liquid were investigated. The type of anion in the ionic liquid significantly influenced on the efficiency of the removal of lignin and hemicellulose. Compared to the chloride anion, the acetate anion was more efficient in the removal of lignin and hemicellulose as well as in the extraction of cellulose from lignocellulose. Concurrently, the thermal stability of the lignocelluloses pretreated with EmimOAC was significantly decreased, indicating the rapid reduction of the molecular weight. Due to the hydrolysis and separation of cellulose, lignin and hemicellulose, the intermolecular interaction of the lignocellulose became remarkably faster, accompanying the increase in chain mobility. The high pretreatment temperature enhanced the removal efficiency and cellulose hydrolysis, in agreement with the reduction of inter-chain constraints. Based on microstructural and rheological date, it was proposed to mechanism that cellulose II was formed from fully swelled lignocellulose with EmimOAC whereas cellulose I or mixture of cellulose I and II was formed from the material with the lignocellulose pretreated with EmimCl. The relaxation of lignocellulose microstructure accelerated chain rearrangement, which resulted in an improvement of structural regularity.

References

1. Ahn, Y.; Hu, D. -H.; Hong, J. H.; Lee, S. H.; Kim, H. J.; Kim, H., Effect of co-solvent on the spinnability and properties of electrospun cellulose nanofiber. *Carbohydrate polymers* **2012,** *89* (2), 340-345.
2. David, K.; Ragauskas, A. J., Switchgrass as an energy crop for biofuel production: A review of its ligno-cellulosic chemical properties. *Energy & Environmental Science*. **2010**, *3* (9), 1182-1190.
3. Hendriks, A.; Zeeman, G., Pretreatments to enhance the digestibility of lignocellulosic biomass. *Bioresource technology*. **2009,** *100* (1), 10-18.
4. Huber, G., W.; Iborra, S.; Corma, A., Synthesis of transportation fuels from biomass: chemistry, catalysts, and engineering. *Chemical reviews.* **2006,** *106* (9), 4044-4098.
5. Kumar, P.; Barrett, D. M.; Delwiche, M. J.; Stroeve, P., Methods for pretreatment of lignocellulosic biomass for efficient hydrolysis and biofuel production. *Industrial & Engineering Chemistry Research*. **2009,** *48* (8), 3713-3729.
6. Mosier, N.; Wyman, C.; Dale, B.; Elander, R.; Lee, Y.; Holtzapple, M., Features of promising technologies for pretreatment of lignocellulosic biomass. *Bioresource technology*. **2005**; *96* (6), 673-686.
7. Esteghlalian, A. R.; Mansfield, S. D.; Saddler, J. N., Cellulases: Agents

for Fiber Modification or Bioconversion? The effect of substrate accessibility on cellulose enzymatic hydrolyzability. *Progress in Biotechnology*. **2002**, *21,* 21-36.

8. Sannigrahi, P.; Kim, D. H.; Jung, S.; Ragauskas, A., Pseudo-lignin and pretreatment chemistry. *Energy & Environmental Science*. **2011**, *4* (4), 1306-1310.
9. Brandt, A,; Gräsvik, J,; Hallett, J. P.; Welton, T., Deconstruction of lignocellulosic biomass with ionic liquids. *Green chemistry*. **2013,** *15* (3), 550-583.
10. Laureano-Perez, L.; Teymouri, F.; Alizadeh, H.; Dale, B. E., Understanding factors that limit enzymatic hydrolysis of biomass. *Applied biochemistry and biotechnology*. **2005**, *124* (1-3), 1081-1099.
11. Li, C.; Knierim, B.; Manisseri, C.; Arora, R.; Scheller, H. V.; Auer, M. et al., Comparison of dilute acid and ionic liquid pretreatment of switchgrass: Biomass recalcitrance, delignification and enzymatic saccharification. *Bioresource Technology*. **2010**, *101* (13), 4900-4906.
12. Zhang, Y. H. P.; Lynd, L. R., Toward an aggregated understanding of enzymatic hydrolysis of cellulose: noncomplexed cellulase systems. *Biotechnology and bioengineering*. **2004**, *88* (7), 797-824.
13. Swatloski, R. P.; Spear, S. K.; Holbrey, J. D.; Rogers, R. D., Dissolution of cellose with ionic liquids. *Journal of the American Chemical Society*.

2002, *124* (18), 4974-4975.

14. Dadi, A. P.; Schall, C. A.; Varanasi, S., Mitigation of cellulose recalcitrance to enzymatic hydrolysis by ionic liquid pretreatment. *Applied Biochemistry and Biotecnology*: Springer; **2007**, p. 407-421.
15. Cheng, G.; Varanasi, P.; Li, C.; Liu, H.; Melnichenko, Y. B.; Simmons, B. A., et al., Transition of cellulose crystalline structure and surface morphology of biomass as a function of ionic liquid pretreatment and its relation to enzymatic hydrolysis. *Biomacromolecules*. **2011,** *12* (4), 933-941.
16. Samayam, I. P.; Hanson, B. L.; Langan, P.; Schall, C. A., Ionic-liquid induced changes in cellulose structure associated with enhanced biomass hydrolysis. *Biomacromolecules*. **2011**, *12* (8), 3091-3098.
17. Clough, M. T.; Geyer, K.; Hunt, P. A.; Mertes, J.; Welton, T., Thermal decomposition of carboxylate ionic liquids: trends and mechanisms. *Physical Chemistry Chemical Physics*. **2013**, *15* (47), 20480-20495.
18. Sun, N.; Rahman, M.; Qin, Y.; Maxim, M. L.; Rodríguez, H.; Rogers, R. D., Complete dissolution and partial delignification of wood in the ionic liquid 1-ethyl-3-methylimidazolium acetate. *Green Chemistry*. **2009**, *11* (5), 646.
19. Lee, S. H.; Doherty, T. V.; Linhardt, R. J.; Dordick, J. S., Ionic liquid-mediated selective extraction of lignin from wood leading to enhanced

enzymatic cellulose hydrolysis. *Biotechnology and bioengineering*. **2009**, *102* (5), 1368-1376.

20. Sluiter, A.; Hames, B.; Ruiz, R.; Scarlata, C.; Sluiter, J.; Templeton, D. et al., Determination of structural carbohydrates and lignin in biomass. Laboratory analytical procedure. **2008**.
21. Zhu, L.; O'Dwyer, J. P.; Chang, V. S.; Granda, C. B.; Holtzapple, M. T., Structural features affecting biomass enzymatic digestibility. *Bioresource Technology*. **2008**, *99* (9), 3817-3828.
22. McCormick, C. L.; Callais, P. A., Hutchinson Jr BH. Solution studies of cellulose in lithium chloride and N, N-dimethylacetamide. *Macromolecules*. **1985**, *18* (12), 2394-2401.
23. Nelson, M. L.; O'Connor, R. T., Relation of certain infrared bands to cellulose crystallinity and crystal lattice type. Part II. A new infrared ratio for estimation of crystallinity in celluloses I and II. *Journal of Applied Polymer Science*. **1964,** *8* (3), 1325-1341.
24. Naik, S.; Goud, V. V.; Rout, P. K.; Jacobson, K.; Dalai, A. K., Characterization of Canadian biomass for alternative renewable biofuel. *Renewable energy*. **2010**, *35* (8), 1624-1631.
25. Carrillo, F.; Colom, X.; Sunol, J.; Saurina, J., Structural FTIR analysis and thermal characterisation of lyocell and viscose-type fibres. *European Polymer Journal*. **2004**, *40* (9), 2229-34.

26. Du, H.; Qian, X., The effects of acetate anion on cellulose dissolution and reaction in imidazolium ionic liquids. *Carbohydrate research*. **2011**, *346* (13), 1985-1990.

27. Wang, H.; Gurau, G.; Rogers, R. D., Ionic liquid processing of cellulose. *Chemical Society Reviews*. **2012**, *41* (4), 1519-1537.

28. Fengel, D., IDEAS ON ULTRASTRUCTURAL ORGANIZATION OF CELL-WALL COMPONENTS. *Journal of Polymer Science Part C-Polymer Symposium*. **1971,** (36), 383.

29. Gazit, O. M.; Katz, A., Dialkylimidazolium ionic liquids hydrolyze cellulose under mild conditions. *ChemSusChem*. **2012**, *5* (8), 1542-1548.

30. Kang, Y.; Ahn, Y.; Lee, S. H. .; Hong, J.H.; Ku, M. K.; Kim, H., Lignocellulosic nanofiber prepared by alkali treatment and electrospinning using ionic liquid. *Fibers and Polymers*. **2013,** *14* (4), 530-536.

31. Calahorra, M.; Cortazar, M.; Eguiazabal, J.; Guzmán, G., Thermogravimetric analysis of cellulose: effect of the molecular weight on thermal decomposition. *Journal of Applied Polymer Science*. **1989**, *37* (12), 3305-3314.

32. Tamai, N.; Tatsumi, D.; Matsumoto, T., Rheological properties and molecular structure of tunicate cellulose in LiCl/1, 3-dimethyl-2-imidazolidinone. *Biomacromolecules*. **2004**, *5* (2), 422-432.

33. Lewin, M.; Goldstein, I. S., Wood structure and composition: M. Dekker; **1991**.
34. Plaza, A.; Montoro, P.; Benavides, A.; Pizza, C.; Piacente, S., Phenylpropanoid glycosides from Tynanthus panurensis: characterization and LC-MS quantitative analysis. *Journal of agricultural and food chemistry*. **2005**, *53* (8), 2853-2858.
35. Whetten, R. W.; MacKay, J. J.; Sederoff, R. R., Recent advances in understanding lignin biosynthesis. *Annual review of plant biology*. **1998**, *49* (1), 585-609.
36. Segal method is not used to directly compare crystallinities of cellulose I and II because crystallinity for cellulose II against cellulose I could be overestimated. Despite this possibility, the values obtained from our data clearly showed crystallinity was rapidly reduced during crystalline transition from cellulose I to II. It explicitly reflected that the original crystalline of the lignocellulose was considerably collapsed and less transformed to cellulose II. Considering all of these things, we used the Segal method to quantitatively analyze changing tendency of the crystallinity according to pretreatment conditions. Needless to say, Segal method was not applied for unclear diffraction patterns.
37. Cao, Y.; Li, H.; Zhang, Y.; Zhang, J.; He, J., Structure and properties of novel regenerated cellulose films prepared from cornhusk cellulose in

room temperature ionic liquids. *Journal of applied polymer science*. **2010**, *116* (1), 547-554.

38. Ding, Z. -D.; Chi, Z.; Gu, W. -X.; Gu, S. -M.; Liu, J. -H.; Wang, H. -J., Theoretical and experimental investigation on dissolution and regeneration of cellulose in ionic liquid. *Carbohydrate Polymers*. **2012,** *89* (1), 7-16.
39. Iguchi, M.; Aida, T. M.; Watanabe, M.; Smith, Jr. R. L., Dissolution and recovery of cellulose from 1-butyl-3-methylimidazolium chloride in presence of water. *Carbohydrate polymers*. **2013**, *92* (1), 651-658.
40. Zhang, H.; Wu, J.; Zhang, J.; He, J., 1-Allyl-3-methylimidazolium chloride room temperature ionic liquid: a new and powerful nonderivatizing solvent for cellulose. *Macromolecules*. **2005**, *38* (20), 8272-8277.

CHAPTER 5

Formation of cellulose nanoparticles with high uniformity and dispersity

5.1. Introduction

At the nanosized level, materials reveal extraordinary features mainly due to dangling bonds on enlarged surfaces. The revelation of these features has motivated many researchers to decrease the sizes of materials to the nanolevel and utilize their novel features for various applications, such as electronic, optical, magnetic and catalytic devices. However, the attractions between particles dramatically increase as the material size decreases. When particles decrease below 1 μm, van der Waals forces acting between particles overcome the forces of separation. Furthermore, particles smaller than 100 nm cannot be separated in any media even under intensive mechanical agitation. Aggregation is the main reason for the loss of the valuable features of nanoparticles and causes defects when the particles are used with polymers or various media. For stable dispersions of nanoparticles, the particle surfaces must be modified sterically and/or electrostatically.

Cellulose, the most abundant natural polymer on earth, shows remarkable properties for biomedical and eco-friendly applications when its size is reduced to the nanolevel. Cellulose nanoparticles exhibit beneficial properties as nanocarriers for bioactive molecules in nanobiotechnology and nanomedicine.[1-3] For the applications in biomedical fields, the surface charge is one of the most important factors affecting the performance of the nanoparticles. An increase in surface charge influences the colloidal stability in complex fluids, since the nanoparticles are prone to aggregation in aqueous media.[4] Conventionally, cellulose nanoparticles have been prepared by breaking the building blocks of cellulose fibrils using mechanical or chemical methods, such as homogenization,[5] acid hydrolysis,[6,7] and TEMPO oxidation.[8] However, these "top-down" methods exhibit difficultly to obtain a uniform morphology and to control the preparation conditions for different cellulose sources. Such problems encourage the development of a new nanofabrication method. Self-assembly and anti-solvent precipitation, as a "bottom-up" method, have been recently reported for the fabrication of nanoparticles of lignocellulosic materials.[9-11]

As reported in previous work[12], positive charges can be induced at the reducing end of cellulose during dissolution in an ionic liquid. This

finding provides the possibility for the preparation of aqueous dispersions of cellulose nanoparticles without any stabilizing agents or extra surface modifications. Although submicron particles from cellulose/IL solutions have already been reported by several researchers, [13,14] it is still unclear how the microstructures and the morphologies of the precipitated cellulose particles change or whether those particles are stable in aqueous media. These limitations encourage a novel approach to interpret the formation of cellulose nanoparticles on the molecular level. Such an approach would also provide a fundamental understanding of the relationship between the molecular properties and the particle formation during self-assembly and precipitation.

In this chapter, auto-dispersing nanospheres with a uniform diameter of 20 nm were successfully fabricated via molar mass control and self-assembly of cellulose chains in an IL. The fundamental understanding for reducing cellulose size was provided, including the preparation method of cellulose nanoparticle with improved dispersity in aqueous media. Without extra treatment, the particles were stably dispersed in aqueous media for longer than a month due to the positive charges on their surfaces. The comprehensive analysis demonstrated that the molar mass and the

imidazolium at the reducing ends simultaneously played important roles in increasing the crystallinity and the size uniformity.

5.2. Experimental

5.2.1. Preparation of cellulose nanoparticles

Cellulose for this study was kindly provided in a powder form by Hyosung Co. (Republic of Korea). The cellulose sample had a number average molar mass of 229 $kg \cdot mol^{-1}$ and a weight average molar mass of 283 $kg \cdot mol^{-1}$. The ionic liquid, 1-butyl-3-methylimidazolium chloride ($[C_4C_1Im][Cl]$), was purchased from Sigma Aldrich. All chemicals were used as-received without further purification. Cellulose powder was washed with deionized water and subsequently stored at 80 °C before dissolution. The cellulose was placed in a sealed reaction vessel and IL was added to form a 7 wt% solution. Samples were gently stirred at 200 rpm and heated at 90 °C for the desired time (24- 240 h). After dissolution, all solutions were immersed in a coagulation bath consisting of deionized water with vigorous agitation and repeatedly washed in the same manner. Cellulose nanoparticles were obtained by centrifugation from the cellulose/water suspension and dried in a vacuum oven for one day.

5.2.2. Morphological properties

The formation and the morphology of cellulose nanoparticles were examined using a TEM (LIBRA 120, Carl Zeiss) operating at 120 kV. The

average size and size distribution of cellulose nanocrystals were measured by dynamic light scattering (DLS), using a photal DLS-7000 spectrophotometer equipped with a photal GC-1000 digital autocorrelator (Otuka Electronics Co.). In this procedure, the wavelength of the argon laser was 488 nm and the scattering angle was 90° with respect to the incident beam. Intensity-average and number-average particle size distributions were analyzed by the conventional CONTIN algorithm to estimate the diameter of cellulose nanocrystals. Zeta potential was measured by a zeta potential analyzer with an ELS-8000 spectrophotometer (Otsuka Electronics Co.) using the Smoluchowski relationship.

5.2.3. Observation for reaction of imidazole at reducing end

The induced nitrogen content of cellulose nanocrystals was measured by elemental analysis (Flash2000, Thermo Fisher Scientific).

Measurements of ^{13}C NMR spectra of glucose/$[C_4C_1Im][Cl]$ (7 wt%) was performed on a Burker Advanced-400 spectrometer. The solutions used for the ^{13}C NMR experiments were prepared after dissolution for the desired time, and then inserted into a capillary tube containing DMSO-d_6. The samples were subjected to FTIR spectroscopy using a PerkinElmer spectrum BX spotlight spectrophotometer with a diamond Attenuated Total Reflectance attachment. Scanning was conducted from 4000 to 700 cm^{-1} with 64 repetitious scans averaged for each spectrum. The resolution was 4 cm^{-1} and interval scanning was 2 cm^{-1}.

5.2.4. Structural properties

The X-ray diffraction measurement was conducted using Powder X-ray diffraction (Ultima IV, Rigaku, Japan) with Cu K_α (λ = 0.154 nm) at 45 kV and 40 mA. A reflection-transmission spinner was used as a sample holder and the spinning rate was set at 10 rpm throughout the experiment. The patterns were collected in the 2θ range of 8-40° with a step size of 0.05° and an exposure time 180 s. To quantitatively estimate the

conversion to crystalline, the following empirical equation was adopted in the recrystallized cellulose substitutes; [9]

$$CrI = \frac{I_{total} - I_{am}}{I_{total}} \times 100$$

where, *CrI* is the crystallinity index for cellulose II structure, I_{total} is the diffraction intensity at the peak position at 21.5°, and I_{am} is the intensity at suitable locations for the amorphous background (16°).

Thermogravimetric analysis of the biomass samples was performed using a PerkinElmer instrument, Pyris Diamond TG/DTA. The thermal stability of 0.5 mg of each sample was investigated starting at room temperature to 700 °C at a rate of 10 °C·min^{-1}. The rate of purge gas (nitrogen) flow was controlled at 70 mL·min^{-1}.

5.3. Results and Discussion

5.3.1. Morphological change depending on molar mass

Figure 5-1 shows the schematic representation for the fabrication of cellulose nanoparticles from a cellulose solution (283 kg·mol^{-1}, 7 wt%) dissolved in 1-butyl-3-methylimidazolium chloride ([C_4C_1Im][Cl]). To control the molar mass, the dissolution time was changed from 24 to 240 h. During the dissolution and depolymerization, imidazolium was combined with the reducing ends, especially when the molar mass was smaller than 100 kg·mol^{-1}.[12] Cellulose nanoparticles were then obtained by precipitation of the prepared solution in deionized water. The molar mass and molecular size of the precipitated cellulose are summarized in Table 5-1.

The nanoparticles from the cellulose solutions with two different molar masses were observed by TEM (Figure 5-1, inserted images). Similar to typical cellulose nanocrystals,[6] the nanoparticles prepared from high molar mass cellulose (252 kg·mol^{-1}) had irregular and long-grain shapes with large sizes. The apparent aspect ratio of the cellulose nanoparticles was approximately 100 (average thickness and length were calculated as 10 nm and 100 nm, respectively). When the molar mass was decreased to 55 kg·mol^{-1}, the shapes of the precipitated particles changed from long

grains to spheres. The diameters of the cellulose nanospheres were measured as 20 nm. It is noteworthy that the diameters of the spheres were almost identical to each other, which, to the best of our knowledge, has not been reported yet. This result implies that the morphology and shape of the cellulose particles are strongly dependent on their molar mass.

Figure 5-2 shows the hydrodynamic radius (R_h) distribution of the cellulose nanoparticles from the high and low molar mass groups. For the high molar mass cellulose, the nanoparticles exhibited a large R_h with a broad distribution. Compared to the diameter measured from the TEM images, the R_h showed a larger value because of the agglomeration of the nanoparticles in aqueous media. However, the nanoparticles from the low molar mass group had a sharp and narrow peak located at 20 nm, indicating that the cellulose nanoparticles were stably isolated and dispersed in aqueous media without aggregation.

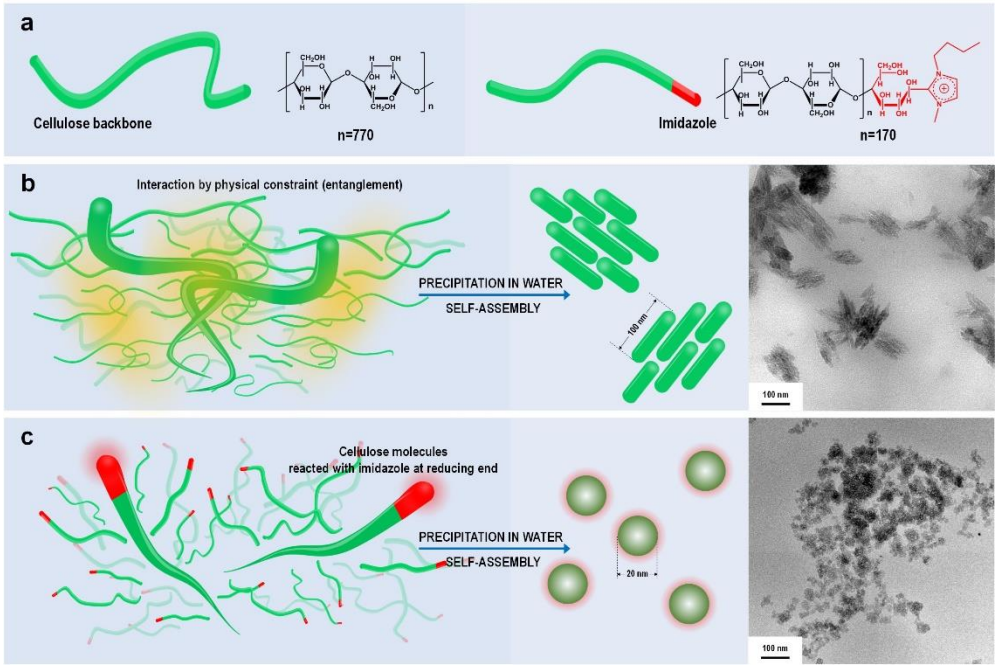

Figure 5-1. (a) Structure of cellulose molecules reacted with/without imidazole at the reducing end. (b) Nanograin formation of cellulose (252 $kg \cdot mol^{-1}$) after precipitation in water. (c) Nanosphere formation of cellulose (55 $kg \cdot mol^{-1}$) reacted with imidazole at the reducing end prepared under the same condition. The inserted images were obtained from TEM.

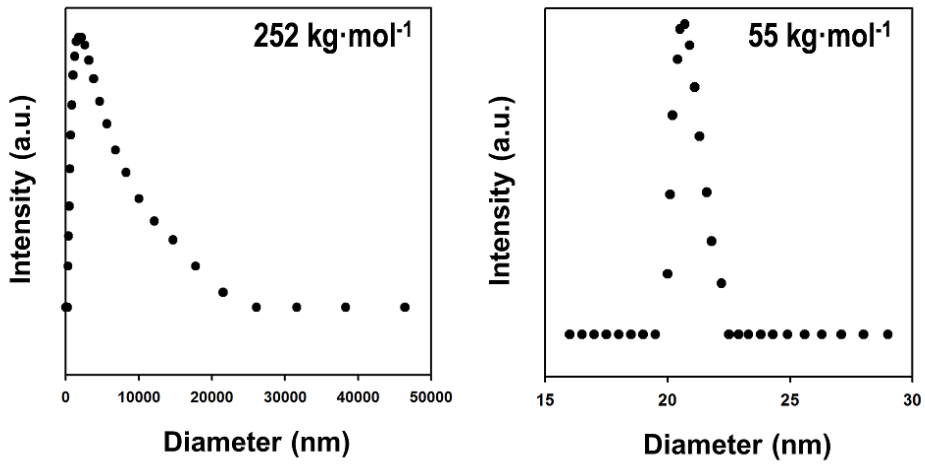

Figure 5-2. Size distribution curve for cellulose nanoparticles having different molar masses, as measured by DLS.

Table 5-1. Characterization data including the molar mass, radius of gyration and elemental analysis for cellulose from $[C_4C_1Im][Cl]$ after various dissolution time.

Dissolution time (h)	M_w ($kg \cdot mol^{-1}$)	R_g (nm)	Elemental analysis (wt%)		
			C	H	N
24	252	21.8	43.6	6.2	-
72	165	20.6	43.8	6.3	-
120	128	17.1	43.9	6.3	0.1
168	92	14.8	46.2	6.8	0.6
216	63	12.9	46.6	6.9	0.9
240	55	11.3	47.1	6.9	1.1

5.3.2. Reaction of imidazole at reducing end

The drastic decrease in hydrodynamic radius suggest that the dispersity of the nanoparticles was improved by the IL-catalyzed depolymerization. The improvement of dispersity is ascribed to the positive charge introduced by the reaction of imidazolium with the reducing ends, as described in a previous study.[12] To simulate the reactivity of the reducing ends of cellulose, we used a fitting model using D-glucose, which was ^{13}C-labeled at C-1 (>99%). Figure 5-3a shows the ^{13}C NMR spectrum of $[C_4C_1Im][Cl]$ and 7 wt% 1-^{13}C-D-glucose solutions dissolved with different dissolution times. The resonances at 99 and 93 ppm correspond to β-D-glucopyranose and α-D-glucopyranose, respectively.[15] After 120 h of dissolution, two new signals (at 65 and 67 ppm) were observed, which originated from the additional products formed by the electrophilic attack of C-2 of the imidazolium at the anomeric carbon. These signals became stronger in the solution dissolved for 240 h. This is solid evidence that the reaction of the imidazolium with the reducing ends was accelerated with longer dissolution times, i.e., with more severe depolymerization.

The physical and chemical structures of the nanoparticles were examined by Fourier transform infrared (FTIR) spectroscopy, as shown in Figure 5-3b. The pristine cellulose contained broad bands in the 3650-3000 cm^{-1}

region (corresponding to O–H stretching vibrations) and a peak at 2900 cm^{-1} (corresponding to –CH stretching vibrations). After precipitation from [C_4C_1Im][Cl], the –CH stretching vibrations shifted from 1033 to 1025 cm^{-1}, and the C–O–C vibration of the β-glycosidic linkage shifted from 897 to 894 cm^{-1}. These shifts can be explained in terms of the change of the torsion angles of the glycosidic linkage in the crystalline phase.[16] The peak at 1562 cm^{-1} (C-N stretching vibration) was observed for the nanoparticles precipitated from the extensively depolymerized cellulose. This result, along with the elemental analysis results (Table 5-1), confirms that the cellulose reducing ends were chemically combined with the imidazolium from [C_4C_1Im][Cl]. Although the pristine cellulose did not contain nitrogen, the precipitated cellulose had a small amount of nitrogen originating from the imidazolium. As suggested in other works,[17,18] ionic interactions between anions and cations can produce free protons and carbene intermediates in ILs. The reactive intermediates can further react with the reducing ends of cellulose. Since the formation of the carbene was simultaneously increased with proton generation, the reducing ends of the depolymerized cellulose had a higher chance to combine with the carbene.

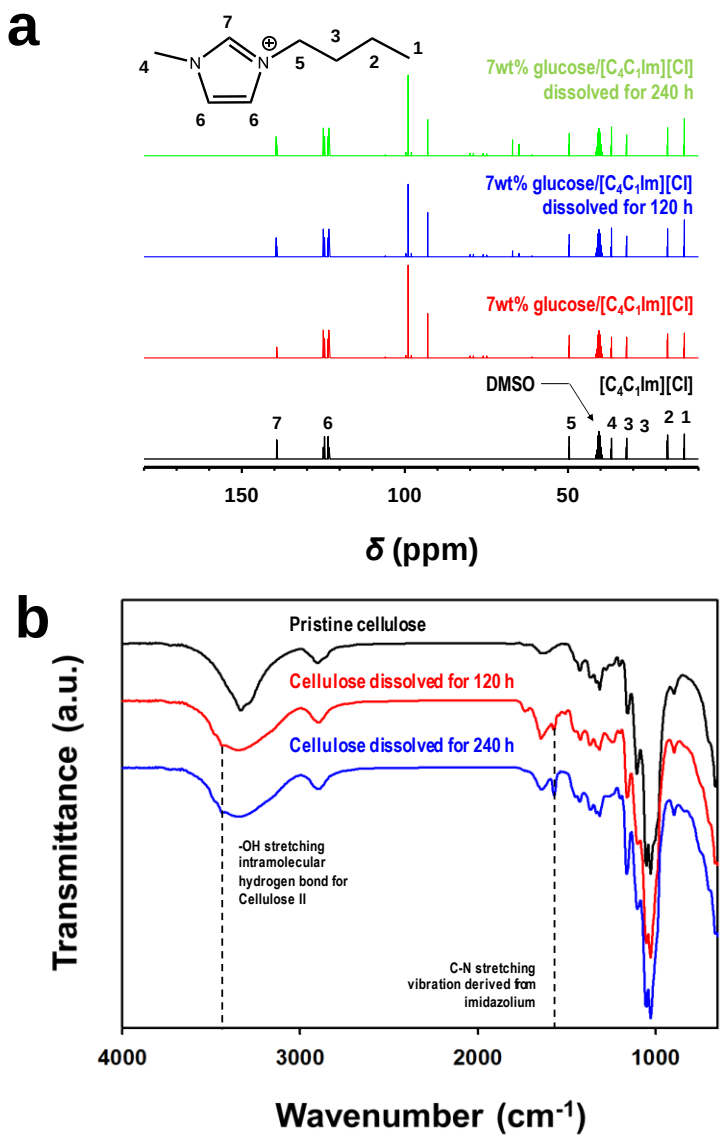

Figure 5-3. (a) ^{13}C NMR spectra of $[C_4C_1Im][Cl]$ and 7 wt% 1-^{13}C-D-glucose/$[C_4C_1Im][Cl]$ solutions acquired immediately after dissolution, after 120 h and after 240 h. (b) FTIR spectra of cellulose precipitated from $[C_4C_1Im][Cl]$ after dissolution for 120 and 240 h.

5.3.3. Dependence of molar mass on morphology

The above results strongly suggest that both the morphology and the dispersity are greatly dependent on the degree of depolymerization of cellulose in the IL. To confirm this dependence, we investigated the effect of the molar mass on the morphology using a series of cellulose samples with varying molar masses controlled by the dissolution time. Figure 5-4a shows the TEM images of the cellulose nanoparticles obtained from cellulose with molar masses ranging from 63 to 252 $kg \cdot mol^{-1}$. Above approximately 100 $kg \cdot mol^{-1}$, all particles had fibril-containing debris. As the molar mass was decreased below 92 $kg \cdot mol^{-1}$, the particles started to show spherical-like shapes with different diameters. When the molar mass was 63 $kg \cdot mol^{-1}$, the particles had spherical shapes with a 20 nm diameter. Compared to the particles with a molar mass of 92 $kg \cdot mol^{-1}$, the particles with a molar mass of 55 $kg \cdot mol^{-1}$ were individually isolated and had more uniform sizes. These changes of the shape and size can be quantitatively compared using an average R_h value measured by dynamic light scattering (DLS), as shown in Figure 5-4b. The average size of the nanoparticles slowly decreased with a decrease in the molar mass due to their poor dispersity. With a further decrease of the molar mass, the R_h value also sharply decreased, indicating the enhanced stability in the isolated state. This dispersity was strongly supported by the results of the aqueous

suspensions (Figure 5-4a, inserted image). When the molar mass decreased below 100 kg·mol^{-1}, the cellulose nanoparticles were stably dispersed for longer than a month without any extra agitation or surface modification. The dispersities and shapes of the nanoparticles are attributed to the particle charge, mainly located on the surface. As shown in Figure 5-4b, the zeta potential increased with a decrease in the molar mass, and its sign changed from negative to positive at 92 kg·mol^{-1}. The charge mainly originated from the carbene intermediate (i.e., imidazolium in this study) reacting with the reducing ends of the cellulose chain. In addition, the reaction between the reducing ends and imidazolium was facilitated when the cellulose chains were severely depolymerized below 100 kg·mol^{-1}.[12] Due to their strong positive charges, the reducing ends tend to locate on the particle surfaces during precipitation, similarly to micelles.[19] For an even distribution of the surface charge, it is more favorable for the particles to have spherical shapes.

The surface charge also had a significant influence on the particle size. The size of a particle is determined by the balance between the surface energy and the volumetric free energy of the system. The charge on a particle surface increases the surface energy, which results in a smaller particle size and uniform distribution. As a result, the size cannot be

reduced below a certain level (which is 20 nm in this study) due to an increase in the surface charge density with a smaller size. In contrast, the size increase was not preferable due to the higher surface energy. In addition to the energy balance, the phase separation and solvent exchange process also have considerable influences on the particle size. When the polymer solution is immersed in a non-solvent, the solution system is divided into polymer-rich and polymer-deficient phases with different sizes. The volume of the polymer-rich phase is increased by solvent exchange and fusion with the neighboring polymer-rich phase. In this system, the imidazolium on the boundary electrostatically hindered the fusion with the neighboring phase. As explained above, the imidazolium at the reducing ends is located on the boundary between the polymer-rich and polymer-deficient phases due to its strong positive charge. Apparently, the number of imidazolium compounds on the boundary were statistically proportional to the size of the polymer-rich phase. Therefore, the electrostatic hindrance of this fusion is more severe for the large phase than for the small phase. Furthermore, the reduced molecule length by depolymerization can contribute to forming a small particle size, corresponding to the value of the radius of gyration (R_g), as shown in Table 5-1. Due to the fusion between the small phases, the sizes of the synthesized particles are uniform with a diameter of 20 nm.

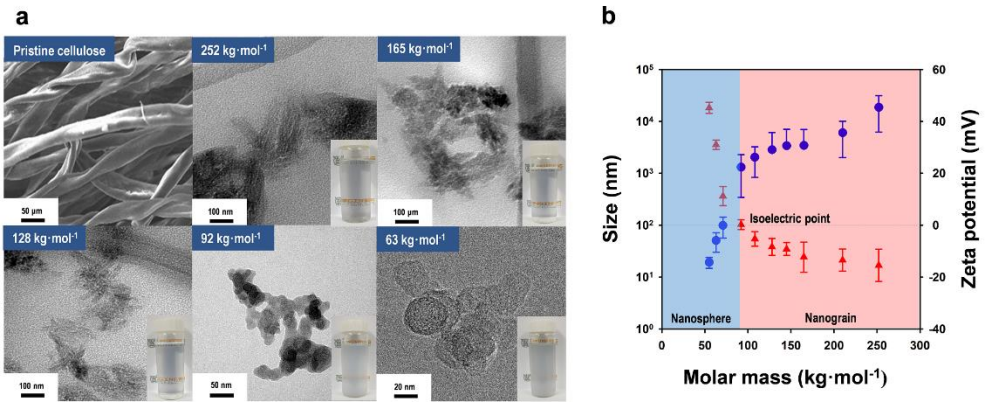

Figure 5-4. (a) SEM and TEM images of pristine cellulose and the cellulose nanoparticles with different molar masses controlled by the dissolution time. The inserted photographs represent the stability in aqueous media. All samples were adjusted to the same concentration of 0.1 wt%, and each image was captured for the suspension after a month of sample preparation. (b) Dependence of the molar mass on the average size and zeta potential; the circle and triangle symbols represent the average size and zeta potential, respectively.

5.3.4. Structural properties of cellulose nanoparticles

The reaction at the reducing ends with the imidazole also contributed to the microstructures of the cellulose nanoparticles. As shown in Figure 5-5a, the crystallinity significantly changed with a variation in the molar mass. Regardless of the molar mass, all nanoparticles had a cellulose II crystalline structure with corresponding characteristic peaks at 2θ = 11.7 ($11\bar{0}$), 20.1 (110), and 21.6 (020). The nanoparticles from the high molar mass cellulose did not exhibit a clear diffraction pattern, indicating the formation of a disordered structure during precipitation. The peaks became sharper and more intense when the particles had spherical shapes. The degree of crystallinity was higher than 85%, similar to cellulose in native pulp, when the molar mass was 55 $kg \cdot mol^{-1}$. The high crystallinity is due to the molecular interactions, chain conformation, and surface charge. As reported in a previous study,[20] hydrogen bonding between the hydroxyl groups, the extended chain conformation, and the independent chain movement drive the ordered chain alignment during precipitation. For cellulose with a high molar mass, the interaction and entanglement between the chains hindered the formation of ordered patterns. The reducing ends with imidazolium appeared to play an important role in the formation of an ordered structure. The positive charges at the chain ends hindered the random packing of the chain during solidification. The

repulsive forces at the chain ends helped the formation of an anti-parallel structure and resulted in a more ordered structure of cellulose II.

The thermogravimetric analysis (TGA) curves of the cellulose nanoparticles are presented in Figure 5-5b. There was a significant difference in their thermal degradation characteristics. The thermal degradation of pristine cellulose showed typical decomposition behavior with an onset degradation temperature of 300 °C. Another major thermal degradation event occurred at approximately 350 °C, which corresponds to the cracking of the organic compounds. The nanoparticles from the high molar mass cellulose exhibited slightly less thermal stability because of their loose structure (lower crystallinity).[21] Compared to the particles from the high molar mass cellulose, the spherical particles from the low molar mass cellulose started to decompose at lower temperatures. However, the residual weight loss at 700 °C was approximately 60%, which was less than the particles from the high molar mass group (~80%). Although comprehensive results were not provided in this study, the results suggest that the particles with higher crystallinity produced more stable bio-char, which has a higher carbon content.

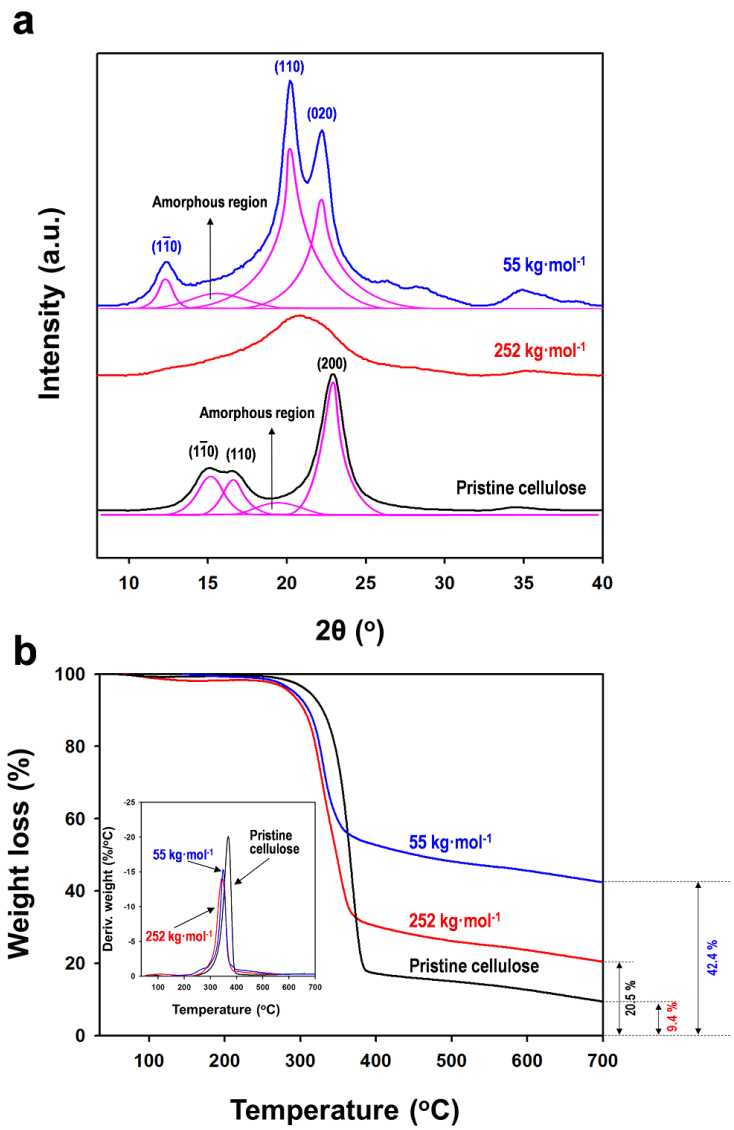

Figure 5-5. (a) XRD curves of pristine cellulose and the cellulose nanoparticles with different molar masses controlled by the dissolution time. (b) TGA curves and differential thermal analysis (insert) of pristine cellulose and the cellulose nanoparticles with different molar masses.

5.4. Conclusions

In this chapter, auto-dispersing cellulose nanospheres with a uniform size were successfully prepared via self-assembly of cellulose chains depolymerized in an IL. The dispersion of the nanospheres was stabilized due to inter-particle electrostatic repulsion, which originated from the imidazolium combining with the reducing ends. The balance between the surface energy and the surface charge determined the particle size and its distribution. In addition, the conformational change of cellulose played critical roles in determining the microstructures and sizes of the nanospheres.

References

1. Champion, J. A.; Mitragotri, S. Role of target geometry in phagocytosis. *Proceedings of the National Academy of Sciences of the United States of America* **2006**, 103, 4930-4934.
2. Eyley, S.; Thielemans, W. Surface modification of cellulose nanocrystals. *Nanoscale* **2014**, *6*, 7764-7779.
3. Edgar, K. J.; Heinze, T.; Buchanan, C. M. *Polysaccharide Materials: Performance by Design.* American Chemical Society: 2009.
4. Fröhlich, E. The role of surface charge in cellular uptake and cytotoxicity of medical nanoparticles. *Int J Nanomedicine* **2012**, *7*, 5577-91.
5. Liu, D.; Chen, X.; Yue, Y.; Chen, M.; Wu, Q. Structure and rheology of nanocrystalline cellulose. *Carbohydrate Polymers* **2011**, *84*, 316-322.
6. Lin, N.; Huang, J.; Dufresne, A. Preparation, properties and applications of polysaccharide nanocrystals in advanced functional nanomaterials: a review. *Nanoscale* **2012**, *4*, 3274-3294.
7. Zhang, J.; Elder, T. J.; Pu, Y.; Ragauskas, A. J. Facile synthesis of spherical cellulose nanoparticles. *Carbohydrate Polymers* **2007**, 69 (3), 607-611.

8. Isogai, A.; Usuda, M.; Kato, T.; Uryu, T.; Atalla, R. H. Solid-state CP/MAS carbon-13 NMR study of cellulose polymorphs. *Macromolecules* **1989**, *22*, 3168-3172.
9. Qian, Y.; Qiu, X.; Zhong, X.; Zhang, D.; Deng, Y.; Yang, D.; Zhu, S., Lignin reverse micelles for UV-absorbing and high mechanical performance thermoplastics. *Industrial & Engineering Chemistry Research* **2015**, 54, 12025-12030.
10. Richter, A. P.; Brown, J. S.; Bharti, B.; Wang, A.; Gangwal, S.; Houck, K.; Hubal, E. A. C.; Paunov, V. N.; Stoyanov, S. D.; Velev, O. D., An environmentally benign antimicrobial nanoparticle based on a silver-infused lignin core. *Nature nanotechnology* **2015**, 10, 817-823.
11. Zhao, W.; Simmons, B.; Singh, S.; Ragauskas, A.; Cheng, G., From lignin association to nano-/micro-particle preparation: extracting higher value of lignin. *Green Chemistry* **2016**, 18, 5693-5700.
12. Ahn, Y.; Song, Y.; Kim, H.; Kwak, S.-Y. Formation of cellulose-carbene complex via depolymerization in ILs: Dependence of IL types on kinetics, conformation and dispersity. *Carbohydrate Polymers* **2017**, *159*, 86-93.
13. Chang, P. R.; Jian, R.; Zheng, P.; Yu, J.; Ma, X. Preparation and properties of glycerol plasticized-starch (GPS)/cellulose nanoparticle (CN) composites. *Carbohydrate Polymers* **2010**, *79*, 301-305.

14. Li, J.; Wei, X.; Wang, Q.; Chen, J.; Chang, G.; Kong, L.; Su, J.; Liu, Y. Homogeneous isolation of nanocellulose from sugarcane bagasse by high pressure homogenization. *Carbohydrate Polymers* **2012**, *90*, 1609-1613.
15. Potthast, A.; Röhrling, J.; Rosenau, T.; Borgards, A.; Sixta, H.; Kosma, P. A novel method for the determination of carbonyl groups in cellulosics by fluorescence labeling. 3. Monitoring oxidative processes. *Biomacromolecules* **2003**, *4*, 743-749.
16. Carrillo, F.; Colom, X.; Sunol, J.; Saurina, J. Structural FTIR analysis and thermal characterisation of lyocell and viscose-type fibres. *European Polymer Journal* **2004**, *40*, 2229-2234.
17. Du, H.; Qian, X. The effects of acetate anion on cellulose dissolution and reaction in imidazolium ionic liquids. *Carbohydrate research* **2011**, *346*, 1985-1990.
18. Ebner, G.; Schiehser, S.; Potthast, A.; Rosenau, T. Side reaction of cellulose with common 1-alkyl-3-methylimidazolium-based ionic liquids. *Tetrahedron Letters* **2008**, *49*, 7322-7324.
19. Duncan, R. The dawning era of polymer therapeutics. *Nature reviews Drug discovery* **2003**, *2*, 347-360.
20. Ahn, Y.; Song, Y.; Kwak, S.-Y.; Kim, H. Highly ordered cellulose II crystalline regenerated from cellulose hydrolyzed by 1-butyl-3-methylimidazolium chloride. *Carbohydrate polymers* **2016**, *137*, 321-327.

21. Rodrigues Filho, G.; de Assunção, R. M.; Vieira, J. G.; Meireles, C. d. S.; Cerqueira, D. A.; da Silva Barud, H.; Ribeiro, S. J.; Messaddeq, Y. Characterization of methylcellulose produced from sugar cane bagasse cellulose: Crystallinity and thermal properties. *Polymer degradation and stability* **2007**, *92*, 205-210.

CHAPTER 6

Preparation of cellulose NF membrane for separation of free fatty acid and chlorophyll in extra virgin olive oil

6.1. Introduction

The traditional Mediterranean diet is characterized by the preferential consumption of vegetables, legumes, fruit, nuts, and cereals, and olive oil is the main dietary fat. Extra virgin olive oil (EVOO) is obtained from pressing Olea europea (olive) fruit.[1] The characteristic aroma, taste and color of this oil distinguish it from other edible vegetable oils. The excellent organoleptic and nutritional properties of EVOO and the current tendency of consumers to select minimally processed food, have prompted a re-assessment of its consumption in daily diet.[2] Furthermore, the increase in EVOO intake is related to the healthier characteristics of some of its minor constituents, such as phenolic compounds.[3] Because of the diverse benefits of EVOO, Mediterranean countries have commonly used EVOO to cook, and frying is an important technique employed in industrial food preparation. More recently, the consumption of olive oil blended with other refined vegetable oils is increasing for use as frying

oil, due to economic reasons and customer desire for taking healthy components.[4]

EVOO quality is related to its composition, and the free fatty acid (FFA) content is one of the main parameters to evaluate EVOO quality in frying condition.[1, 5-6] Freshly produced EVOO is naturally turbid, containing micro-droplets of water and solid particles from the olive fruits.[7] The polar phase content may accelerate a series of reactions, namely, hydrolysis, oxidation, isomerization and polymerization. Among various routs of oxidative and hydrolytic degradation processes, several papers[8-10] have been reported on the prooxidant action of FFA. It seems to be exerted by the carboxylic molecular group of FFA, which accelerates the rate of decomposition of hydroperoxides.[10] Oxidation leads to the formation of volatile products and a dramatic decrease in the smoking point, which change the initial flavor of EVOO and decrease its nutritional quality, possibly leading to the formation of toxic products.[11-12] Furthermore, chlorophyll is a critical ingredient in frying. During the olive pressing process, chlorophyll is readily included in EVOO, resulting in greenish color. Chlorophyll can thermally decompose into the pigment pheophytin, resulting in a dull, dark-colored oil. This pigment also contributes to an off-flavor and may promote oil oxidation, thus reducing the oil stability.[13]

Food manufacturers commonly treat crude olive oils with various process to improve their nutritional quality and cooking performance. However, those processes are not always completely effective, and some processes remove the problematic ingredients along with the minor ingredients that represent flavor, taste and health properties. Thus, developing suitable material and process to remove the problematic ingredients in EVOO while minimizing the loss of beneficial and essential ingredients is necessary.

Membrane technology is emerging as a viable process for molecular separation that offers numerous benefits over the conventional processes.[14-15] It consumes lower energy, generates smaller footprint, and can be operated in a much simpler way. In particular, nanofiltration (NF) is developed for molecular separation on the basis of size and charge differences. Beyond drinking water production and wastewater treatment, NF technology has also been applied for the separations carried in organic solvents such as in the pharmaceutical,[16-17] petroleum and food industry.[18] It is essential to produce membranes with sufficiently high flux and rejection, but it is at least as important to identify an environmentally friendly and simple manufacturing process.

Cellulose has emerged as an indispensable membrane material due to its abundant availability, low cost, and environment benignancy. However,

this unique molecular architecture also leads to cellulose insolubility in the common organic solvents. Only very few usable solvents are known and those are often highly reactive, toxic or impractical for industrial use. Moreover, cellulose membranes typically have meso- or macro-pores,[19-26] making them suitable only for ultra- or microfiltration. In previous chapter, it was proposed that the morphology of cellulose can be controlled by the cellulose molar mass of the cellulose in an ionic liquid. Compaing to the typical cellulose membranes, cellulose formed from ionic liquid is expected to possess micropores suitable for nanofiltration that can separate from molecular level.

In this study, a simple method is provided to prepare cellulose NF membrane from cellulose hydrolyzed in ionic liquid, and then it was applied to the selective separation of FFAs and chlorophyll from EVOO. To verify the effects of pore size and surface functionality, a series of cellulose NF memebrane with various pore size was prepared, and then they were functionalized by tosyl and amine group, in turns. The fatty acid composition and anti-oxidant content (total phenols and tocopherol) were analyzed to demonstrate the selective separation of the amino-functionalized cellulose NF membrane without a component conversion. To confirm the thermal stability, we observed the smoking point of EVOO filtrated by cellulose NF memebrane and compared the smoking point

with that of crude and physically refined EVOO. This study can provide a facile method for enhancing thermal stability of EVOO and thus aid the development of better treatment process for crude oils using cellulose NF membrane.

6.2. Experimental

6.2.1. Materials

The crude and physically refined EVOO (Piqual, Catalunya) were supplied by Genesis bbq (Korea). Cellulose was dried at 100 °C for 3 h under vacuum before use. 1-butyl-3-methylimidazolium chloride (purity≥ 99%) were purchased from BASF (Germany). All other reagents were of analytical grade and used without pretreatment.

6.2.2. Preparation of cellulose NF membrane

Cellulose powder with controlled molar mass (92, 165 and 252 kg/mol) was washed with deionized water and subsequently stored at 80 °C before dissolution. The cellulose was placed in a sealed reaction vessel and IL/1-methylimidazole was added to form a 12 wt% solution. Samples were gently stirred at 200 rpm and heated at 90 °C for the desired time (24- 240 h). After dissolution, the homogeneous viscous solution was transferred to 3 appropriate molds and sealed individually. All samples underwent cyclic freeze-thaw treatment. The typical Freeze-thaw process is described as follows: freeze-thaw treatment was frozen at -20 ºC for 10 h; then, it was vacuum-thawed for 6 h to room temperature. The required cryogenic temperature in this process was <17 ºC and the thawing temperature ought to be >17 ºC. After

undergoing freeze-thaw treatment, The dope solution was cast on a glass plate with a 200 μm gap casting knife and the glass plate then immediately immersed into a DI water bath as the nonsolvent. The resulting membrane was rinsed with DI water to remove the solvent. The NF membrane prepared according to their molar masses are referred to as CNM92, CNM165 and CNM252, respectively..The overall procedure used to prepare the cellulose nanomemebrane is schematically illustrated in Figure 6-1.

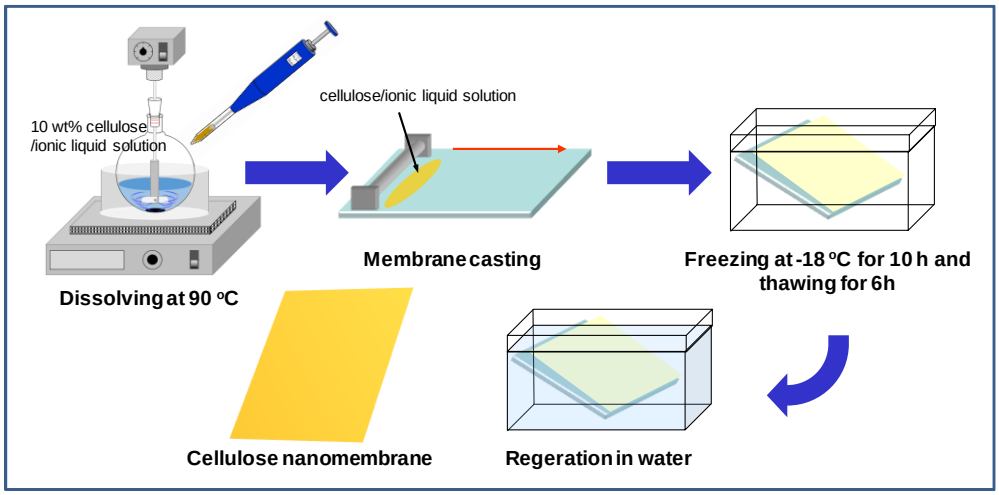

Figure 6-1. Schematic representation of preparation procedure for cellulose NF membrane via freeze-thaw process

6.2.3. Tosylation of cellulose

The prepared cellulose NF membrane was emerged in DI water. p-toluenesulfonyl chloride(37.8 mmol) and polyethylene glycol alkyl-(C_{11}–C_{15}) ether (12.3 mmol) were added to the cellulose/water mixture. After 15 min a modification of the texture of the reaction mixture occurred. The mixture was stirred vigorously at 25 °C for 5 h. The product washed three times with ethanol, and dried under vacuum at 60 °C. The substituted NF membrane are referred to as CNM-tosyl92, CNM-tosyl165 and CNM-tosyl252, respectively.

6.2.4. Synthesis of 6-deoxy-6-(ω-aminoethyl)amino cellulose

The tosyl cellulose (1.6 mmol, DS_{tos} = 0.95) was emerged in DMF. Ethylene diamine (40.5 mmol, 25 mol per mol modified AGU) were added at 100 °C. The mixture was allowed to react for 6 h at 100 °C under stirring. After cooling to room temperature, the product was washed three times with acetone and two times with ethanol and dried at 60 °C under vacuum. The amino-functionalized NF membrane are referred to as CNM-$NH_2$92, CNM-tosyl-$NH_2$165 and CNM-tosyl-$NH_2$252, respectively.

6.2.5. Characterizations

NMR spectra were acquired at 25 °C in deuterated dimethylsulfoxide (DMSO-d_6) or D_2O using Bruker Avance 250 MHz and 400 MHz spectrometers. ^{13}C NMR spectra were recorded with at least 10,000 scans and a sample concentration of 50 mg mL^{-1}. FTIR spectra were recorded on a Nicolet Avatar 370 DTGS spectrometer. A CHNS 932 Analyzer (Leco) was used for elemental analyses. Field-emission scanning electron microscopy (FE-SEM) was employed to observe the morphology of cellulose NF membrane. High-resolution transmission electron microscopy (HR-TEM) experiments were conducted using a JEM-3010 microscope operated at 300 kV to observe the pore structure, and pore size of the cellulose NF membrane. N_2 adsorption-desorption isotherms were measured with a 3FLEX Micromeritics instrument at liquid nitrogen temperature. The specific surface area of the samples was calculated utilizing the Brunauer-Emmett-Teller (BET) method. Using the Barrett-Joyner-Halenda (BJH) model, the pore volumes and pore size distribution curves were obtained.

To further confirm the pore size distribution of cellulose NF membrane, a capillary flow porometer was employed. Pore properties was calculated from the measured differential pressures and gase flow rates. The correlation between the pore size and applied pressure can be expressed by Young-Laplace equation:

$$R = \frac{2\gamma}{\Delta P}\cos\theta$$

where, R is radius of the believed capillary-shaped pore, γ is the surface tension at the liquid/air interface (here, γ = 15.9 $\times$ 10^{-5} N/cm), and θ is the contact angle. When an air bubble penetrates through the pore, its radius is equal to that of the pore and if wetting of the polymer by the solvent is good, then θ is 0° (cos θ = 1).

6.2.6. Filtration test

Filtration efficiency of cellulose NF membrane for free fatty acid and chlorophyll was measured using an Amicon 8050 dead-end stirred cell (Millipore corp.) connected to a pressure vessel filled with crude EVOO. It can work in a pressure operating range of 100–1000 kPa, temperature up to 60 ^{o}C and a recirculation rate from 1 to 6 $ms^{-}1$. The duration of each test normally varied from one to three hours. Permeate and concentrate samples were taken and an average sample was analyzed.

6.2.7. Characteristic analysis for EVOO

The measurement of the FFA concentration, peroxide values and K232 and K270 spectrophotometric indices were carried out according to the European Official Methods of Analysis Regulation 2568/91. K232 (dienes conjugates) and K270 (trienes conjugates) were the extinction coefficients calculated respectively on the absorption at 232 and 270 nm wavelength by using a 1% solution of oil in isooctane and a path length of 1 cm.

The chlorophyll content in the EVOO was determined using the American Oil Chemists' Society (AOCS) method Cc13d-55. The chlorophyll concentration was calculated by the following Eq. (1).

$$\text{Chlorophyll}_a \text{ content (ppm)} = A_{670} - \frac{A_{630} + A_{710}}{2 \times 0.0965} \qquad (1)$$

where A630, A670 and A710 are the absorbance values corresponding to wavenumbers 630, 670 and 710 nm, respectively.

6.3. Results and Discussion

6.3.1. Morphological change depending on molar mass

The compactness degree of the cross-linking network can be adjusted by different molar mass of cellulose. The morphology of the cellulose NF membrane according to SEM images is shown in Figure 6-2. The microstructure of the specimen with large molar mass (CNM252) shows no evidence of cellulosic network structure. In contrast, As molar mass decreased, the uncollapsed columnar NF membrane (CNM165) showed a porous structure. Additionally, the distribution of the pores became denser with the decrease in cellulose molar mass (CNM92). However, the microporous structure disappeared, and a dense film-like structure, which is associated with common open-pore web structure, was observed from the samples having low molar mass. As presented in SEM image of CNM92 in Figure 6-2, the film-like structure rather than a network structure was observed. The construction of cellulose fibril networks should be ascribed to the formation of the IL crystal during the freezing process.

The TEM images of the cellulose fibril networks of CNM165 and CNM92 are compared. Bottom images in Figure 6-2 shows that the net-shaped structure of CNM165 contained fewer layers, and TEM images of CNM92 presents compacter networks with multiple layers with the decrease in molar mass.

TEM images are in good agreement with the morphology shown in SEM results. This confirms that molar mass of cellulose play an important role in the formation of physical cross-linking network.

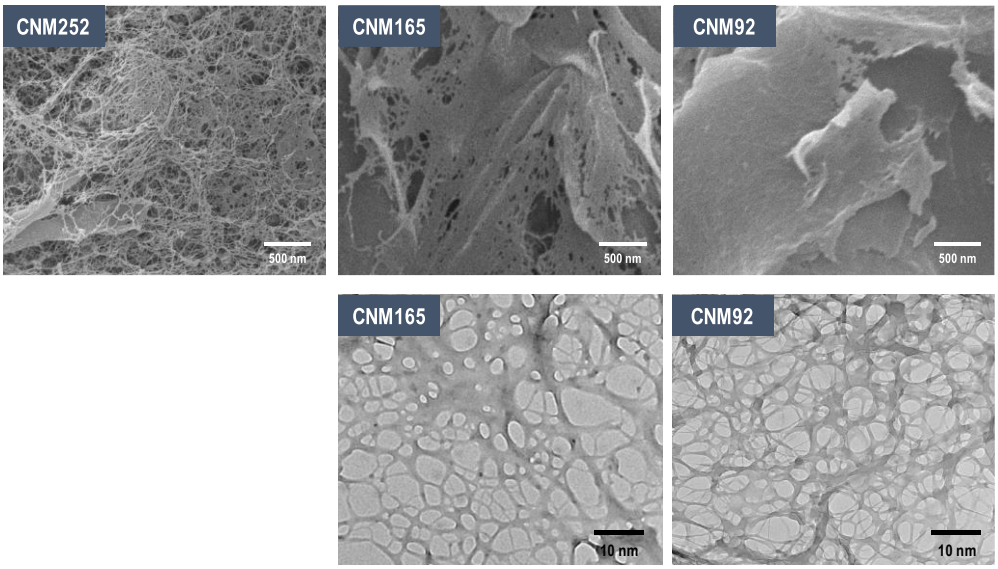

Figure 6-2. SEM (upper) and TEM (bottom) images of cellulose nanomemebrane with different molar mass

6.3.2. Tosylation and amination of cellulose

Tosylation of cellulose having different pore structure was analyzed using ^{13}C NMR in DMSO-d_6 at 25 °C,as shown in Figure 6-3. Signals for the *p*-substituted toluene ring and the methyl group of the tosyl moiety can be found at 128 and 146 ppm, and 22 ppm,[27] respectively. As DS_{tos} indicating a tosylation of the primary hydroxyl group, increased, the signal intensity at 69 ppm became strong. Because the cellulose tosylation occurs mainly at the primary hydroxyl group, the signal intensity presenting an unmodified C-6 atom (61 ppm) was decreased. Signal for chlorination at position 6 (45 ppm) disappeared, while The signals for the C atoms of the secondary hydroxyl groups appear at ～73 ppm. A new signal appeared at 78 ppm in tosyl celluloses 7 and 9, indicating secondary positions modified with tosyl moieties. The cellulose tosylation resulted in a splitting of the signal C-1 (C-1′). The FT-IR spectra of tosylated cellulose clearly indicate the introduction of tosyl groups into the polysaccharides (Figure 6-5). With increasing DS_{tosyl}, different signals emerged that can be attributed to the sulfonic acid ester group and to the p-substituted toluene ring.

As shown in Figures 6-3, the tosylation of cellulose would be closely related to the pore size of the NF membrane. In the case of the cellulose NF membrane with the large pore size among samples, the DS_{tosyl} value was 0.5. For CNM-

92, the DS value is observed to increase to 1.7. These results would be considered to be due to the amount of hydroxyl groups exposed on the surface. With decreasing molar mass, fibrillated cellulose exposes more hydroxyl groups to the surface, thereby providing more opportunities to contact the tosylation agent and increasing the DS_{tosyl} value. This point is dicussed later in section 6.3.3

It has been confirmed that tosyl cellulose is a key precursor for the synthesis of 6-deoxy-6-substituted cellulose derivatives. The substitution of tosyl groups at position 6 occurred by SN reaction. Figure 6-4 shows the ^{13}C NMR spectra of 6-deoxy-6-(ω-aminoethyl)amino-cellulose synthesized from tosyl cellulose with different morphology. The characteristic signal for ethylenediamine (49 ppm) substituting the position C-6 was clearly observed. The presence of the free amine is also corresponded with results of FT-IR spectra, exhibiting the broad N−H stretching band at 3764 cm^{-1} and the N−H bend at 1570 cm^{-1}, as shown in Figure 6-5.

Similar to tosylation, the degree of amination on the surface of the cellulose increased as the NF membrane became more porous. Especially, it was observed that the increase of the degree of substitution was significantly changed compared to the case of tosylation. These results indicate that not

only the specific surface area is increased but also the site of the tosyl group capable of reacting with ethylenediamine increases at the same time.

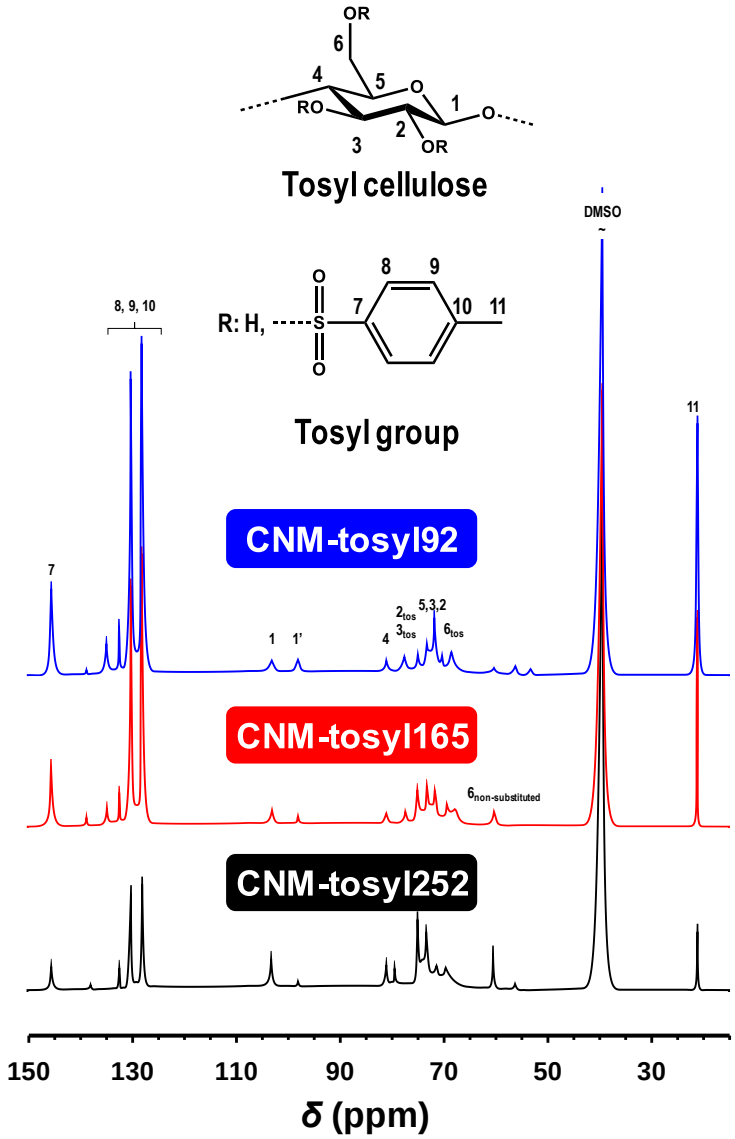

Figure 6-3. ^{13}C NMR spectra of tosyl cellulose NF membrane with degree of substitution DS_{tos} = 0.48, CNM-tosyl252, DS_{tos} = 0.95, CNM-tosyl165, and DStos = 1.71, CNM-tosyl92 recorded in DMSO-d_6 at 25 °C.

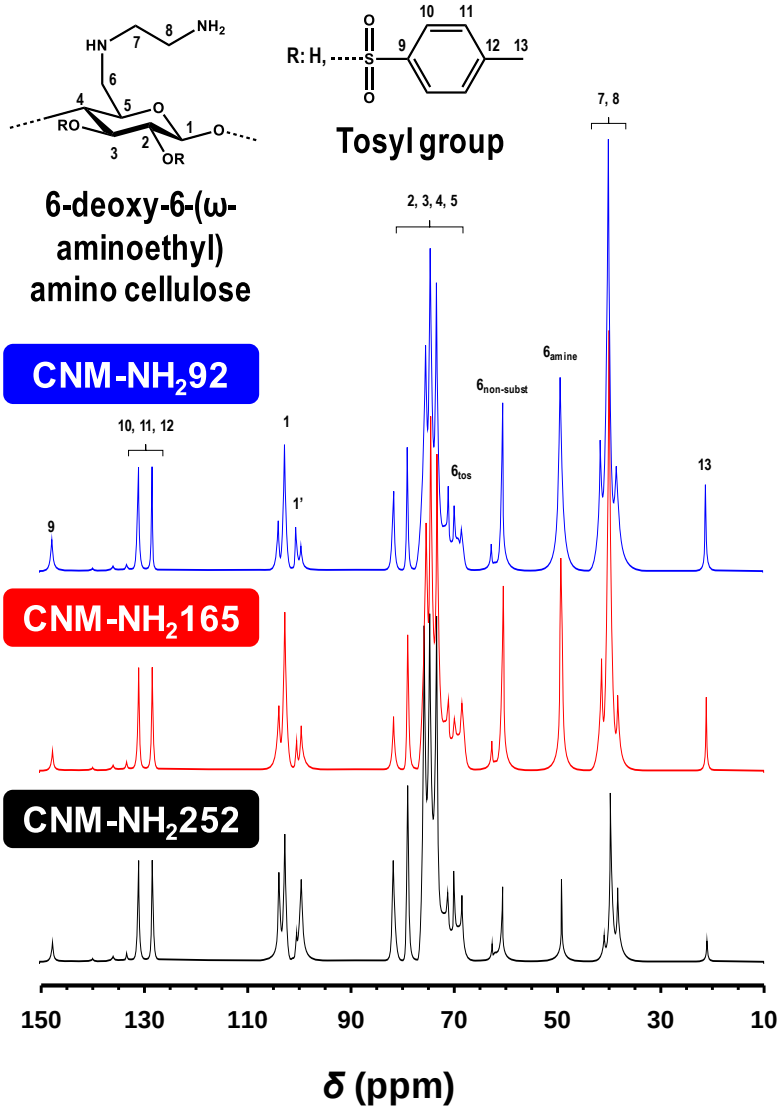

Figure 6-4. ^{13}C NMR spectra of CNM-$NH_2$252 (DS_{tos} = 0.07 and DSamine = 0.32), CNM-$NH_2$165 (DS_{tos} = 0.05 and DS_{amine} = 0.51) and CNM-$NH_2$92 (DS_{tos} = 0.05 and DS_{amine} = 0.63), recorded in D_2O at 25 °C.

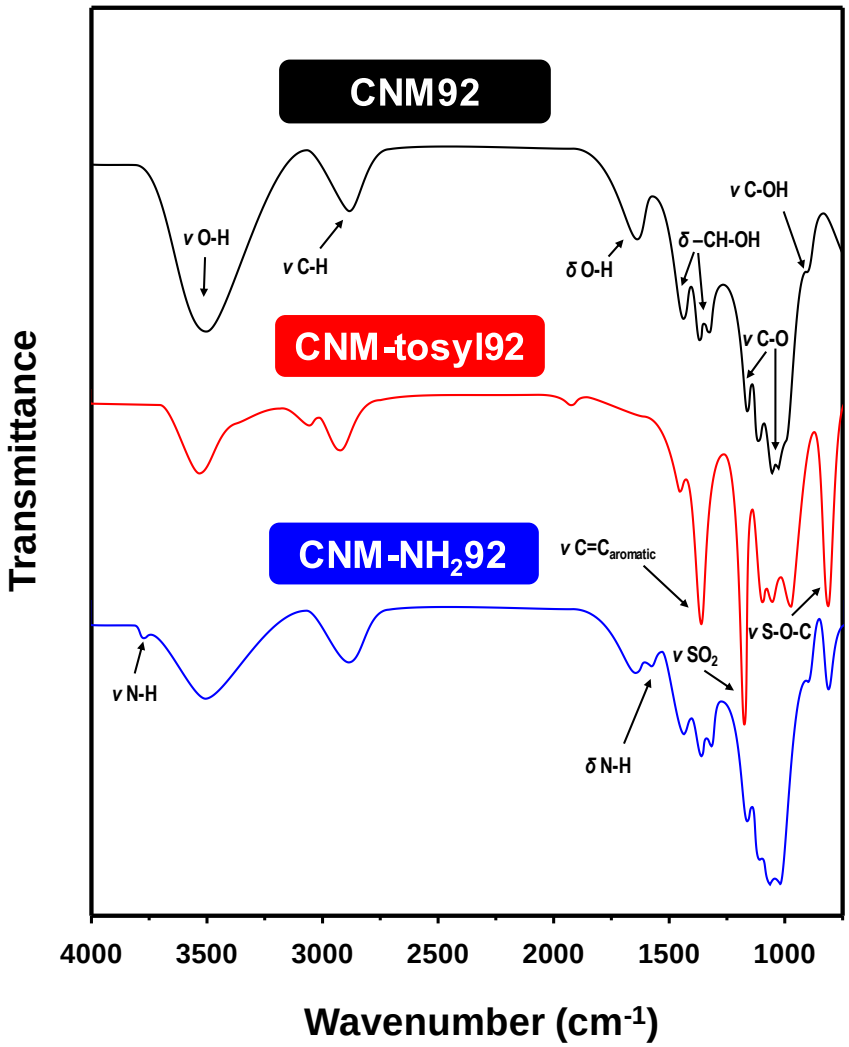

Figure 6-5. FT-IR spectra of neat and functionalized cellulose NF membrane with 92 kg/mol of molar mass

6.3.3. Structural properties

The structural properties of cellulose NF membrane was confirmed by the nitrogen-sorption analysis and BET and BJH calculations, as shown in Figure 6-6. The physisorption measurements exhibited type-IV isotherms with H1-type hysteresis, which indicated the mesoporous structure. A small decrease in the specific surface area and pore diameter was observed after the functionalization, and the surface area decreased in all the samples (Figure 6-7 and Table 6-1). As mentioned above, the morphology change was a result of the nanomembrnae and pore surfaces being covered by tosyl and amino groups.

.The effect of amination was observed in the change in the surface charge (Table 6-1). The zeta potential of the pristine membrane indicates a negative charge due to the high amount of hydroxy groups on the cellulose surface. For the amino-functionalized cellulose, the zeta potential values indicated a positive charge, which can be attributed to the insertion of ethylenediamine chains. The results indicate the surface of the cellulose NF membrane was successfully modified by ethylenediamine.

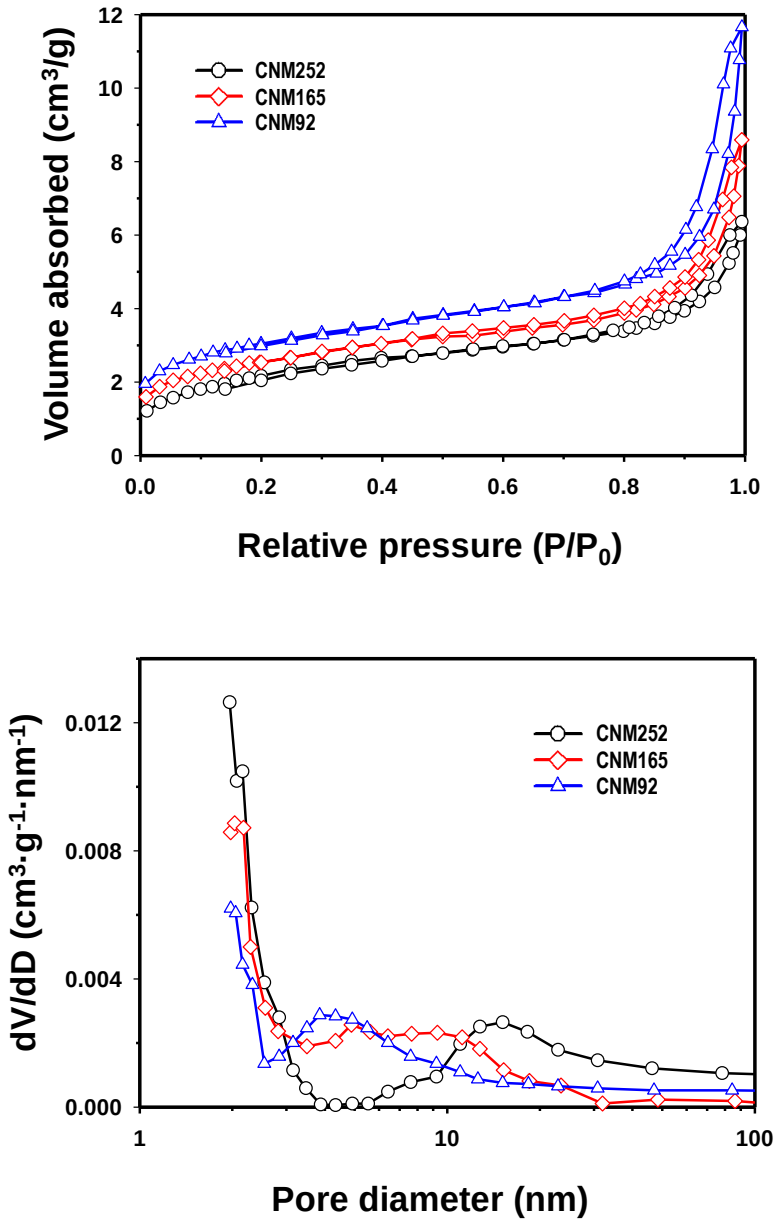

Figure 6-6. BET isotherms and BJH pore size distribution of neat cellulose nanomembrnae

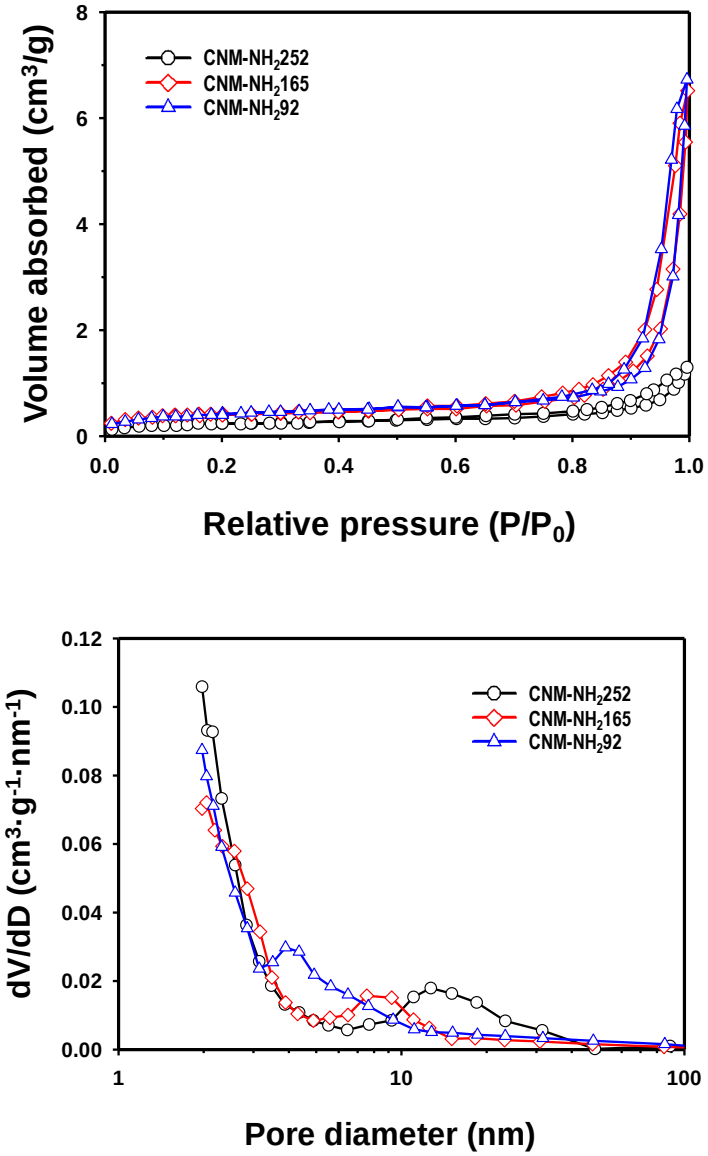

Figure 6-6. BET isotherms and BJH pore size distribution of amine-functionalized cellulose nanomembrnae

Table 6-1. Structure and surface properties of neat and amino-functionalized cellulose NF membrane

Sample	Surface area (m^2/g)	Average pore size (nm)[a]	Zeta potential (mV)	Average pore size (nm)[b]
Pristine cellulose	2.00	21.40	-19.82	-
CNM252	5.28	13.18	-16.57	12.52
CNM165	5.95	8.42	-15.92	7.98
CNM92	7.12	5.80	-2.54	5.24
CNM-$NH_2$252	5.10	12.34	15.24	11.92
CNM-$NH_2$165	5.52	7.11	18.65	7.25
CNM-$NH_2$92	6.94	4.57	19.19	4.40

[a]Calculated by BJH method

[b]Calculated by Young-Laplace equation

6.3.4. Permeability test of extra virgin olive oil

Figure 6-7 shows the results obtained for the NF membrane of the amino-functionalized cellulose consisting of different pore size. The permeability test of cellulose NF membrane was conducted with different transmembrane pressure, indicating the difference in pressure between the concentrated side and the permeate side. The high operating pressure resulted in an initial greater flux. However, rapid flux decrease was observed when the applied pressure is 400 and 600 kPa, while the flux under 200 kPa was almost constant during permeability test. This behavior resulted from the fouling phenomenon, which is ascribed to unstable pressure.[28] The fouling effect occurred differently under applied pressure. In all samples, the decrease rate of flux under 600 kPa is higher than one under other pressure. In addition, permeating rate under 600 kPa was lower than one measured in 200 kPa after 200 min of operating time. Based on results of flux behavior, the optimal pressure seems to be 200 kPa when operating stability was considered during filtration.

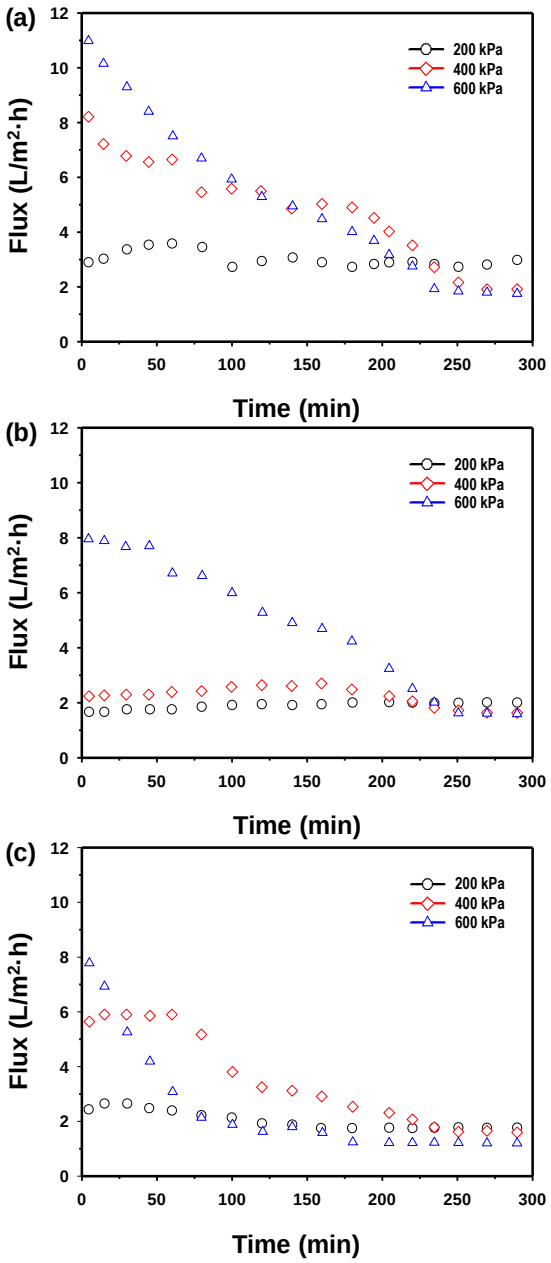

Figure 6-7. Filtration test of (a) CNM-$NH_2$282, (b) CNM-$NH_2$165 and (c) CNM-$NH_2$92

6.3.5. Optimal pore size for filtration

To determine the optimal pore size, the resulting cellulose NF membrane were employed for filtration of crude EVOO containing FFAs and chlorophyll at 30 ^{o}C under 200 kPa of pressure, and the remaining EVOO was analyzed, as shown in Figure 6-8. For the FFA filtration, the efficiency of amino-cellulose NF membrane was 9-fold higher than that of pristine one, regardless of the pore size. This trend demonstrates that the adsorption ability can be improved by functionalizing the cellulose surface with ethylenediamine. For chlorophyll, the adsorption strongly depended on the channel diameter of the nanoporous membrane. Rejection efficiency of the chlorophyll rapidly increased for pore sizes smaller than 7 nm. The results show that a critical pore size exists to allow chlorophyll to penetrate the pore interior and be captured in the pore volume.

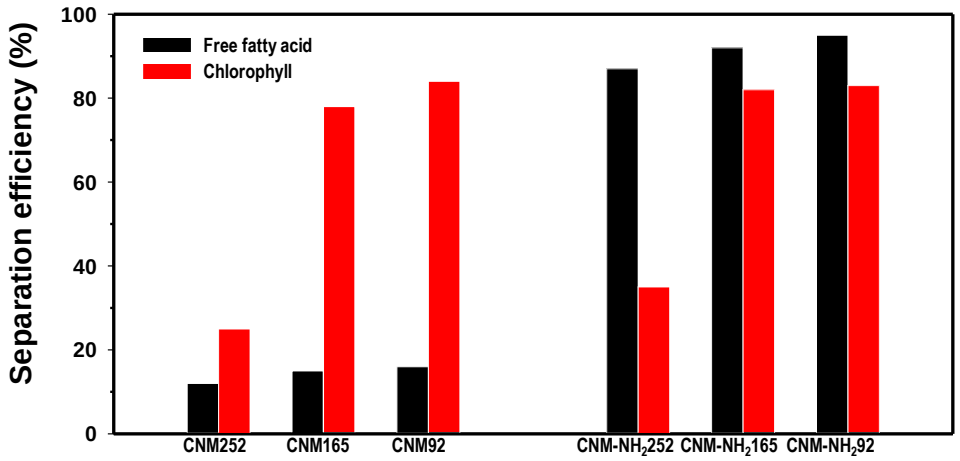

Figure 6-8. Separation efficiency of FFAs and chlorophyll by neat and amine-functionalized cellulose NF membrane

6.3.6. Composition analysis

A composition analysis was carried out on crude EVOO, physically refined EVOO and filtrated EVOO, and the results are given in Table 6-2. Filtrated EVOO refers to EVOO filtrated by CNM-$NH_2$92. Refined EVOO (Genesis bbq, Korea) refers to EVOO treated by a conventional process (degumming, bleaching and deodorization), and we used refined EVOO to demonstrate the selective seperation ability of CNM-$NH_2$92.

The fatty acid compositions of crude EVOO, physically refined EVOO and filtrated EVOO were in good agreement with their typical ranges.[29] All oils mainly consisted of oleic, palmitic, linoleic and stearic acids, comprising 67%, 14%, 8% and 3%, respectively. No significant difference was observed between the fatty acid ratios, which showed that the fatty acid composition of EVOO filtrated with CNM-$NH_2$92 was preserved.

'Extra virgin olive oil' in Europe is required to have the following: (i) FFA content: <0.8% oleic acid, (ii) peroxide values <20 meqO_2/kg and (iii) K232 and K270 spectrophotometric indexes <2.5 and 0.2, respectively. In terms of FFA content and peroxide value quality regulation, all olive oils used in this study were in the 'extra virgin' commodity class. The free acidity values were very low in all the samples, i.e., lower than 0.35%. The peroxide values varied among the samples and were 9.87, 4.52 and 9.89 meqO_2/kg in crude EVOO,

physically refined EVOO and filtrated EVOO, respectively. The low peroxide value of refined EVOO is because hydroperoxides decompose during the bleaching and deodorization process.[30] However, the K232 and K270 values of the refined oil exceeded the regulatory limits for the 'extra virgin' class, while the absorbances of the filtrated EVOO were similar to that of the crude EVOO. The rapid increase in the absorbance is due to the formation of dienes and trienes.[31] Hydroxy acids form because hydroperoxides undergo partial dehydration during bleaching. Because the functional group is at an allylic position, a rapid increase in the UV absorption at 232 nm is observed due to the formation of conjugated dienes from oleic acid hydroperoxides and conjugated trienes from linoleic acid hydroperoxides. Consequently, these results suggest that an EVOO treatment using CNM-$NH_2$92 can remove FFAs and chlorophyll without converting the FFAs.

Phenols are another typical component of EVOO. Olive fruits contain large amounts of water-soluble phenolic compounds and flavonoids with potent antioxidant properties. The total phenols were observed to be significantly reduced only in the refined olive oil. The tocophenol reduction trend agreed with the phenol results. The total phenol and tocopherol contents in refined EVOO indicated they were largely lost during the degumming and deodorization process that uses a large amount of water. The similarity in the

functional ingredient contents of crude EVOO and filtrated EVOO is proof of the selective removal of FFAs and chlorophyll.

Table 6-2. Component characterization of crude, refined and filtrated EVOO[a]

	Crude EVOO	Refined EVOO	Filtrated EVOO
Fatty acid composition (%)			
C16:0	14.31±0.25	14.38±0.08	14.39±0.21
C16:1	1.18±0.05	1.16±0.03	1.18±0.04
C17:0	0.04±0.00	0.04±0.00	0.04±0.01
C18:0	2.67±0.12	2.63±0.07	2.65±0.15
C18:1	69.84±0.39	70.06±0.06	69.71±0.35
C18:2	10.92±0.15	10.75±0.08	10.94±0.18
C18:3	0.06±0.01	0.05±0.00	0.06±0.00
C20:0	0.45±0.08	0.44±0.02	0.49±0.11
C20:1	0.26±0.04	0.27±0.01	0.27±0.02
C22:0	0.13±0.02	0.12±0.00	0.13±0.04
C24:0	0.04±0.01	0.03±0.00	0.04±0.00
FFA (% oleic acid)	0.35±0.09	0.03±0.01	0.04±0.00
Peroxide value (meqO_2/kg)	9.8±0.35	4.52±0.07	10.4±0.45
K232	2.02±0.03	2.42±0.01	2.15±0.00
K270	0.08±0.02	0.23±0.00	0.14±0.01
A-tocopherols (mg/kg)	334±11	37±2	329±8
Total phenols (mg/kg)	328±13	21±1	312±15
Smoke point (°C)	192±2	213±1	210±2

[a]All measurements are average of triplicate samples

6.3.7. Smoke point

The smoke point is a typical indicator of the thermal and oxidation stability of frying oil (Stevenson, Vaisey-Genser, & Eskin, 1984). The smoke points of crude EVOO, refined EVOO and filtrated EVOO are summarized in Table 6-2. The smoke point was observed to significantly increase when crude EVOO was refined or filtrated with CNM-$NH_2$92. The smoke point of frying oil should be at least 200 °C. Therefore, filtrated EVOO may be suitable for frying based on the smoke point of commercially used oil.

6.4. Conclusions

In this chapter, selective separation of FFAs and chlorophyll in crude EVOO was described using amino-functionalized cellulose NF membrane. The surface functionalization and pore size of NF membrane significantly influenced the separation efficiency for FFAs and chlorophyll, respectively. It was found that the amine group on the surface of cellulose was necessary to improve the selectivity and adsorption capacity. It also demonstrated that the chlorophyll separation efficiency was optimized when the pore size was smaller than 7 nm. The resulting absorbent selectively removed 90% and 81% of FFAs and chlorophyll, respectively, without the composition change of fatty acids. The EVOO filtrated by amino-functionalized cellulose NF membrane had a smoke point high enough to be used as a commercial frying oil.

References

1. Gordillo, B.; Ciaccheri, L.; Mignani, A. G.; Gonzalez-Miret, M. L.; Heredia, F. J., Influence of turbidity grade on color and appearance of virgin olive oil. *Journal of the American Oil Chemists' Society* **2011,** *88* (9), 1317-1327.
2. Fregapane, G.; Lavelli, V.; León, S.; Kapuralin, J.; Desamparados Salvador, M., Effect of filtration on virgin olive oil stability during storage. *European Journal of Lipid Science and Technology* **2006,** *108* (2), 134-142.
3. Tripoli, E.; Giammanco, M.; Tabacchi, G.; Di Majo, D.; Giammanco, S.; La Guardia, M., The phenolic compounds of olive oil: structure, biological activity and beneficial effects on human health. *Nutrition research reviews* **2005,** *18* (1), 98-112.
4. Casal, S.; Malheiro, R.; Sendas, A.; Oliveira, B. P.; Pereira, J. A., Olive oil stability under deep-frying conditions. *Food and chemical toxicology* **2010,** *48* (10), 2972-2979.
5. Hatzakis, E.; Dais, P., Determination of water content in olive oil by 31P NMR spectroscopy. *Journal of agricultural and food chemistry* **2008,** *56* (6), 1866-1872.
6. Ruiz-Domínguez, M. L.; Raigón, M. D.; Prohens, J., Diversity for olive

oil composition in a collection of varieties from the region of Valencia (Spain). *Food research international* **2013,** *54* (2), 1941-1949.

7. Bubola, K. B.; Koprivnjak, O.; Sladonja, B., Influence of filtration on volatile compounds and sensory profile of virgin olive oils. *Food chemistry* **2012,** *132* (1), 98-103.
8. Catalano, M.; De Felice, M., autossidazione delle sostanze grasse. I. Influenza degli acidi grassi liberi. *Riv Ital Sostanze Grasse* **1970**.
9. Kiritsakis, A.; Tsipeli, A., Relationship of the acidity of olive oil to its resistance to oxidation. *Rivista Italiana Delle Sostanze Grasse* **1992,** *69* (10), 513-515.
10. Miyashita, K.; Takagi, T., Study on the oxidative rate and prooxidant activity of free fatty acids. *Journal of the American Oil Chemists' Society* **1986,** *63* (10), 1380-1384.
11. Bendini, A.; Valli, E.; Rocculi, P.; Romani, S.; Cerretani, L.; Gallina Toschi, T., A new patented system to filter cloudy extra virgin olive oil. *Current Nutrition & Food Science* **2013,** *9* (1), 43-51.
12. Stefanoudaki, E.; Williams, M.; Harwood, J., Changes in virgin olive oil characteristics during different storage conditions. *European Journal of Lipid Science and Technology* **2010,** *112* (8), 906-914.
13. Diosady, L. L., Chlorophyll removal from edible oils. *Int. J. Appl. Sci. Eng* **2005,** *3* (2), 81-88.

14. Marchetti, P.; Solomon, M. F. J.; Szekely, G.; Livingston, A. G., Molecular Separation with Organic Solvent Nanofiltration: A Critical Review. *Chemical Reviews* **2014,** *114* (21), 10735-10806.
15. Sholl, D. S.; Lively, R. P., Seven chemical separations to change the world. *Nature* **2016,** *532* (7600), 435-437.
16. Ormerod, D.; Sledsens, B.; Vercammen, G.; Van Gool, D.; Linsen, T.; Buekenhoudt, A.; Bongers, B., Demonstration of purification of a pharmaceutical intermediate via organic solvent nanofiltration in the presence of acid. *Separation and Purification Technology* **2013,** *115*, 158-162.
17. Szekely, G.; Bandarra, J.; Heggie, W.; Sellergren, B.; Ferreira, F. C., Organic solvent nanofiltration: A platform for removal of genotoxins from active pharmaceutical ingredients. *Journal of Membrane Science* **2011,** *381* (1-2), 21-33.
18. Ribeiro, A. P. B.; de Moura, J.; Goncalves, L. A. G.; Petrus, J. C. C.; Viotto, L. A., Solvent recovery from soybean oil/hexane miscella by polymeric membranes. *Journal of Membrane Science* **2006,** *282* (1-2), 328-336.
19. Abe, Y.; Mochizuki, A., Hemodialysis membrane prepared from cellulose/N-methylmorpholine-N-oxide solution. II. Comparative studies on the permeation characteristics of membranes prepared from N-methylmorpholine-N-oxide and cuprammonium solutions. *Journal of*

Applied Polymer Science **2003,** *89* (2), 333-339.

20. Liang, S. M.; Zhang, L.; Xu, H., Morphology and permeability of cellulose/chitin blend membranes. *Journal of Membrane Science* **2007,** *287* (1), 19-28.
21. Liu, S. L.; Zeng, J. A.; Tao, D. D.; Zhang, L. N., Microfiltration performance of regenerated cellulose membrane prepared at low temperature for wastewater treatment. *Cellulose* **2010,** *17* (6), 1159-1169.
22. Livazovic, S.; Li, Z.; Behzad, A. R.; Peinemann, K. V.; Nunes, S. P., Cellulose multilayer membranes manufacture with ionic liquid. *Journal of Membrane Science* **2015,** *490*, 282-293.
23. Mao, Y.; Zhou, J. P.; Cai, J.; Zhang, L. N., Effects of coagulants on porous structure of membranes prepared from cellulose in NaOH/urea aqueous solution. *Journal of Membrane Science* **2006,** *279* (1-2), 246-255.
24. Nevstrueva, D.; Pihlajamaki, A.; Manttari, M., Effect of a TiO2 additive on the morphology and permeability of cellulose ultrafiltration membranes prepared via immersion precipitation with ionic liquid as a solvent. *Cellulose* **2015,** *22* (6), 3865-3876.
25. Xiong, X. P.; Duan, J. J.; Zou, W. W.; He, X. M.; Zheng, W., A pH-sensitive regenerated cellulose membrane. *Journal of Membrane Science* **2010,** *363* (1-2), 96-102.
26. Yang, G.; Xiong, X. P.; Zhang, L., Microporous formation of blend

membranes from cellulose/konjac glucomannan in NaOH/thiourea aqueous solution. *Journal of Membrane Science* **2002,** *201* (1-2), 161-173.

27. Gericke, M.; Schaller, J.; Liebert, T.; Fardim, P.; Meister, F.; Heinze, T.; European Polysaccharide, N., Studies on the tosylation of cellulose in mixtures of ionic liquids and a co-solvent. *Carbohydrate Polymers* **2012,** *89* (2), 526-536.
28. Schafer, A. I.; Fane, A. G.; Waite, T. D., Fouling effects on rejection in the membrane filtration of natural waters. *Desalination* **2000,** *131* (1-3), 215-224.
29. Aranda, F.; Gomez-Alonso, S.; Del Álamo, R. R.; Salvador, M.; Fregapane, G., Triglyceride, total and 2-position fatty acid composition of Cornicabra virgin olive oil: Comparison with other Spanish cultivars. *Food Chemistry* **2004,** *86* (4), 485-492.
30. Zschau, W., Bleaching. AOCS Press, Champaign, IL, USA: 2000; pp 158-178.
31. Cert, A.; Lanzón, A.; Carelli, A. A.; Albi, T.; Amelotti, G., Formation of stigmasta-3, 5-diene in vegetable oils. *Food chemistry* **1994,** *49* (3), 287-293.

국문 초록

지구상에서 가장 풍부한 고분자 중 하나인 셀룰로오스는 고강도, 생분해성, 생체적합성 등과 같은 우수한 성질을 지니고 있다. 그러나 셀룰로오스는 용융이 되지 않으며 용해할 수 있는 용매가 매우 제한적이기 때문에 공정적으로 불합리한 조건을 가지고 있다. 최근, 상온에서 쉽게 셀룰로오스를 용해할 수 있는 이온성 액체가 개발된 이후, 관련 연구는 막대히 증가하고 있다. 이온성 액체는 거대 양이온 분자와 상대적으로 작은 음이온이 이온결합을 하고 있는 염으로 구성되어 있다. 셀룰로오스 용해 원리는 수소결합이 가능한 음이온이 셀룰로오스 수소결합 네트워크를 붕괴시키고 이 공간을 양이온이 채워서 셀룰로오스의 견고한 구조를 해리시키는 것으로 알려져 있다. 많은 연구에도 불구하고, 이온성 액체 내에서 셀룰로오스의 분자량이 감소되는 현상과, 재생 후 결정성이 회복되지 않아 강도가 저하되는 문제점이 발생한다. 따라서 본 연구에서는 이온성 액체내에서 셀룰로오스의 해중합에 대한 근본적 고찰과 동시에 미세구조를 제어하여 균일한 나노구조를 갖는 셀룰로오스 소재를 개발하는 것을 주요 목표로 한다.

첫째로, 서로 다른 음이온을 갖는 이온성 액체를 사용하여 셀룰로오스를 용해 후, 해중합되는 속도와 원인을 관찰하였다. 셀룰로오스의 해중합은 이온성 액체에서 발생하는 산에 의한 가수분해 현상으로 밝혀졌다. 이온성 액체에서 발생한 산은 음이온의 염기도가 클수록 많이 생성되는 것을 확인하였다. 산 가수분해에 의해 분자량의 낮아진 셀룰로오스를 이용하여 점도평균분자량 상수를 구할 수 있었다. 또한 기존에 보고되지 않았던 셀룰로오스의 유방성 액정현상을 관찰하였다.

둘째로, 이온성 액체 내에서 가수분해된 셀룰로오스 분자의 운동성을 평가하고 결정화 거동과의 상관관계를 조사하였다. 분자량이 낮아진 셀룰로오스는 운동성이 점차 향상되며, 특히 얽힘 분자량 이하에서 급격히 증가하였다. 이를 증명하기 위해 분자 확산 계수와 점도의 상관관계를 분석하여 운동 상수를 계산하였다.

셋째로, 가수분해 거동과 운동성 데이터를 바탕으로 리그노셀룰로오스 바이오매스 전처리 공정에 이온성 액체를 적용하였다. 리그노셀룰로오스 전처리는 구조의 이완과 분자량의 감소를 목적으로 한다. 이온성 액체의 용해도가 증가할수록 비셀룰로오스계 성분의 제거 효율은 증가하였나 재결정화도가 크게

증가하였다. 이 연구를 통해 각 리그노셀룰로오스의 구조에 최적화된 이온성 액체 선정에 대한 레퍼런스를 제시하였다.

넷째로, 분자 운동성이 조절된 셀룰로오스 분자를 이용하여 균일한 크기와 우수한 분산성을 갖는 셀룰로오스 나노입자를 제조하였다. 가수분해 도중 이온성 액체의 양이온이 셀룰로오스 환원성 말단에 치환되는 반응을 유도하여 마이셀과 유사한 셀룰로오스 나노입자를 형성시켰다. 표면의 양이온에 의해 셀룰로오스 나노입자는 높은 분산성을 나타내었다.

다섯째로, 나노기공을 갖는 셀룰로오스 분리막을 제조하고 표면에 아민기 도입을 통해 엑스트라 버진 올리브유의 산패성분을 분리하는 공정을 제시하였다. 앞서 나노입자 제조의 원리와 마찬가지로, 운동성이 향상된 셀룰로오스 분자 사슬은 높은 기공성을 나타내었다. 제조된 셀룰로오스 나노분리막에 토실기와 에틸렌디아민을 차례대로 치환하여 아민기를 도입하였다. 엑스트라 버진 올리브유의 산패성분으로 알려진 유리지방산과 엽록소는 각각 분리막 표면의 아민기와 기공크기에 의해 분리되었다. 또한 엑스트라 버진 올리브유의 성분 변화없이 산패성분만 선택적으로 제거 가능함을 확인하였다.

본 연구에서는 다양한 조건에서 셀룰로오스를 이온성 액체에 용해하고 분자의 특성 변화를 규명하였다. 이를 기반으로 셀룰로오스의 나노화에 대한 기술을 확립하였다. 특히, 이온성 액체에서 재생된 기존 셀룰로오스의 한계로 여겨지는 분자량의 감소와 낮은 결정성을 극복하고 분산성과 크기 균일성을 확보하는 방법을 개발하여 셀룰로오스/이온성 액체 공정의 새로운 지평을 열 수 있을 것으로 기대된다.

Paper lists

1. Ahn, Y.; Kim, H.; Kwak, S. -Y., Self-reinforcement of alginate hydrogel via conformational control. *European Polymer Journal*. **2019**, *116*,480-487.
2. Ahn, Y.; Song, Y.; Kim, H.; Kwak, S. -Y., In Situ Formation of Autodispersing Cellulose Nanoparticles with Extreme Uniformity. *ACS Macro Letters*. **2017**, *6*, 762-767.
3. Ahn, Y.; Song, Y; Kim, H.; Kwak, S. -Y., Formation of cellulose-carbene complex via depolymerization in ILs:Dependence of IL types on kinetics, conformation and dispersity. *Carbohydrate Polymers*. **2017**, *159*, 86-93.
4. Ahn, Y.; Kim, H.; Kwak, S. -Y., Comparing the influence of acetate and chloride anions on the structure of ionic liquid pretreated lignocellulosic biomass. *Biomass and Bioenergy*. **2016**, *93*, 243-253.
5. Ahn, Y.; Song, Y; Kim, H.; Kwak, S. -Y., Highly ordered cellulose II crystalline regenerated from cellulosehydrolyzed by 1-butyl-3-methylimidazolium chloride. *Carbohydrate Polymer*, **2016**, *137*, 321-327.
6. Ahn, Y.; Kwak, S. -Y.; Song, Y; Kim, H., Physical state of cellulose in BmimCl: dependence of molar mass on viscoelasticity and sol-gel transition. *Phys. Chem. Chem. Phys*. **2016**, *18*, 1460-1469.

Patent lists

1. 곽승엽, 안용준, ‘유/무기 재료의 표면에 커플링제를 도입하기 위한 반응 용액 순환형 반응 장치 및 상기 반응 장치를 이용한 커플링제 도입 방법’ 대한민국 특허출원 10-2018-0117223 (출원일 2018. 10. 01.)
2. 곽승엽, 안용준, 윤홍근, 이성우, ‘엑스트라 버진 올리브유에 함유된 산패인자를 선택적으로 흡착하여 정제하는 흡착필터 및 이를 이용한 정제방법’ 대한민국 특허등록 제1833932호 (등록일 2018. 02. 23.)

Symposium lists

1. 2018년, Waset 2018 New York Conference, “Dependence of free fatty acid and chlorophyll content on thermal stability of extra virgin olive oil”
2. 2016년, 추계 섬유공학회, “이온성 액체에 의해 가수분해된 셀룰로오스 용액의 유변학적 거동과 상전이”
3. 2015년, MRS fall meeting, “Preparation of high crystallinity bionanofibers from ionic liquid-cosolvent system”
4. 2015년, The Fiber Society’s Spring 2015 Conference, “Effect of lignin

content on electrospinning of lignocellulose solution”

5. 2014년, MRS fall meeting, “Influence of Anion Type on Ionic Liquid Pretreated Lignocellulosic Biomasses”